UNIVERSITY OF CALIFORNIA
RIVERSIDE

Control-Theoretic Methods for the Robustness of Network Systems: Application to Traffic Control and Cyber-Physical Security

A Dissertation submitted in partial satisfaction
of the requirements for the degree of

Doctor of Philosophy

in

Mecahnical Engineering

by

Gianluca Bianchin

March 2020

Dissertation Committee:

Dr. Fabio Pasqualetti, Chairperson
Dr. Matthew Barth
Dr. Wei Ren
Dr. Jun Sheng

The Dissertation of Gianluca Bianchin is approved:

Committee Chairperson

University of California, Riverside

Acknowledgments

First, I would like to express my deepest gratitude to my Ph.D. advisor Fabio Pasqualetti. He guided and oriented my doctoral work with his vision, inspired me with his "message-oriented" research ideas, pushed me to learn the beauty of "linear writing", and made my whole Ph.D. experience an enjoyable journey by accommodating a good work-life balance.

I am grateful to my committee members, Dr. Matthew Barth, Dr. Wei Ren, and Dr. Jun Sheng for our constructive interactions. Their research ideas inspired me, and their comments stimulated my doctoral research and helped me identifying interesting directions.

Many thanks to all my friends, labmates, and colleagues at the University of California, Riverside. Many of these left an indelible mark: Rajasekhar, Tommaso, Siddharth, Giacomo, Chiara, Lorenzo, Mika, Christian, Adriano, Yin-Chen, to name a few.

To all my mentors and instructors at the University of Padova, I owe a great debt of thanks. I was fortunate to study in such an outstanding institution, full of excellent instructors, brilliant students, and all surrounded by beautiful history. I am especially grateful to Prof. Angelo Cenedese and Prof. Ruggero Carli, who guided me towards this exciting career, and to all my former classmates for all the wonderful interactions.

My most sincere thank you goes to my family: they are the basis of all my achievements. They provided me the best education, they supported me in all my decisions, and most importantly they withstood the stress of me living in the opposite corner of the world.

Finally, during my five-year journey in the United States I was constantly helped and guided by friends, mentors, or simply strangers. A great thank you to all the people I met during this journey, because a great success requires the help of many.

To to all those who have helped me during this journey.

ABSTRACT OF THE DISSERTATION

Control-Theoretic Methods for the Robustness of Network Systems:
Application to Traffic Control and Cyber-Physical Security

by

Gianluca Bianchin

Doctor of Philosophy, Graduate Program in Mecahnical Engineering
University of California, Riverside, March 2020
Dr. Fabio Pasqualetti, Chairperson

Network systems model natural and engineered processes composed of groups of physical components that interact with the environment, and that are coupled with each other by means of an intricate communication network. Network systems have been widely adopted to model and understand many complex physical processes, ranging from stock markets in economics, transportation networks in engineering, to evolutionary processes in biology. A fundamental property of these systems is their robustness to contingencies, that is, the capability of operating effectively despite external perturbations, such as accidental component failures, malicious targeted attacks, or external disturbances. In this dissertation, we address four engineering problems concerning robustness in network systems.

First, we study robustness in highway transportation systems where travelers follow routing suggestions provided by modern navigation apps (such as GoogleMaps, Waze, Inrix, etc.). Navigation apps provide minimum-time routing directions to the travelers based on global and instantaneous congestion information, thus transforming the way users behave and impacting the aggregate system behavior. We propose and analyze new models

to capture the routing decisions of app-informed travelers that are inspired from selection and learning mechanisms in biology. Our analysis and techniques are rigorous, and can be applied to any traffic network topology, independently of its size or interconnection patterns. Our findings demonstrate that among numerous favorable benefits, routing apps can introduce new undesirable congestion phenomena, and that appropriate information design will be necessary to ensure the robustness of modern traffic infrastructures. Second, we propose a set of robust control algorithms to optimize the operation of the signalized traffic intersections in an urban traffic network in order to guarantee system-level optimality. Our methods are computationally-tractable, outperform state-of-the-art intersection control policies, and are effective to reduce congestion in major cities, as demonstrated by our simulations for Manhattan, NY. Third, with a focus on networks with linear dynamics, we develop theories and tools to study the robustness of a network against changes in the the communication links. Our methods include both rigorous algebraic conditions and tractable numerical algorithms, and ultimately relate the robustness of a system to the graph-theoretical properties of the underlying network interconnection. Fourth, with an application focus to robotics, we tackle the problem of ensuring robust navigation despite maliciously-compromised localization sensors. Our methods rely on the nonlinear notion of *zero dynamics*, and unveil fundamental limitations for attack detection. More generally, our results demonstrate for the first time that the choice of inputs adopted for control affects the security of a dynamical system.

Contents

List of Figures

List of Tables

Chapter 1

Introduction

Robustness is the ability to withstand unforeseen perturbations, failures, or possibly malicious attacks while ensuring nominal performance. While the concept of robustness is generic and applicable to many domains, this notion becomes exceedingly important when groups of components are interconnected by means of a network. In fact, networks are often nature's solution to ensure the robustness of components that individually are exceedingly fragile, thanks to their capability to quickly redistribute remotely located resources. The application-domain of particular interest for this dissertation is networked dynamical systems (or network systems). Network systems model groups of physical components that are interconnected through a network, such as coupled physical processes, production or economic activities, biological processes, or groups of computational resources. Due to their crucial role in real-world applications, ensuring the robustness of network systems is a central engineering goal, aiming to design transportation systems, power networks, robots, cars, or airplanes that can perform basic functions despite occasional failures of their components.

This dissertation addresses four main engineering questions concerning robustness in network systems: (i) how do we ensure network robustness in the face of fluctuations in the behavior of its users or components, (ii) how do we adjust the network parameters to ensure optimality in a variety of operating regimes, (iii) how robust are certain network properties to changes in the communication arcs, and how do we identify the arcs that mainly originate these fragilities, and (iv) how do we design controls to ensure robustness in the face of targeted malicious attacks. These four research questions are addressed along two main application domains: traffic control in transportation systems, and security in cyber-physical systems.

1.1 Application to Traffic Control in Transportation Systems

Traffic networks are fundamental components of modern societies, making economic activity possible by enabling the transfer of passengers, goods, and services in a timely and reliable fashion. Despite their economic importance, traffic networks are impaired by the outstanding problem of traffic congestion, which wastes billions of gallons of fuel each year in the United States [16]. Recent advances in vehicle technologies, such as vehicle communication and vehicle automation, have demonstrated an enormous potential to overcome the inefficiencies of traditional transportation systems. Notwithstanding, because of the tremendous complexity of these infrastructures, the development efficient and robust control algorithms capable of effectively engaging these capabilities is an extremely challenging task that often results in suboptimal performance [17], or can originate novel

system fragilities [13, 18]. The increasing need for robust control algorithms to effectively operate transportation infrastructures motivates our first two research questions.

How do we ensure network robustness in the face of fluctuations in the behavior of its users? Increasing levels of congestion are affecting nominal travel times of freeways and urban roads, thus incentivizing travelers to adopt alternative routes that are often undesirable and suboptimal. These route alternatives are increasingly made available by advanced traveler information systems, such as navigation apps (or routing apps), which provide reliable minimum-time routing suggestions to the travelers based on real-time congestion information. Yet, among numerous favorable advantages, routing apps can sometimes deteriorate traffic congestion and originate undesirable behaviors at the system level, a phenomenon that is studied here for the first time.

In this dissertation, we focus on studying the impact of app-informed routing on the dynamical properties of the traffic infrastructure, and on characterizing the consequences of real-time traffic information on the stability of the traffic system. Our results show that the general adoption of navigation apps will maximize the throughput of flow across the network in the long run. Hence, these devices bring valuable system-level benefits to modern transportation systems. Unfortunately, our findings also demonstrate that navigation apps can deteriorate the stability of the system, and can results in emerging undesirable traffic phenomena such as temporal oscillations of traffic congestion. Hence, our results demonstrate that the benefits in the adoption of real-time routing systems come at the cost of increased system fragility, and suggest that adequate information design is necessary to overcome these limitations.

How do we adjust the network parameters to ensure optimality in a variety of operating regimes? Modern urban transportation architectures comprise two fundamental components: roads and traffic intersections. Intersections connect and regulate conflicting traffic flows among adjacent roads, and their effective control can sensibly improve travel time and prevent congestion. The ability to control modern signalized intersections, combined with the increasing availability of sensors for vehicle detection and flow estimation, have inspired the development control algorithms that adjust the operation of the infrastructure in relation to the current traffic conditions and congestion regimes.

In this dissertation, we propose a simplified version of classical models for urban traffic networks, and we study the problem of optimizing the network overall efficiency by controlling the signalized intersections. Differently from classical approaches to control traffic signaling, our models are tractable, they allow us to effectively model large-scale interconnections, and enable the design of critical parameters while considering system-level measures of efficiency. By adopting these tractable models, we cast an optimization problem to minimize network congestion by controlling the green times at the signalized intersections. Our results and simulations demonstrate that tractable optimization frameworks can outperform state-of-the art intersection control policies, and suggest that the increase in system performance obtained by our control method justifies the increment in complexity deriving from the adoption of a global system description.

1.2 Application to Security in Complex Networks and Robotics

Complex Networks are a class of network systems where the physical components have linear dynamics and the network interconnections is large-scale, namely, the number of nodes and links is increasingly large. Complex networks are broadly used to model engineering, social, and natural systems, such as power networks, social networks, and networks of epidemic processes. On the other hand, Robotic Networks are a class of network systems where the physical components are autonomous robots. In recent years, autonomous robots have gained exceptional popularity thanks to their flexibility, their capability to accomplish complex tasks, and broad range of civilian and military applications. Ensuring robustness in complex and robotic networks motivates our second two research questions.

How robust are certain network properties to changes in the communication arcs? Observability of a linear network guarantees the ability to reconstruct the state of each node from sparse measurements, and is a fundamental property to ensure that the state of the system can be correctly estimated from the available measurements. In this part of the dissertation, we measure the robustness of a network based on the size of the smallest perturbation needed to prevent observability. We consider linear networks, where the dynamics are described by a weighted adjacency matrix, and dedicated sensors are positioned at a subset of the nodes. We allow for perturbations of certain edge weights, with the objective of preventing observability of some modes of the network dynamics. To comply with the network setting, our work considers perturbations with a desired sparsity structure, thus extending the classic literature on the observability radius of linear systems.

This dissertation proposes two sets of results. First, we propose an optimization framework to determine the smallest perturbation that renders a desired mode unobservable from the existing sensor nodes. Second, we study the expected observability radius of networks with given structure and random edge weights. We provide fundamental robustness bounds that depend on the connectivity properties of the network and we analytically characterize optimal perturbations of line and star networks, showing that networks with line topology are inherently more robust than networks with star topology.

How do we design controls to ensure robustness in the face of targeted malicious attacks? In this part of the dissertation, we study the problem of navigating a robot in an adversarial environment, where the objective is to perform localization and trajectory planning despite the malicious and unknown action of an attacker. We consider robots equipped with a Global Navigation Satellite System (GNSS) sensor and a Radio Signal Strength Indicator (RSSI) sensor that provides relative positioning information with respect to a group of radio stations, each with limited communication range. The attacker can simultaneously spoof the sensor readings and send falsified control inputs to the robot, so as to deviate its trajectory from the nominal path. We demonstrate the existence of undetectable attacks, that is, attack actions that deviate the robot from the nominal trajectory and cannot be detected by detection algorithms. Conversely, we show that by appropriately designing the control inputs and by selecting certain intermediate waypoints, a trajectory planner can ensure the detectability of any attack and thus secure navigation.

1.3 Organization and Summary of Contributions

The contents of this dissertation are organized into seven main chapters, followed by a shared conclusion. The main contributions of each chapter are as follows.

Chapter 2 - Preliminaries in Control Theory, Graph Theory, and Nonlinear Control. In this chapter, we define the main notation adopted in this dissertation, and we introduce few fundamental notions from Control Theory and Graph Theory that will be used throughout this document. The chapter also includes a primer on concepts from passivity in nonlinear dynamical systems that will be instrumental in Chapter 3.

Chapter 3 - Changes in User Behavior: The Impact of Navigation Apps. In this chapter, we study the impact of navigation apps on the stability of transportation systems. The bulk of literature on understanding the routing decisions of human drivers in traffic congestion has been developed mainly by adopting simplified traffic models in a game-theoretic setting (see e.g. [17, 19, 20]). In these models, traffic flows propagate *instantaneously* across the network, and drivers make route choices by minimizing their personal travel times in response to day-to-day information regarding traffic congestion [21]. Our approach, instead, is based on models that capture finite flow propagation times and the availability of real-time traffic information, and focuses on understanding the dynamical interplay between traffic congestion and routing behaviors.

The contribution of this chapter is fourfold. First, we propose a dynamical decision model to capture the routing behavior of app-informed travelers in response to traffic congestion. Our model is inspired from evolutionary models (or learning models) in biology and game theory, and models scenarios inspired by the real-world where travelers

make decisions iteratively and use the observations of other travelers to adjust their next decision. Second, we study the properties of the fixed point of a traffic system where the dynamical routing decision model is coupled with a dynamical traffic model, and we establish a relationship between the properties of the equilibrium points and the well-established notion of Wardrop equilibria [21]. Third, we characterize the stability of the equilibrium points, and we demonstrate the existence of periodic orbits for the system, demonstrating the existence of temporal oscillations of traffic congestion. Fourth, we propose a control technique to ensure the asymptotic stability of the fixed points. Our methods rely on regulating the rates at which travelers react to congestion information, a behavior that can be achieved by appropriately designing the frequency at which navigation apps update the routing suggestions provided to the travelers. Throughout this chapter, we also develop important insights into the system-level benefits of using navigation apps, and demonstrate for the first time the existence of temporal oscillations of traffic congestion.

Chapter 4 - Robust Network Optimization: Application to Traffic Intersections. In this chapter, we study the problem of controlling the signalized intersections in an urban traffic network with the goal of minimizing system-level congestion. Our work is motivated by the fact that most of the state-of-the-art control policies adopted in major cities are distributed, namely, the operation of a certain signalized intersection only depends on the traffic congestion in the proximity of that intersection. Hence, research is needed for the development of tractable models and optimization techniques that can guarantee system-level performance and traffic efficiency.

The contribution of this chapter is fourfold. First, we propose a simplified model to capture the behavior of traffic networks operating in free-flow regimes with arbitrary travel speeds. The adoption of a simplified model is motivated by the exceeding complexity of urban transportation systems, and represents a novel, computationally-tractable, way of capturing the macroscopic behavior of large traffic intersections. Second, we employ the proposed model to design the durations of the green times at the signalized intersections. Our methods relate congestion objectives with the problem of optimizing a metric of controllability of the dynamical system associated with the traffic network. We use the concept of smoothed spectral abscissa [22] to solve the optimization, and we demonstrate that our methods outperform common intersection control algorithms. Third, we propose a technique to efficiently solve the optimization by parallelizing the computation among a group of distributed agents, demonstrating that our methods can be solved efficiently in a distributed fashion. Fourth, we assess the benefits of the proposed modeling and optimization framework through macroscopic (based on Cell Transmission Model) and microscopic (based on SUMO) simulations on daily commutes for the urban interconnection of Manhattan, NY.

Chapter 5 - Optimization-Based Techniques to Quantify Resilience. In this chapter, we discuss the use of vehicle communication to partially influence the routing decisions of drivers in a traffic network with the goal of optimizing a global measure of traffic congestion. We define link-wise levels of trust to tolerate the non-cooperative behavior of a certain fraction of the drivers, and we develop an optimization-based control mechanism to provide real-time routing suggestions based on the current congestion levels. Differently

from classical approaches to design routing suggestions, our methods focus on scenarios with quickly-varying traffic volumes, and do not require the knowledge of the traffic demands.

The contribution of this chapter is threefold. First, we formulate and solve an optimization problem to design optimal routing suggestions with the goal of minimizing the travel time experienced by all network users. The optimization problem incorporates link-wise trust parameters that describe the extent to which drivers on that link are willing to follow the suggested routing policy. Second, we develop an online update scheme that takes into account instantaneous changes in the levels of trust on the provided routing suggestions. Third, we study the resilience of the network, measured as the smallest change in the trust parameters that results in roads reaching their maximum capacity. We present an efficient numerical technique to approximate the resilience of the network links, and we discuss how these quantities can be computed from the output of the optimization problem.

Chapter 6 - Robustness Against Perturbations of the Network Edges. In this chapter, we measure robustness of a network based on the size of the smallest perturbation needed to prevent its observability. While network observability is a binary notion [23], the degree of observability can be quantified in different ways, including the energy associated with the measurements [24, 25], the novelty of the output signal [26], the number of necessary sensor nodes [27, 28], and the robustness to removal of interconnection edges [29]. A quantitative notion of observability is preferable over a binary one, as it allows to compare different observable networks, select optimal sensor nodes, and identify topological features favoring observability.

The contribution of this chapter is threefold. First, we introduce a metric of robustness that captures the capability of a network to withstand structural perturbations of the communication edges. Our metric evaluates the magnitude of a perturbation needed to make some of its states unobservable. Second, we formulate a problem to determine optimal perturbations (with smallest Frobenius norm) preventing observability. Our findings demonstrate that the problem is in general not convex, and we derive optimality conditions that relate to a nonlinear generalized eigenvalue problem. To solve this problem, we then propose a numerical procedure based on the power iteration method. Third, we derive a fundamental bound on the expected observability radius for edges with random weights. We characterize the robustness of networks with line and star topologies, and we demonstrate that line networks are inherently more robust than star networks to perturbations of the edge weights.

Chapter 7 - Robustness Against Attacks: Secure Navigation of Robots. In this chapter, we study the problem of navigating a robot in an adversarial environment, where the objective is to perform localization and trajectory planning despite the malicious and unknown action of an attacker. We assume robots are equipped with a GPS sensor, which provides absolute positioning information, and a RSSI sensor, which provides relative positioning information with respect to a group of radio stations, each with limited communication range. Moreover, we assume an attacker can simultaneously spoof the sensor readings and send falsified control inputs to the robot, so as to deviate its trajectory from the nominal path.

The contribution of this chapter is threefold. First, we characterize undetectable attacks, that is, the general form of attack inputs and spoofing signals that cannot be detected by a security monitor. Moreover, we show how an attacker can systematically design attacks that are undetectable, and we demonstrate that attacks can exist only when the robot is located in certain regions of the plane. Second, we solve the problem of designing optimal attacks, that is, attack inputs that maximally deviate the robot's trajectory from the nominal path. Third, we formalize the trajectory planner's goal of designing secure control inputs, that is, inputs that allow the detection of any attack action, and we demonstrate that secure control inputs can only exist between certain subsets of initial and final positions.

Chapter 8 - Conclusions. This chapter concludes the dissertation and outlines some aspects for future research in the area of network system robustness.

Chapter 2

Preliminaries in Control Theory, Graph Theory, and Nonlinear Control

This chapter includes a primer on concepts from Control Theory, Algebraic Graph Theory, and Nonlinear Control that will be used throughout this dissertation.

2.1 Control Theory and Algebraic Graph Properties

On the one hand, Control Theory is the fundamental mathematical framework used for the study of dynamical systems. On the other hand, Algebraic Graph Theory provides a link between the theory of graphs (Graph Theory) and the theory of matrices (matrix theory in Linear Algebra), and it is a fundamental tool for the analysis and control

of dynamical systems over networks. We begin this section by introducing some of the fundamental notation adopted in this dissertation.

Vector notation, matrix notation, and basic linear algebra definitions. Let $\mathbb{R}$, $\mathbb{R}_{>0}$, $\mathbb{R}_{\geq 0}$, $\mathbb{C}$, and $\mathbb{N}$ denote the set of real numbers, the set of positive real numbers, the set of nonnegative real numbers, the set of complex numbers, and the set of positive integers, respectively. For $n, p \in \mathbb{N}$, a vector $x \in \mathbb{R}^n$, and a matrix $A \in \mathbb{R}^{n \times n}$, we let $\|x\|_p$ be the Euclidean p-norm of x, and $\|A\|_p$ be the induced p-norm of A. We denote by x^T the row vector obtained by transposing x, and by A^T the transpose of matrix A. We denote the n-dimensional vector of all ones by $\mathbb{1}_n$, the n-dimensional vector of all zeros by 0_n, and the $(n \times n)$-dimensional identity matrix by I_n.

Let A be a matrix describing a linear map between two subspaces $\mathcal{X}$ and $\mathcal{Y}$, i.e., $A : \mathcal{X} \to \mathcal{Y}$. The *image or range space* of A is defined as

$$\mathrm{Im}(A) := \{Ax \ : \ x \in \mathcal{X}\},$$

and the *kernel or null space* of A is defined as

$$\mathrm{Ker}(A) := \{x \in \mathcal{X} \ : \ Ax = 0\}.$$

We say that A is *surjective* if $\mathrm{Im}(A) = \mathcal{Y}$ and *injective* if $\mathrm{Ker}(A) = \emptyset$. Also, the map A is *bijective* (or invertible) if A is injective and surjective. In this case, the map A admits an inverse map, denoted by A^{-1}.

Fora matrix A, $\lambda \in \mathbb{C}$ is an *eigenvalue* of A if there exists a nonzero vector $v \in \mathcal{X}$ such that $Av = \lambda v$. The set of eigenvalues, which contains at most n elements, is called the spectrum of A and is denoted by $\lambda(A)$. The matrix A is *Hurwitz stable* if $\Re(\lambda) < 0$ for all $\lambda \in \lambda(A)$, where $\Re(\lambda)$ denotes the real part of the complex number λ. The matrix A is *Schur stable* if $|\lambda| < 1$ for all $\lambda \in \lambda(A)$, where $|\lambda|$ denotes the absolute value of the complex number λ.

Linear dynamical systems. A *continuous-time linear time-invariant* system is defined by the equations

$$\begin{aligned} \dot{x}(t) &= Ax(t) + Bu(t), \\ y(t) &= Cx(t) + Du(t), \end{aligned} \tag{2.1}$$

where $x \in \mathcal{X} \subseteq \mathbb{R}^n$, $u \in \mathcal{U} \subseteq \mathbb{R}^m$, $y \in \mathcal{Y} \subseteq \mathbb{R}^p$ and A, B, C, and D are constant matrices of appropriate dimensions. The signals x, u, and y are called the state, input, and output of the system, respectively.

The *controllability Gramian* of the linear time-invariant system (2.1) is the $n \times n$ matrix defined by

$$\mathcal{W}_T(A, B) = \int_0^T e^{-A\sigma} B B^{\mathsf{T}} e^{-A^{\mathsf{T}}\sigma} \, d\sigma.$$

The controllability Gramian has widely been adopted as a quantitative measure of the degree of controllability of a dynamical system. In fact, the unique minimum-energy control that steers the system from the initial state $x(0) = x_0$ to the final state $x(T) = x_T$ at time

$T \in \mathbb{R}_{>0}$ is given by [30]

$$u(t) = -B^{\mathsf{T}} e^{A^{\mathsf{T}}(T-t)} \mathcal{W}_T^{-1}(A,B)(e^{AT}x_0 - x_T),$$

where $t \in [0,T]$. Hence, the controllability Gramian encodes the amount of energy needed to control a dynamical system to a certain final state. Examples of quantitative measure of controllability include the smallest eigenvalue of the controllability Gramian, the trace of its inverse, and its determinant [31].

Basic graph definitions. A directed graph $\mathcal{G} = (\mathcal{V}, \mathcal{L})$, consists of a set of vertices (or nodes) $\mathcal{V}$ and a set of directed edges (or links) $\mathcal{L} \subseteq \mathcal{V} \times \mathcal{V}$. We use the notation $\ell = (v,w)$ to denote a directed link from node $v \in \mathcal{V}$ to node $w \in \mathcal{V}$ and, for each node v, we let $v^{\text{out}} = \{(z,w) \in \mathcal{L} \ : \ z = v\}$ be the set of its outgoing links and $v^{\text{in}} = \{(w,z) \in \mathcal{L} \ : \ z = v\}$ the set of its incoming links. A path in $\mathcal{G}$ is a subgraph $p = (\{v_1, \ldots, v_k\}, \{\ell_1, \ldots, \ell_k\})$, such that $v_i \neq v_j$ for all $i \neq j$, and $\ell_i = (v_i, v_{i+1})$ for each $i \in \{1, \ldots, k-1\}$. We will say that a path starts at v_1 and ends at v_k. A path p is simple (or edge-disjoint) if no link is repeated in p. A cycle is a path where the first and last vertex are identical, i.e., $v_1 = v_k$. Finally, $\mathcal{G}$ is acyclic if it contains no cycles.

A weighted graph is a graph $\mathcal{G}$ where a scalar weight $a_{vw} \in \mathbb{R}$ is associated to each link $\ell = (v,w)$. In compact form, a weighted graph is described by an *adjacency matrix*, that is, a matrix whose entries are the edge weights $[A]_{vw} = a_{vw}$.

2.2 Basic Notions on Nonlinear Systems

In this brief section, we gather some preliminary results and basic concepts on nonlinear dynamical systems that are used throughout this dissertation. A continuous-time nonlinear time-invariant dynamical system is described by the equations

$$\begin{aligned} \dot{x} &= f(x, u), \\ y &= g(x, u), \end{aligned} \tag{2.2}$$

where $x \in \mathcal{X} \subseteq \mathbb{R}^n$, $u \in \mathcal{U} \subseteq \mathbb{R}^m$, $y \in \mathcal{Y} \subseteq \mathbb{R}^p$, are the state, input, and output of the system, respectively. We observe that this definition generalizes that of (2.1) by considering differential equations that do not necessarily satisfy the linearity property.

In the following, we summarize the basic definitions of equilibrium points.

- A point $x^* \in \mathcal{X}$ and an input $u^* \in \mathcal{U}$ are a *fixed point* (or equilibrium) of the dynamics (2.2) if, for the initial condition $x(0) = x^*$ and constant input $u(t) = u^*$ at all times,

$$f(x^*, u^*) = 0.$$

- A fixed point is *stable* if, for every $\epsilon > 0$ there exists $\delta > 0$ such that

$$\|x(0) - x^*\| < \delta \Rightarrow \|x(t) - x^*\| < \epsilon, \text{ for all } t \geq 0.$$

- A fixed point is *asymptotically stable* (or locally asymptotically stable) if it is stable and

$$\lim_{t \to +\infty} x(t) = x^*.$$

- A fixed point is *globally asymptotically stable* if it is stable and for every $x(0) \in \mathcal{X}$

$$\lim_{t \to \infty} x(t) = x^*.$$

- A fixed point is *unstable* if it is not stable.

The dynamical system (2.2) is *zero-state detectable* if $u(t) = 0$ and $y(t) = 0$ for all $t \geq 0$ implies $\lim_{t \to +\infty} x(t) = 0$.

Next, we recall some basic definitions and results on passivity in nonlinear dynamical systems that are instrumental for the analysis presented in Chapter 3. We begin by recalling the notions of passivity [32].

- The dynamical system (2.2) is *passive with respect to the input-output pair* (u, y) if there exists a differentiable function $V : \mathcal{X} \to \mathbb{R}_{\geq 0}$, called *storage function*, such that for all initial conditions $x(0) = x_0 \in \mathcal{X}$, for all allowed input functions $u \in \mathcal{U}$, and $t \geq 0$, the following inequality holds

$$V(x(t)) - V(x_0) \leq \int_0^t u(\sigma)^{\mathsf{T}} y(\sigma) d\sigma. \tag{2.3}$$

- A dynamical system is *input strictly passive* if there exists a function $\varphi : \mathcal{U} \to \mathbb{R}^m_{>0}$ such that $u^\mathsf{T}\varphi(u) > 0$ for all $u \neq 0$ and

$$V(x(t)) - V(x_0) \leq \int_0^t u(\sigma)^\mathsf{T} y(\sigma) - u(\sigma)^\mathsf{T}\varphi(u(\sigma))\ d\sigma.$$

- A dynamical system is *output strictly passive* if there exists a function $\rho : \mathcal{Y} \to \mathbb{R}^p_{>0}$ such that $y^\mathsf{T}\rho(y) > 0$ for all $y \neq 0$ and

$$V(x(t)) - V(x_0) \leq \int_0^t u(\sigma)^\mathsf{T} y(\sigma) - y(\sigma)^\mathsf{T}\rho(y(\sigma))\ d\sigma.$$

Loosely speaking, a system is passive if the increase in its storage function in the time interval $[0, t]$ (left hand side of (2.3)) is no larger than the energy supplied to the system during that interval (right hand side of (2.3)). Passivity is a useful tool to assess the Lyapunov stability of a feedback interconnection. The Passivity Theorem [32, Proposition 4.3.1], [33, Theorem 2.30] is summarized next.

Theorem 2.1. ***(Passivity Theorem)*** *Consider the pair of systems*

$$\begin{aligned} \dot{x}_i &= f(x_i, u_i), \\ y_i &= g_i(x_i, u_i), \qquad\qquad i \in \{1, 2\}, \end{aligned}$$

where $x_i \in \mathcal{X}_i \subseteq \mathbb{R}^n$, $u_i \in \mathcal{U}_i \subseteq \mathbb{R}^m$, $y_i \in \mathcal{Y}_i \subseteq \mathbb{R}^m$, and assume the two systems are coupled through a negative feedback interconnection, namely $u_2 = y_1$, $u_1 = -y_2$. Moreover, assume each system is passive with storage functions $V_i : \mathcal{X}_i \to \mathbb{R}_{\geq 0}$. Then,

(i) if V_1, V_2 have strict local minimum at x_1^*, x_2^*, then (x_1^*, x_2^*) is a stable fixed point of the negative feedback interconnection.

(ii) Assume V_1, V_2 have strict local minimum at x_1^*, x_2^*. Moreover, assume each system is zero-state detectable and input-strictly passive or output strictly passive, namely, each system admits a storage function that satisfies

$$V_i(x(t)) \; - \; V_i(x_0) \;\; \leq \;\; \int_0^t u_i(\sigma)^{\mathsf{T}} y_i(\sigma) \; - \; u_i(\sigma)^{\mathsf{T}} \varphi_i(u_i(\sigma)) \; - \; y_i(\sigma)^{\mathsf{T}} \rho_i(y_i(\sigma)) \;\; d\sigma.$$

for (possibly zero) functions $\varphi_i : \mathcal{U}_i \to \mathbb{R}^m_{\geq 0}$ and $\rho_i : \mathcal{U}_i \to \mathbb{R}^m_{\geq 0}$. If

$$\begin{aligned} &v^{\mathsf{T}} \varphi_1(v) + v^{\mathsf{T}} \rho_2(v) > 0, \;\; \textit{and} \\ &v^{\mathsf{T}} \varphi_2(v) + v^{\mathsf{T}} \rho_1(v) > 0, \end{aligned} \tag{2.4}$$

for all $v \neq 0$, then (x_1^*, x_2^*) is a locally asymptotically stable fixed point of the negative feedback interconnection.

Part I

Application to Traffic Control in Transportation Systems

Chapter 3

Changes in User Behavior: The Impact of Navigation Apps

Traffic networks are fundamental components of modern societies, making economic activity possible by enabling the transfer of passengers, goods, and services in a timely and reliable fashion. Despite their economical importance, traffic networks are impaired by the outstanding problem of traffic congestion, which wastes over 3 billions of gallons of fuel each year in the United States [16]. This chapter tackles the problem of reducing traffic congestion by studying the effects of navigation and routing apps on the robustness of modern traffic networks. We refer the reader to [1, 6] for an exhaustive discussion of the technical results contained in this chapter.

3.1 Introduction

In modern transportation systems, escalating levels of congestion are affecting nominal travel times of freeways and urban roads, incentivizing travelers to adopt alternative routes that are often undesirable and suboptimal. These route alternatives are increasingly made available through advanced traveler information systems, such as navigation apps (or routing apps), which provide reliable minimum-time routing suggestions to the travelers based on real-time congestion information. Yet, among numerous favorable advantages, routing apps can sometimes deteriorate traffic congestion and originate undesirable behaviors at the system level, a phenomenon that is studied here for the first time.

In this chapter, we focus on studying the impact of app-informed routing on the dynamical properties of the traffic infrastructure, and on characterizing the consequences of real-time traffic information on the stability of the traffic system. Differently from classical results on congestion-responsive traffic routing, the focus of this work is on the dynamical behavior of the transportation infrastructure, rather than on the economic properties of its equilibria. In particular, our models allow us to take into account the fact that travelers react instantaneously to changes in traffic congestion (other than from day to day), and to study the interplay between the rates of reaction to traffic information and the physical limitations of the traffic roads, such as capacities and delays in the propagation of flows. Our results show that the general adoption of navigation apps can maximize the throughput of flow across the network, and thus these devices bring valuable benefits to the traffic infrastructure. Unfortunately, our findings also demonstrate that navigation apps can deteriorate the stability of the traffic system, and can results in emerging undesirable

traffic phenomena such as temporal oscillations of traffic congestion. Hence, our results demonstrate that the benefits in the adoption of real-time routing systems come at the cost of increased system fragility, and suggest that adequate information design is necessary to overcome these limitations.

This work brings together two streams of independent literature. On the one hand, dynamical traffic network models have widely been studied after the popularization of the Cell Transmission Model [34]. In this line of research, the main emphasis has been on the development of accurate models that can capture the behavior of the network in several congestion regimes [35], and on characterizing the properties of the equilibria of the network [36], while considering simplified (often time-invariant) routing models.

On the other hand, the routing decisions of the travelers have been studied by adopting simplified traffic models in the game-theoretic setting of a routing game (see e.g. [19, 20, 17]). In these models, traffic flows propagate *instantaneously* across the network, and drivers make route choices by minimizing their personal travel times in response to day-to-day information regarding traffic congestion [21]. Recently, Evolutionary Game-Theory [37] has been applied to the routing game [38, 39], to capture not only the properties of the equilibria of the system, but also the time evolution of its trajectories. Although these works represent an important step towards understanding the dynamical properties of traffic networks under real-time congestion-responsive routing, the results have been limited to simplified traffic models and day-to-day driver behavior.

An important attempt to characterize the impact of congestion-dependent routing on the dynamical behavior of traffic are the recent works [40, 41], which are however limited

to routing models that are local, that is, where travelers make decisions based on one-road-ahead congestion information. Finally, to the best of the author's knowledge, the pioneering work [42] was one of the few attempts to highlight that simplifications in either the traffic model or the routing model are inadequate to accurately predict traffic patterns. In fact, the authors demonstrate through simulations that in certain regimes static flow model indicate that routing apps can improve network congestion, whereas dynamical models demonstrate the opposite.

The contribution of this work is fourfold. First, we propose a dynamical decision model to capture the routing behavior of app-informed travelers in response to traffic congestion. Our model is inspired from evolutionary models (or learning models) in biology and game theory, and models a setting where travelers make decisions iteratively and use the observations of other travelers to adjust their next decision. Moreover, our dynamical routing model can be naturally coupled with dynamical traffic models, and it allows us to effectively study the interplay between traffic congestion and routing behavior in time-varying congestion regimes.

Second, we study the properties of the fixed point of a traffic system where our routing decision model is coupled with a dynamical traffic model. We establish a connection between the properties of the equilibrium points and the well-established notion of Wardrop equilibria [21]. Our results show that, when travelers update their routing preferences at every junction of the network based on the instantaneous congestion information, the system admits an equilibrium point that satisfies the Wardrop First Principle. This observation extends Wardrop's practical observations, which were so far limited to scenarios where

travelers update their congestion information from day to day and the traffic system operates at equilibrium.

Third, we characterize the Lyapunov stability of the fixed points of the system. Our analysis relies on the theory of passive nonlinear dynamical systems [32], and it demonstrates that the open-loop dynamics of traffic models and the open-loop aggregate routing model satisfy the passivity property.

Fourth, we propose a control technique to ensure the asymptotic stability of the fixed points. Our methods rely on regulating the rates at which travelers react to congestion information, a behavior that can be achieved by appropriately designing the frequency at which navigation apps update the routing suggestions provided to the travelers. Our results suggest that, in order to achieve asymptotic stability of the equilibrium points, travelers that are close to the network origin must react faster to traffic congestion as opposed to travelers that are located in the proximity of the destination.

This chapter is organized as follows. Section 3.2 illustrates our traffic network model, our routing decision model, and reviews the Wardrop First Principle. Section 3.3 characterizes the properties of the equilibrium points, and contains a set of necessary and sufficient conditions for their existence. Section 3.4 contains the stability analysis of the equilibrium points, and illustrates through an example the existence of oscillatory trajectories. Section 3.5 proposes a control technique to ensure the asymptotic stability of the fixed points, and Section 3.6 illustrates our findings through a set of simulations.

3.2 Traffic Network and App Routing Models

This section is organized into three main parts. First, we discuss a traffic model that captures the physical characteristics of roads and traffic junctions. Second, we introduce a decision model to capture the routing behavior of app-informed travelers in response to traffic congestion. Third, we review the framework that describes the well-established Wardrop First Principle. We begin with some preliminary notation.

Notation. A directed graph $\mathcal{G} = (\mathcal{V}, \mathcal{L})$, consists of a set of vertices $\mathcal{V}$ and a set of directed links (or edges) $\mathcal{L} \subseteq \mathcal{V} \times \mathcal{V}$. We use the notation $\ell = (v, w)$ to denote a directed link from node $v \in \mathcal{V}$ to node $w \in \mathcal{V}$ and, for each node v, we let $v^{\text{out}} = \{(z, w) \in \mathcal{L} \ : \ z = v\}$ be the set of its outgoing links and $v^{\text{in}} = \{(w, z) \in \mathcal{L} \ : \ z = v\}$ be the set of its incoming links. A path in $\mathcal{G}$ is a subgraph $p = (\{v_1, \ldots, v_k\}, \{\ell_1, \ldots, \ell_k\})$, such that $v_i \neq v_j$ for all $i \neq j$, and $\ell_i = (v_i, v_{i+1})$ for each $i \in \{1, \ldots, k-1\}$. A path p is simple (or edge-disjoint) if no link is repeated in p. We will say that a path starts at v_1 and ends at v_k, and use the compact notation $p = p_{v_1 \to v_k}$. A cycle is a path where the first and last vertex are identical, i.e., $v_1 = v_k$. Finally, $\mathcal{G}$ is acyclic if it contains no cycles.

3.2.1 Traffic Network Model

We model a traffic network as a directed acyclic graph $\mathcal{G} = (\mathcal{V}, \mathcal{L})$, where $\mathcal{L} = \{1, \ldots n\} \subseteq \mathcal{V} \times \mathcal{V}$ models the set of traffic roads (or links), and $\mathcal{V} = \{v_1, \ldots, v_\nu\}$ models the set of traffic junctions (or nodes). Every traffic junction is composed of a set of ramps, each interconnecting a pair of freeways. We denote the set of traffic ramps (or adjacent links)

by $\mathcal{A} \subseteq \mathcal{L} \times \mathcal{L}$ and we let $\mathcal{A}_\ell$ be the set of ramps available upon exiting ℓ, that is,

$$\begin{aligned} \mathcal{A} &:= \{(\ell, m) \ : \ \exists \ v \in \mathcal{V} \text{ s.t. } \ell \in v^{\text{in}} \text{ and } m \in v^{\text{out}}\}, \\ \mathcal{A}_\ell &:= \{m \in \mathcal{L} \ : \ \exists (\ell, m) \in \mathcal{A}\}. \end{aligned} \tag{3.1}$$

We describe the macroscopic behavior of each link $\ell \in \mathcal{L}$ by means of a dynamical equation that captures the conservation of flows between upstream and downstream:

$$\dot{x}_\ell = f_\ell^{\text{in}}(x) - f_\ell^{\text{out}}(x_i),$$

where $x_\ell : \mathbb{R}_{\geq 0} \to \mathcal{X}$, $\mathcal{X} \subseteq \mathbb{R}_{\geq 0}$, is the traffic density in the link, $f_\ell^{\text{in}} : \mathcal{X} \to \mathcal{F}$, $\mathcal{F} \subseteq \mathbb{R}_{\geq 0}$, is the inflow of traffic at the link upstream, and $f_\ell^{\text{out}} : \mathcal{X} \to \mathcal{F}$ is the outflow of traffic at the link downstream. We make the following technical assumption.

(A1) For all $\ell \in \mathcal{L}$, $f_\ell^{\text{out}}(x_\ell) = 0$ only if $x_\ell = 0$. Moreover, f_ℓ^{out} is differentiable, non-decreasing, and upper bounded by the flow capacity of the link $C_\ell \in \mathbb{R}_{\geq 0}$:

$$\frac{d}{dx_\ell} f_\ell^{\text{out}}(x_\ell) \geq 0 \text{ and } \sup_{x_\ell} f_\ell^{\text{out}}(x_\ell) = C_\ell.$$

We discuss in the following remark possible choices of outflow functions commonly adopted in practice.

Example 3.1. ***(Common Link Outflow Functions)*** *A common choice for the link outflow function is the linear saturation function, originally adopted by the Cell Transmission*

Model [34], described by

$$f_\ell^{\text{out}}(x_\ell) = \min\{v_\ell x_\ell, C_\ell\},$$

where $v_\ell \in \mathbb{R}_{>0}$ models the free-flow speed of the link. Linear outflow functions have also been considered in the literature thanks to their simplicity [4]:

$$f_\ell^{\text{out}}(x_\ell) = v_\ell x_\ell,$$

where, in this case, $C_\ell = +\infty$. Alternatively, exponential saturation functions have widely been adopted in the recent literature (see e.g. [36]):

$$f_\ell^{\text{out}}(x_\ell) = C_\ell(1 - \exp(a_\ell x_\ell)),$$

where $a_\ell \in (0, \infty)$. □

We associate a routing ratio $r_{\ell m} \in [0, 1]$ to every pair of adjacent links $(\ell, m) \in \mathcal{A}$ to describe the fraction of traffic flow entering link m upon exiting ℓ, with $\sum_m r_{\ell m} = 1$. We combine the routing ratios into a matrix $R = [r_{\ell m}] \in \mathbb{R}^{n \times n}$, where we let $r_{\ell m} = 0$ if ℓ and m are not adjacent $(\ell, m) \notin \mathcal{A}$, and we denote by $\mathcal{R}_\mathcal{G}$ the set of feasible routing ratios for the network defined by $\mathcal{G}$. That is,

$$\mathcal{R}_\mathcal{G} := \{r_{\ell m} : r_{\ell m} = 0 \text{ if } (\ell, m) \notin \mathcal{A}, \text{ and } \sum_{m \in \mathcal{L}} r_{\ell m} = 1\}.$$

At every ramp, traffic flows are transferred from the incoming link to the outgoing link as described by the routing ratios:

$$f_m^{\text{in}}(x) = \sum_{\ell \in \mathcal{L}} r_{\ell m} f_\ell^{\text{out}}(x_\ell).$$

We focus on single-commodity networks, where an inflow of vehicles $\bar{\lambda} : \mathbb{R}_{\geq 0} \to \mathcal{F}$ enters the network at a (unique) source link $s \in \mathcal{L}$, and traffic flows exit the network at a (unique) destination link $d \in \mathcal{L}$. In the remainder, we adopt the convention $s = 1$ and $d = n$. We describe the overall network dynamics by combining the dynamical models of all links in a vector equation of the form

$$\dot{x} = (R^{\mathsf{T}} - I) f(x) + \lambda, \tag{3.2}$$

where $I \in \mathbb{R}^{n \times n}$ denotes the identity matrix, $x = [x_1, \ldots, x_n]^{\mathsf{T}}$ is the vector of traffic densities in the links, $f = [f_1^{\text{out}}, \ldots, f_n^{\text{out}}]^{\mathsf{T}}$ is the vector of link outflows, and $\lambda = [\bar{\lambda}, \ldots, 0]^{\mathsf{T}}$ denotes the inflow vector. Finally, we illustrate our model of traffic network in Example 3.2, and we discuss the relationship between our model and the well-established Cell Transmission Model in Remark 3.3.

Example 3.2. ***(Dynamical Traffic Model)*** *Consider the seven-link network illustrated in Fig. 3.1. The traffic network model* (5.6) *is composed of the following seven dynamical*

equations:

$$\dot{x}_1 = -f_1^{\text{out}}(x_1) + \bar{\lambda},$$

$$\dot{x}_2 = -f_2^{\text{out}}(x_2) + r_{12} f_1^{\text{out}}(x_1),$$

$$\dot{x}_3 = -f_3^{\text{out}}(x_3) + r_{13} f_1^{\text{out}}(x_1),$$

$$\dot{x}_4 = -f_4^{\text{out}}(x_4) + r_{24} f_2^{\text{out}}(x_2),$$

$$\dot{x}_5 = -f_5^{\text{out}}(x_5) + r_{25} f_2^{\text{out}}(x_2),$$

$$\dot{x}_6 = -f_6^{\text{out}}(x_6) + f_3^{\text{out}}(x_3) + f_4^{\text{out}}(x_4),$$

$$\dot{x}_7 = -f_7^{\text{out}}(x_7) + f_5^{\text{out}}(x_5) + f_6^{\text{out}}(x_6),$$

where

$$\mathcal{R}_{\mathcal{G}} = \{r_{12}, r_{13}, r_{24}, r_{25} \ : \ r_{12} + r_{13} = 1, r_{24} + r_{25} = 1\}.$$

□

Remark 3.3. ***(Capturing Backwards Propagation)*** *Our model can be interpreted as a simplified version of the Cell Transmission Model [34]. In fact, while in the Cell Transmission Model highways are characterized by two fundamental functions (a link demand function and a link supply function), our model only captures capacities in the flows through the link outflow functions f_ℓ^{out}. As a result, in our model density accumulation can happen on the links and congestion does not propagate through the junctions (and thus corresponds to a vertical queue model). While more general traffic models could be considered in future*

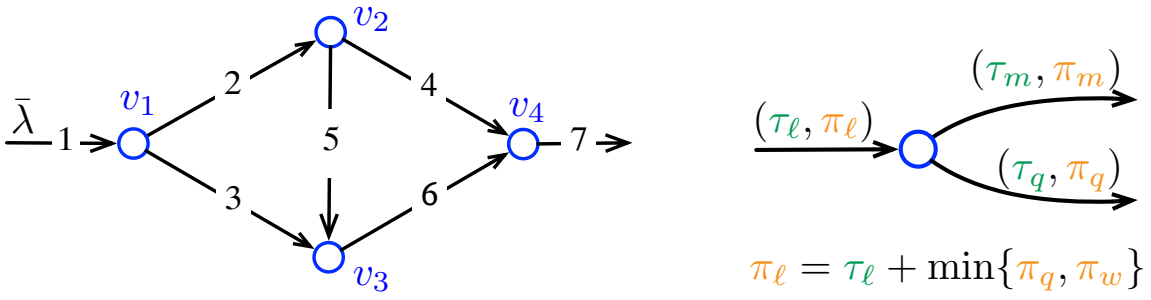

(a) (b)

Figure 3.1: (a) Seven-highway network discussed in examples 3.2 and 3.6. (b) We associate two variables to each link: the link travel cost τ_ℓ (the travel time to traverse that link) and the link perceived cost π_ℓ (the total travel cost of reaching the network destination from that link).

works, we note that density capacities can be captured in our model by considering unbounded link delay functions, as we do in Section 3.3.3. □

3.2.2 Congestion-Responsive Routing Model

In what follows, we present a dynamical decision model to capture the behavior of app-informed travelers in response to congestion. To this aim, we associate a state-dependent travel cost to each link of the network

$$\tau_\ell : \mathcal{X} \to \mathcal{T}, \mathcal{T} \subseteq \mathbb{R}_{\geq 0},$$

which describes the instantaneous travel cost (or travel delay) of traversing link ℓ. We denote by $\tau(x) = [\tau_1, \ldots, \tau_n]^\mathsf{T}$ the joint vector of travel costs, and we make the following technical assumption.

(A2) For all $\ell \in \mathcal{L}$, the travel cost $\tau_\ell(x_\ell)$ is differentiable and non-decreasing.

To capture the fact that travelers wish to minimize the overall (total) travel time between their current location and their destination, we associate to each link ℓ a perceived cost:

$$\pi_\ell : \mathcal{X}^n \to \mathcal{T},$$

which describes the cost of link ℓ that is *perceived* by the travelers. The perceived cost is a quantity that, in general, includes the combined cost of traversing multiple links (e.g. a path in the graph). In this work, we model the perceived costs as the instantaneous minimum travel times to destination (see Fig. 3.1(b))

$$\pi_\ell(x) = \tau_\ell(x_\ell) + \min_{m \in \mathcal{A}_\ell} \pi_m(x). \tag{3.3}$$

We note that the above equation is a recursive definition, and: (i) given the current traffic state, the set of perceived costs can be computed backwards from the network destination to every link in the graph, and (ii) the above equation states that a traveler located at any point in the traffic network perceives a cost that is equal to the instantaneous minimum travel time to destination. We discuss and generalize the choice of perceived costs in Remark 3.4.

Remark 3.4. ***(Choices of Perceived Costs)*** *A choice that generalizes* (3.3) *is the following convex combination:*

$$\pi_\ell(x) = \alpha_\ell \tau_\ell(x_\ell) + (1 - \alpha_\ell) \min_{m \in \mathcal{A}_\ell} \pi_m(x),$$

where $\alpha_\ell \in [0,1]$ *is a parameter that describes the level of confidence in the observed global congestion information. For instance, the special case* $\alpha_\ell = 1$ *correspond to a situation where the drivers rely only local congestion information, while* $\alpha_\ell = 0$ *models a scenario where drivers rely on global congestion information, which is the focus of this work. An intermediate value of* α_ℓ *can be interpreted as the level of confidence in the knowledge of the travel delay of links that are distant in the network. Although all the results presented in this chapter hold for the generalized perceived cost model, in the remainder of this chapter we focus on the model* (3.3) *for the clarity of illustration.* □

To model the reactions of app-informed travelers to changes in the traffic state, we assume that at every node of the network drivers will instantaneously update their routing by increasingly avoiding the links with higher perceived cost (in the current congestion regime). To this aim, we model the aggregate routing ratios as time-varying quantities $r_{\ell m} : \mathbb{R}_{\geq 0} \to [0,1]$ that obey a selection mechanism inspired by the replicator dynamics [37]:

$$\delta_{\ell m}^{-1} \dot{r}_{\ell m} = r_{\ell m} \underbrace{(\sum_q r_{\ell q} \pi_q - \pi_m)}_{a_{\ell m}(x)}, \tag{3.4}$$

where $a_{\ell m} : \mathcal{X}^n \to \mathbb{R}$ is a function that describes the appeal of entering link m upon exiting ℓ, and $\delta_{\ell m} \in \mathbb{R}_{>0}$ is the reaction rate, namely a scalar variable that captures the rate at which travelers react to changes in the traffic state.

The dynamical equation (3.4) describes a real-time reaction mechanism, where routing apps continuously revise their routing recommendations by increasingly suggesting

links that have a more desirable travel time to destination, as detailed next. A positive appeal ($a_{\ell m} > 0$) implies that the perceived travel cost of link m is preferable over the travel cost of alternative links upon exiting ℓ (i.e. $\pi_m < \sum_q r_{\ell q}\pi_q$). Hence, equation (3.4) states that the fraction of travelers choosing m will increase over time ($\dot{r}_{\ell m} > 0$). As a result, the appeal $a_{\ell m}$ can be interpreted as the aggregate interest in selecting to traverse link m upon exiting ℓ.

In compact form, the set of dynamical equations (3.4) describing the routing parameters reads as follows:

$$\dot{r} = \varrho(r, \pi), \tag{3.5}$$

where $r = [\dots, r_{\ell m}, \dots]^{\mathsf{T}}$, $(\ell, m) \in \mathcal{A}$, denotes the joint vector of routing ratios. In the following result, we show that the congestion-responsive routing model (3.5) evolves within the feasible set of routing ratios $\mathcal{R}_{\mathcal{G}}$ at all times.

Lemma 3.5. ***(Conservation of Flows)*** *Let $\mathcal{G}$ be a traffic network and let $\delta_{\ell m} = \delta_\ell \in \mathbb{R}_{>0}$ for all $(\ell, m) \in \mathcal{A}$. If $r(0) \in \mathcal{R}_{\mathcal{G}}$, then the vector of routing ratios is feasible at all times, that is,*

$$r \in \mathcal{R}_{\mathcal{G}} \text{ for all } t \in \mathbb{R}_{>0}.$$

Proof. The proof of this claim is organized into two parts. First, we show that $r_{\ell m} \in [0, 1]$. To show that the routing ratios are non-negative, $r_{\ell m} \geq 0$, we note that

$$r_{\ell m} = 0 \Rightarrow \dot{r}_{\ell m} = r_{\ell m} a_{\ell m}(x) = 0.$$

To show that the routing ratios are upper bounded, $r_{\ell m} \leq 1$, assume the ratio achieves the boundary, i.e. $r_{\ell m} = 1$. Then, since $r \in \mathcal{R}_{\mathcal{G}}$ (i.e., $\sum_q r_{\ell q} = 1$), we have

$$r_{\ell q} = 0 \text{ for all } q \neq m,$$

which implies

$$a_{\ell m}(x) = \sum_q r_{\ell q} \pi_q - \pi_m = r_{\ell m} \pi_m - \pi_m = 0.$$

Hence, the above observations prove the following implication

$$r_{\ell m} = 1 \Rightarrow \dot{r}_{\ell m} = r_{\ell m} a_{\ell m}(x) = 0,$$

which shows that the routing ratios are bounded in $[0, 1]$.

Second, we prove that $\sum_m r_{\ell m} = 1$. To this aim, we equivalently show that $\sum_m \dot{r}_{\ell m} = 0$. By substituting the expression (3.4) in the summation term we obtain

$$\begin{aligned}\sum_m \dot{r}_{\ell m} &= \sum_m r_{\ell m}(\sum_q r_{\ell q}\pi_q - \pi_m) \\ &= \underbrace{\sum_m r_{\ell m}}_{=1} \sum_q r_{\ell q}\pi_q - \sum_m r_{\ell m}\pi_m \\ &= \sum_q r_{\ell q}\pi_q - \sum_m r_{\ell m}\pi_m = 0,\end{aligned}$$

which shows the claim and concludes the proof. ■

We conclude this discussion by illustrating in Example 3.6 our routing model, by discussing in Remark 3.7 the use of the replicator equation to model routing apps, and by clarifying in Remark 3.8 the novelty of our framework with respect to the classical routing game.

Example 3.6. ***(Dynamical Routing Model)*** *Consider the seven-link network illustrated in Fig. 3.1 and discussed in Example 3.2. By assuming that the drivers perceive the global*

cost to destination (3.3)*, the perceived costs read as*

$$
\begin{aligned}
\pi_1 &= \tau_1 + \bar{\pi}_{v_1 \to d}, & \bar{\pi}_{v_1 \to d} &= \min\{\pi_2, \pi_3\},\\
\pi_2 &= \tau_2 + \bar{\pi}_{v_2 \to d}, & \bar{\pi}_{v_2 \to d} &= \min\{\pi_4, \pi_5\},\\
\pi_3 &= \tau_3 + \bar{\pi}_{v_3 \to d}, & \bar{\pi}_{v_3 \to d} &= \pi_6,\\
\pi_4 &= \tau_4 + \bar{\pi}_{v_3 \to d}, & &\\
\pi_5 &= \tau_5 + \bar{\pi}_{v_4 \to d}, & \bar{\pi}_{v_4 \to d} &= \pi_7,\\
\pi_6 &= \tau_6 + \bar{\pi}_{v_4 \to d}, & &\\
\pi_7 &= \tau_7. & &
\end{aligned}
$$

We note that the perceived costs (3.3) *are defined in a recursive way, where for all* $i \in \{1, \dots, 7\}$*,* π_i *can be computed given* $\pi_{i+1}, \dots, \pi_7$ *. Moreover, the aggregate behavior of the population at the nodes is described as in* (3.4) *by*

$$
\begin{aligned}
\dot{r}_{12} &= r_{12}((r_{12} - 1)\pi_2 + r_{13}\pi_3),\\
\dot{r}_{13} &= r_{13}((r_{13} - 1)\pi_3 + r_{12}\pi_2),\\
\dot{r}_{24} &= r_{24}((r_{24} - 1)\pi_4 + r_{25}\pi_5),\\
\dot{r}_{25} &= r_{25}((r_{25} - 1)\pi_5 + r_{24}\pi_4).
\end{aligned}
$$

Finally, we note that Lemma 3.5 ensures $r_{12} + r_{13} = 1$ *and* $r_{24} + r_{25} = 1$ *at all times.* □

Remark 3.7. ***(Modeling Aggregate Learning Through Replicator Equation)*** *The replicator equation was originally developed to study selection in biological evolution. How-*

ever, it was found recently in [43] (see also references therein) that the evolutionary replicator dynamics can also arise from certain models of human learning. Moreover, in a more recent work [44] it was shown that if models of reinforcement learning or other machine learning techniques were aggregated over a large population, the resulting behavior would possess the same qualitative properties as the replicator dynamics. □

Remark 3.8. ***(Relationship to Routing Game)*** *A trend of literature (e.g. see [38, 39]) recently combined the classical routing game with evolutionary models in order to capture dynamics in the path-selection mechanism of new drivers entering the network. Although these works represent a significant step towards understanding the dynamics of traffic routing, they still critically rely on a static flow model, where traffic flows instantaneously propagate across the network. Unfortunately, this assumption lacks to capture the fact that traffic conditions can change while travelers are traversing the network, and that navigation apps will instantaneously respond by updating the route of each driver at her next available junction. To overcome these limitations, our framework (i) leverages a dynamical traffic model that captures finite flow propagation times, and (ii) includes a junction-based routing model where travelers can update their routing behavior at every node of the network in relationship to the current congestion information.* □

3.2.3 The Wardrop First Principle

The goal of this section is to establish a connection between the classical game-theoretic setting and our framework. The routing game [21] consists of a static (time-invariant) traffic model combined with a path-selection model. In this decision model, a

new traveler entering the network selects a certain origin-destination path based on the instantaneous traffic congestion and, because the traffic model is static, drivers do not update their path while they are traversing the network. Once this path-selection mechanism terminates, the network is at an equilibrium point known as the Wardrop Equilibrium, a condition where all the used paths have identical travel time.

Next, we recall the notion Wardrop Equilibrium. To comply with the static nature of the routing game, we will assume that the dynamical system (3.7) is at an equilibrium point. Let x^* be an equilibrium of (5.6), and let

$$f_\ell^* := f_\ell^{\text{out}}(x_\ell^*), \qquad \ell \in \mathcal{L},$$

be the set of equilibrium flows on the links. In vector form, $f^* := [f_1^* \dots, f_n^*]^\mathsf{T}$. Moreover, let $\mathcal{P} = \{p_1, \dots, p_\zeta\}$, $\zeta \in \mathbb{N}$, be the set of simple paths between origin and destination, and let $f_p^* := [f_{p_1}^*, \dots, f_{p_\zeta}^*]^\mathsf{T}$ be the set of flows on the paths. The flows on the origin-destination paths are related to the flows on the links by means of the following relationship:

$$f_\ell^* = \sum_{p \in \mathcal{P} : \ell \in p} f_p^*,$$

which establishes that the flow on each link is the superposition of all the flows in the paths passing through that link. By inverting the above set of equations, the vector of path flows can be computed from the vector of link flows as follows

$$f_p^* = E^\dagger f^*, \tag{3.6}$$

where $E \in \mathbb{R}^{n \times \nu}$ is the edge-path incidence matrix:

$$E_{\ell p} = \begin{cases} 1, & \text{if } \ell \in p, \\ 0, & \text{otherwise,} \end{cases}$$

where $E^{\dagger}$ denotes the pseudoinverse of E. Lemma 3.9 shows that the path flows are unique for any choice of link flows.

Lemma 3.9. ***(Uniqueness of the Path Flow Vectors)*** *Let $\mathcal{G}$ be acyclic. Then, for every vector of link flows $f^* \in \mathcal{F}^n$ there exists a unique vector of path flows $f_p^* \in \mathbb{R}^{\zeta}$ that solves* (3.6)*.*

We extend the definition of travel costs to the origin-destination paths by letting the travel cost of a path be the sum of the cost of all the links in that path, namely,

$$\tau_p^* := E^{\mathsf{T}} \tau(x^*).$$

The Wardrop First Principle states that all paths with nonzero flow have identical travel cost, and is formalized next.

Definition 3.10. **(*Wardrop First Principle*)** *Let x^* be an equilibrium of* (5.6)*. The vector x^* is a Wardrop Equilibrium if the following condition is satisfied for all origin-destination paths $p \in \mathcal{P}$:*

$$f_p^*(\tau_p^* - \tau_{\bar{p}}^*) \leq 0, \ \textit{for all } \bar{p} \in \mathcal{P}.$$

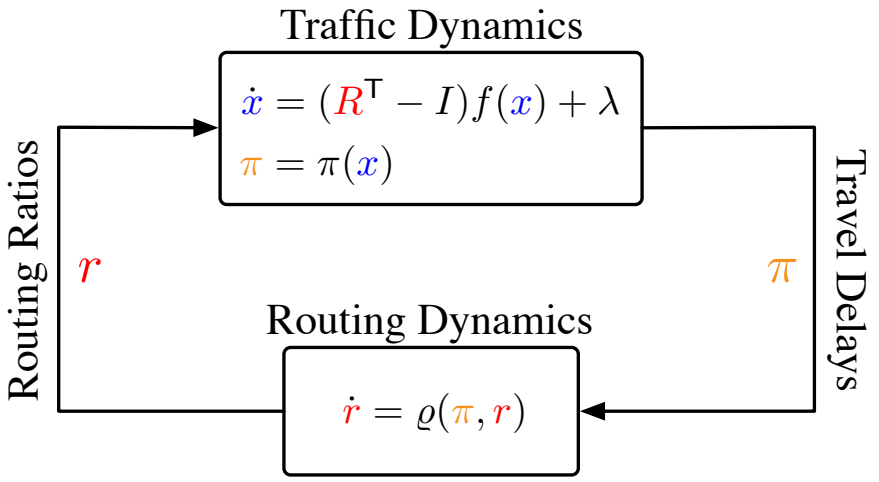

Figure 3.2: Feedback interconnection between traffic and routing dynamics.

3.3 Existence and Properties of the Equilibria

In this section, we characterize the properties of the fixed points of dynamical traffic networks with app-informed routing. Formally, we are interested in characterizing the fixed points of the feedback interconnection between the traffic dynamics (5.6) and the routing dynamics (3.5), which reads as:

$$\begin{aligned} \dot{x} &= (R^\mathsf{T} - I)f(x) + \lambda, & \pi &= \pi(x), \\ \dot{r} &= \varrho(r, \pi). \end{aligned} \tag{3.7}$$

Fig. 3.2 graphically illustrates the interactions between the two systems and depicts the quantities that establish the coupling.

3.3.1 Restricted Set of Equilibria

Let (x^*, r^*) be a fixed point of (3.7). It follows from the expressions of the routing model (3.4) that, for all pairs of adjacent links $(\ell, m) \in \mathcal{A}$, one of the following conditions is satisfied at equilibrium:

$$a_{\ell m}(x^*) = 0, \text{ or } r^*_{\ell m} = 0.$$

We next show that a subset of these points is unstable.

Lemma 3.11. ***(Unstable Equilibria)*** *Let (x^*, r^*) be a fixed point of (3.7) and assume there exists $(\ell, m) \in \mathcal{A}$ such that*

$$r^*_{\ell m} = 0, \text{ and } a_{\ell m}(x^*) > 0.$$

Then, (x^*, r^*) is unstable.

Proof. To prove this lemma, we adopt a perturbation reasoning and show that there exists an infinitesimally-small perturbation from the equilibrium such that $\dot{r}_{\ell m} > 0$. The proof is organized into two main parts.

First, we show that at equilibrium all links alternative to m have identical perceived cost. To this aim, we note that $r^*_{\ell m} = 0$ combined with $r^* \in \mathcal{R}_{\mathcal{G}}$ (i.e. $\sum_q r^*_{\ell q} = 1$) implies that there exists (at least) one alternative link w such that $r^*_{\ell w} > 0$. In general, let $\mathcal{W} = \{w_1, \ldots, w_\xi\}$, $\xi \in \mathbb{N}$, denote the set of all such links. Since $r^*_{\ell w_i} > 0$ and x^* is an

equilibrium, we necessarily have $a_{\ell w_i}(x^*) = 0$ or, equivalently,

$$0 = a_{\ell w_i}(x^*) = \sum_q r^*_{\ell q}\pi^*_q - \pi^*_{w_i},$$

for all $i \in \{1, \dots, \xi\}$. The above system of equations admits the explicit solution $\pi^*_{w_i} = \sum_q r^*_{\ell q}\pi^*_q$ for all $i \in \{1, \dots, \xi\}$, which implies

$$\pi^*_{w_i} = \pi^*_{w_j}, \text{ for all } i, j \in \{1, \dots, \xi\}, \tag{3.8}$$

and proves the first claim.

Second, we show that at equilibrium all links alternative to m (i.e. links $w \in \mathcal{W}$), have strictly suboptimal travel cost: $\pi^*_w > \pi^*_m$. To this aim, we use the assumption $a_{\ell m}(x^*) > 0$ to obtain

$$\begin{aligned} 0 < a_{\ell m}(x^*) &= \sum_q r^*_{\ell q}\pi^*_q - \pi^*_m \\ &= \pi^*_w \sum_q r^*_{\ell q} - \pi^*_m \\ &= \pi^*_w - \pi^*_m, \end{aligned} \tag{3.9}$$

where we substituted (3.4) to obtain the first identity, and (3.8) to obtain the second identity, which proves the second claim.

Finally, let $\epsilon \in \mathbb{R}_{>0}$ be a scalar perturbation. By perturbing (3.4) from the equilibrium point, $r^*_{\ell m} \mapsto r^*_{\ell m} + \epsilon$, we have

$$\begin{aligned}
\dot{r}_{\ell m} &= \epsilon\Big(\sum_{q \neq m,w} r^*_{\ell q}\pi^*_q + (r^*_{\ell m} + \epsilon)\pi^*_m + (r^*_{\ell w} - \epsilon)\pi^*_w - \pi^*_m \Big) \\
&= \epsilon\Big(\sum_{q} r^*_{\ell q}\pi^*_q + \epsilon\pi^*_m - \epsilon\pi^*_w - \pi^*_m\Big) \\
&= \epsilon\Big(\pi^*_w \underbrace{\sum_{q} r^*_{\ell q}}_{=1} + \epsilon\pi^*_m - \epsilon\pi^*_w - \pi^*_m\Big) \\
&= \epsilon(\pi^*_w + \epsilon\pi^*_m - \epsilon\pi^*_w - \pi^*_m) \\
&= \epsilon(\pi^*_w - \pi^*_m)(1 - \epsilon) > 0,
\end{aligned}$$

where we used (3.8) to obtain the third identity, and the final inequality follows from (3.9) and from $\epsilon > 0$. The conclusion follows by observing that infinitely-small perturbations $\epsilon \to 0$ result in systems that depart from the equilibria $\dot{r}_{\ell m} > 0$. ■

Lemma 3.5 shows that equilibrium points where at least one of the links has a positive appeal function are unstable. Such scenarios can be interpreted in practice as a situation where there exists a link in the network with a preferable travel time to destination (i.e. $a_{\ell m} > 0$), but no driver is currently traversing that road (i.e. $r_{\ell m} = 0$). Hence, the navigation app lacks of sufficient observations from other travelers to begin routing vehicles towards that road, thus making the routing algorithm ignore the availability of such option.

In order to disregard the unstable equilibria from the discussion, in the remainder we focus on the equilibria (x^*, r^*) such that, for all $(\ell, m) \in \mathcal{A}$, satisfy:

$$a_{\ell m}(x^*) = 0, \text{ or } r_{\ell m} = 0 \text{ and } a_{\ell m}(x^*) < 0. \tag{3.10}$$

Remark 3.12. ***(Relationship to Game Dynamics)*** *The set of equilibria defined in* (3.10) *is often interpreted in the game-theoretic literature as the set of Nash Equilibria of the game dynamics* (3.4) *(see e.g. [45]). It is worth noting that Lemma 3.5 extends the available results in this line of literature (e.g. see the Folk Theorem of evolutionary game theory [37] and the specific conclusions drawn for the routing game by Fischer and Vöcking [38]), by showing that the set of rest points that are not Nash equilibria are unstable for replicator equations where the payoffs do not depend directly from the strategy.* □

3.3.2 Existence of Equilibria

Next, we characterize the existence of fixed points of the interconnected system (3.7). Our result relies on the following technical assumption.

(A3) The link travel costs are finite, namely, for all $\ell \in \mathcal{L}$

$$\tau_\ell(x_\ell) < \infty \text{ if } x_\ell < \infty.$$

Assumption (A3) disregards cases where travel times are unbounded, and will be relaxed later in this section.

Next, we recall the graph-theoretic notion of min-cut capacity [46]. Let the set of nodes $\mathcal{V}$ be partitioned into two subsets $\mathcal{S} \subseteq \mathcal{V}$ and $\bar{\mathcal{S}} = \mathcal{V} - \mathcal{S}$, such that the network source $s \in \mathcal{S}$ and the network destination $d \in \bar{\mathcal{S}}$. Let $\mathcal{S}^{\text{out}} = \{(v,u) \in \mathcal{L} \ : \ v \in \mathcal{S} \text{ and } u \in \bar{\mathcal{S}}\}$ be a cut, namely, the set of all links from $\mathcal{S}$ to $\bar{\mathcal{S}}$, and let $C_{\mathcal{S}} = \sum_{\ell \in \mathcal{S}^{\text{out}}} C_\ell$ be the capacity of the cut. The min-cut capacity is defined as

$$C_{\text{m-cut}} = \min_{\mathcal{S}} C_{\mathcal{S}}.$$

The following result relates the existence of fixed points to the magnitude of the exogenous inflow to the network.

Theorem 3.13. ***(Existence of Equilibria)*** *Let Assumptions (A1)-(A3) be satisfied. The interconnected system* (3.7) *admits an equilibrium point that satisfies* (3.10) *if and only if the network inflow is no larger than the min-cut capacity:*

$$\bar{\lambda} \leq C_{\text{m-cut}}. \tag{3.11}$$

Proof. (If) The proof is organized into two main parts.

First, we show that, when $\bar{\lambda} \leq C_{\text{m-cut}}$, there exists a pair (x^*, r^*) that is an equilibrium point of the traffic dynamics with finite perceived travel costs, that is,

$$(R^{*\mathsf{T}} - I) f(x^*) + \lambda = 0, \text{ and } \pi(x^*) < \infty.$$

To this aim, consider the graph $\mathcal{G}$ with associated inflow $\bar{\lambda}$. By application of the max-flow min-cut theorem [46], there exists a feasible assignment of flows to the links of the graph $\mathcal{G}$, that is, a set of scalars $\{\varphi_1, \dots, \varphi_n\}$ such that the following conditions are satisfied:

$$
\begin{aligned}
&0 \leq \varphi_\ell \leq C_\ell, && \text{for all } \ell \in \mathcal{L}, \\
&\sum_{\ell \in v^{\text{in}}} \varphi_\ell = \sum_{\ell \in v^{\text{out}}} \varphi_\ell, && \text{for all } v \in \mathcal{V}, \\
&\varphi_1 = \bar{\lambda}.
\end{aligned}
$$

By choosing $r^*_{\ell m} := \varphi_m / \varphi_\ell$ for all $(\ell, m) \in \mathcal{A}$, the above equations imply that

$$
(R^{*\mathsf{T}} - I)\varphi + \lambda = 0,
$$

where $\varphi = [\varphi_1 \dots, \varphi_n]^{\mathsf{T}}$. Finally, by choosing x^*_ℓ so that $f^{\text{out}}(x^*_\ell) = \varphi_\ell$, we have that (x^*, r^*) is a fixed point of the traffic dynamics (5.6), which proves the first claim.

Second, we show that for any traffic state $x^* \in \mathcal{X}$ with finite perceived costs, $\pi(x^*) < \infty$, there exists a vector of feasible routing ratios r^* that is a fixed point of the routing dynamics and satisfies (3.10). To this aim, we first consider a given link $\ell \in \mathcal{L}$ and we prove the claim for the single junction equation (3.4). The statement will then follow by iterating the reasoning for all $\ell \in \mathcal{L}$. We distinguish among two cases.

(Case 1) For all pairs $a, \bar{a} \in \mathcal{A}_\ell$, where $a = (\ell, m)$ and $\bar{a} = (\ell, \bar{m})$, the costs satisfy $\pi_m(x^*) = \pi_{\bar{m}}(x^*)$. In this case, the following identity holds:

$$\begin{aligned}
\dot{r}^*_{\ell m} &= r^*_{\ell m}(\sum_q r^*_{\ell q}\pi^*_q - \pi^*_m) \\
&= r^*_{\ell m}(\pi^*_m \underbrace{\sum_q r^*_{\ell q}}_{=1} - \pi^*_m) \\
&= r^*_{\ell m} \underbrace{(\pi^*_m - \pi^*_m)}_{a_{\ell m}(x^*)} = 0,
\end{aligned}$$

which shows that $\dot{r}^*_{\ell m} = 0$ and $a^*_{\ell m} = 0$, and proves that (x^*, r^*) is an equilibrium point that satisfies (3.10).

(Case 2) There exists $a, \bar{a} \in \mathcal{A}_\ell$, where $a = (\ell, m)$ and $\bar{a} = (\ell, \bar{m})$, such that the costs satisfy $\pi_m \neq \pi_{\bar{m}}$. In this case, let

$$\pi_{\bar{m}} = \max_{a=(\ell,m)\in\mathcal{A}_\ell} \pi_m,$$

be the largest perceived cost at the junction. By letting $r^*_{\ell\bar{m}} = 1$ and $r^*_{\ell m} = 0$ for all $m \neq \bar{m}$ we obtain the following identities

$$\begin{aligned}
\dot{r}^*_{\ell\bar{m}} &= r^*_{\ell\bar{m}}(\sum_q r^*_{\ell q}\pi^*_q - \pi^*_{\bar{m}}) = (\pi^*_{\bar{m}} - \pi^*_{\bar{m}}) = 0, \\
\dot{r}^*_{\ell m} &= r^*_{\ell m}(\sum_q r^*_{\ell q}\pi^*_q - \pi^*_m) = 0,
\end{aligned}$$

which shows that the provided choice of r^* is a fixed point of (3.4). Moreover, the above identities also imply

$$a_{\ell\bar{m}}(x^*) = (\pi^*_{\bar{m}} - \pi^*_{\bar{m}}) = 0,$$

$$a_{\ell m}(x^*) = (\pi^*_{\bar{m}} - \pi^*_{m}) > 0,$$

which shows that the equilibrium point satisfies (3.10).

The conclusion thus follows by combining the two parts of the proof. In fact, when $\bar{\lambda} \leq C_{\text{m-cut}}$ the first part shows that the traffic dynamics admit an equilibrium with finite perceived costs for *some* choice of the routing. The second part of the proof guarantees that the routing dynamics admit an equilibrium for *any* traffic state with finite travel costs.

(Only if) The proof of this statement follows by adopting a contradiction reasoning. To this aim, assume (x^*, r^*) is an equilibrium point and that $\bar{\lambda} > C_{\text{m-cut}}$. The latter assumption, combined with the Maximum Flow Theorem, implies that for any assignment of flows to the links of the graph $\mathcal{G}$ there exists $\ell \in \mathcal{L}$ such that $\varphi_\ell > C_\ell$. In other words, link ℓ is required to transfer a traffic flow $f^{\text{in}}_\ell(x^*) = \varphi_\ell$, and thus:

$$\begin{aligned}\dot{x}_\ell &= f^{\text{in}}_\ell(x^*) - f^{\text{out}}_\ell(x^*_\ell) \\ &= \varphi_\ell - f^{\text{out}}_\ell(x^*_\ell) \\ &\geq \varphi_\ell - C_\ell > 0,\end{aligned}$$

which shows shows that x_ℓ grows unbounded, and hence contradicts the assumption that (x^*, r^*) is an equilibrium. ■

The above theorem bridges an interesting gap between the behavior of dynamical systems and graph-theoretic notions. In fact, it relates the properties of the equilibrium points of a dynamical system with the notion of minimum-cut capacity, which is a feature of static graphs. Two important implications follow from Theorem 3.13. First, by recalling that the minimum-cut capacity equals the maximum flow through a graph (see Maximum-Flow Theorem [46]), the result shows that a dynamical traffic network admits an equilibrium point that transfers a traffic demand equal to the maximum flow. This observation demonstrates that routing apps not only optimize the travelers' commute, but also have a benefit at the system-level. Second, the result shows that when the traffic demand is too large ($\bar{\lambda} > C_{\text{m-cut}}$), then the network does not admit any equilibrium equilibrium point, in fact, it operates at a condition in which traffic densities in the links grow unbounded.

We conclude this section by discussing a special technical assumption that can be used to capture back propagation of traffic congestion, a scenario that is particularly relevant in practice. To this aim, we introduce the following assumption.

(A4) For all $\ell \in \mathcal{L}$, the travel cost becomes unbounded when ℓ reaches its flow capacity, namely,

$$\tau_\ell(x_\ell) = \infty \text{ for all } x_\ell \text{ such that } f_\ell^{\text{out}}(x_\ell) = C_\ell.$$

Assumption (A4) states that if a link is approaching its maximum flow capacity, then the travelers will increasingly avoid it. This setting can also be used to capture back propagation, where if the density of a link reaches a critical value then no additional

vehicles can enter that link (cf. Remark 3.3). The following corollary refines Theorem 3.13 for unbounded costs.

Corollary 3.14. *Let Assumption (A4) replace (A3) in Theorem 3.13. The interconnected system* (3.7) *admits an equilibrium point that satisfies* (3.10) *if and only if the network inflow is strictly lower than the min-cut capacity:*

$$\bar{\lambda} < C_{\text{m-cut}}.$$

3.3.3 Relationship to Wardrop Equilibrium

The following result relates the fixed points of the dynamical system (3.7) with the established notion of Wardrop equilibria.

Theorem 3.15. ***(Relationship Between Fixed Points and Wardrop Equilibria)*** *Consider the interconnected system* (3.7). *The following statements are equivalent:*

(i) $x^* \in \mathcal{X}$ *satisfies the Wardrop First Principle;*

(ii) The pair (x^*, r^*) *is a fixed point of* (3.7) *for some* $r^* \in \mathcal{R}_{\mathcal{G}}$. *Moreover,* (x^*, r^*) *satisfies* (3.10).

Proof. (i) $\Rightarrow$ *(ii)* We begin by observing that, by assumption, a Wardrop equilibrium is also an equilibrium of the traffic dynamics (5.6). Thus, we next prove that given a vector x^* that satisfies the Wardrop conditions, there exists a vector $r^* \in \mathcal{R}_{\mathcal{G}}$ such that (3.10) is satisfied.

Since the graph is acyclic, it admits a shortest path spanning tree [46], that is, a directed tree rooted from the source with the property that the unique path from the source

to any node is a shortest path to that node. Notice that, since in general the Wardrop First Principle allows the existence of multiple paths with optimal travel costs, the shortest-path spanning tree is typically not unique. Next, we distinguish among three cases.

(Case 1) For all $p, \bar{p} \in \mathcal{P}$, $\tau_p^* - \tau_{\bar{p}}^* = 0$, namely, all origin-destination paths have identical travel time. This assumption implies that for every node $v \in \mathcal{V}$ all its outgoing links belong to one of the shortest-path spanning trees. This observation, combined with the fact that the perceived costs are equal to the shorthest travel cost to destination, implies that

$$\pi_q^* = \pi_m^*, \text{ for all pairs } m, q \in v^{\text{out}}.$$

As a result,

$$a_{\ell m}(x^*) = \sum_q r_{\ell q}^* \pi_q^* - \pi_m^* = \pi_m^* (\sum_q r_{\ell q}^* - 1) = 0.$$

By iterating the above equation for all $(\ell, m) \in \mathcal{A}$ we proved that the first condition in (3.10) is satisfied.

(Case 2) There exists a unique $p \in \mathcal{P}$ such that $f_p^* = 0$ and for all $\bar{p} \neq p$, $\tau_{\bar{p}}^* - \tau_p^* \leq 0$, namely, the path p has suboptimal travel time to destination. This assumption implies that there exists a certain node in the network $v \in \mathcal{V}$ such that one of its outgoing links $m \in v^{\text{out}}$ belongs to p (i.e., it does not belong to any shortest-path spanning tree), while $q \in v^{\text{out}}$ belongs to some $\bar{p}$ (i.e., it belongs to a shortest path spanning tree). This observation, combined with the fact that the perceived costs are equal to the shorthest travel cost to

destination, implies

$$\pi_m^* > \pi_q^*.$$

Moreover, since m belongs to an origin-destination path with zero flow, there exists $\ell \in v^{\text{in}}$ such that $r_{\ell m}^* = 0$, and thus

$$\begin{aligned} a_{\ell m}(x^*) &= \sum_q r_{\ell q}^* \pi_q^* - \pi_m^* \\ &= \sum_{q \neq m} r_{\ell q}^* \pi_q^* + \underbrace{r_{\ell m}^*}_{=0} \pi_m^* - \pi_m^* \\ &= \sum_{q \neq m} r_{\ell q}^* \pi_q^* - \pi_m^* \\ &= \pi_q^* \sum_{q \neq m} r_{\ell q}^* - \pi_m^* \\ &= \pi_q^* - \pi_m^* < 0, \end{aligned} \tag{3.12}$$

which proves that $a_{\ell m}(x^*) < 0$, and shows that the second condition in (3.10) is satisfied for the pair $(\ell, m) \in \mathcal{A}$.

(Case 3) There exists multiple $p \in \mathcal{P}$ such that $f_p^* = 0$ and for some $\bar{p} \neq p$, $\tau_{\bar{p}}^* - \tau_p^* \leq 0$, namely, there exists multiple origin-destination paths with suboptimal travel cost. Under this assumption, we note that the bound derived in (3.12) can be iterated for all links m such that $r_{\ell m}^* = 0$, which shows that the second condition in (3.10) is satisfied for all these pairs, and concludes the proof of the implication.

(ii) $\Rightarrow$ (i) To prove this implication we consider three cases.

(Case 1) For all $(\ell, m) \in \mathcal{A}$, $a_{\ell m}(x^*) = 0$, namely, all links have identically zero appeal. Under this assumption, for every $\ell \in \mathcal{L}$, all the perceived travel costs satisfy

$$0 = a_{\ell m}(x^*) = \sum_q r^*_{\ell q}\pi^*_q - \pi^*_m, \text{ for all } m \in \mathcal{A}_\ell, \tag{3.13}$$

which implies that $\pi^*_m = \pi^*_{\bar{m}}$ for all $m, \bar{m} \in \mathcal{A}_\ell$ are identical (i.e. $\pi^*_m = \pi^*_{\bar{m}} = \sum_q r^*_{\ell q}\pi^*_q$). This observation, combined with the fact that the perceived costs are equal to the shorthest travel cost to destination, implies that every link in the network belongs to a shortest path to destination. Hence, all origin-destination paths have identical travel cost, i.e. $\tau^*_p - \tau^*_{\bar{p}} = 0$, which shows that x^* satisfies the Wardrop First Principle.

(Case 2) There exists a unique $(\ell, m) \in \mathcal{A}$ such that $a_{\ell m}(x^*) < 0$ and $r_{\ell m} = 0$. Under this assumption, we first prove that there exists a path $p \in \mathcal{P}$ containing link m such that $f^*_p = 0$. Since the flow on any origin-destination path can be written as the network inflow multiplied by the product of the routing ratios belonging to that path:

$$f^*_p = \bar{\lambda} \prod_{q,w \in p} r^*_{qw},$$

we immediately obtain $f^*_p = 0$.

Second, we prove that for all $\bar{p} \in \mathcal{P}$, $\bar{p} \neq p$, the following inequality holds: $\tau^*_{\bar{p}} - \tau^*_p \leq 0$. By using the assumption $a_{\ell m}(x^*) < 0$, together with $\pi^*_w = \sum_q r^*_{\ell q}\pi^*_q$, which holds for all

$w \in \mathcal{A}_\ell$, $w \neq m$, (see (3.13)), we have

$$\begin{aligned} 0 > a_{\ell m}(x^*) &= \sum_q r^*_{\ell q}\pi^*_q - \pi^*_m \\ &= \pi^*_w \sum_q r^*_{\ell q} - \pi^*_m \\ &= \pi^*_w - \pi^*_m. \end{aligned} \tag{3.14}$$

Since path p contains link w and the minimum travel cost from w to destination is suboptimal ($\pi^*_w > \pi^*_m$), we have that any path $\bar{p} \in \mathcal{P}$ containing link m satisfies

$$\tau^*_{\bar{p}} < \tau^*_p,$$

which shows that x^* satisfies the Wardrop First Principle.

(Case 3) There exists multiple ramps $(\ell, m) \in \mathcal{A}$ such that $a_{\ell m}(x^*) < 0$ and $r^*_{\ell m} = 0$. Under this assumption, we note that equation (3.14) still applies because $r^*_{\ell m} = 0$. Hence, the reasoning adopted for *(Case 2)* can be iterated for all (ℓ, m) such that $a_{\ell m}(x^*) < 0$ and $r^*_{\ell m} = 0$. ■

Three important implications follow from the above theorem. First, the result shows that a Wardrop equilibrium is also an equilibrium of the dynamical model (3.7), thus showing that if a dynamical network starts at a Wardrop equilibrium it will remain at that equilibrium at all times. Second, the result shows that dynamical systems in which travelers update their routing in real-time at every junction by minimizing their perceived travel cost admit equilibrium points that satisfy the Wardrop conditions. This observation supports our

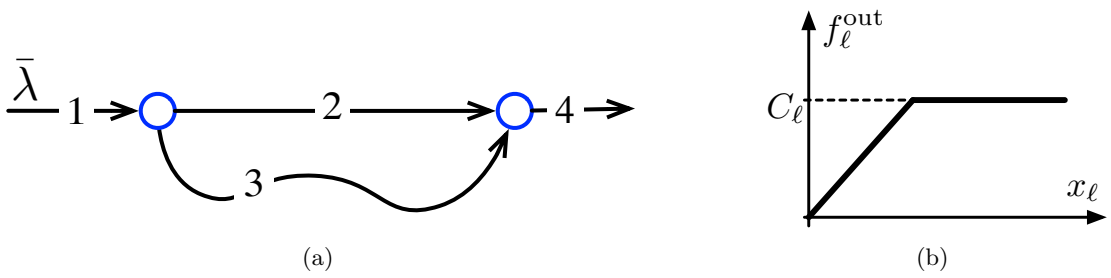

Figure 3.3: Two-link network (a), and piecewise affine outflow function (b).

modeling choices, and demonstrates that the perceived costs are representative quantities to describe the economical decisions of routing apps. Third, by combining Theorem 3.15 with (3.10), it follows that a Wardrop Equilibrium is perceived by the travelers when all the network links have a nonpositive appeal function. This condition corresponds to a situation where at every junction no link is more appealing that others.

3.4 Stability Analysis

In this section, we characterize the stability of the fixed points of the feedback interconnection (3.7). Our main findings are summarized in the following theorem.

Theorem 3.16. ***(Stability of Interconnected Dynamics)*** *Let* (x^*, r^*) *be a fixed point of* (3.7) *satisfying the conditions* (3.10)*. Then,* (x^*, r^*) *is stable.*

The proof of this theorem is postponed to later in this section.

The simple stability of the fixed points implies that the state trajectories are not guaranteed to decay asymptotically towards the equilibrium points, and can result in nontrivial behaviors, such as oscillations, as illustrated in the following example.

Example 3.17. ***(Existence of Oscillations in Two Parallel Roads)*** *Consider the network illustrated in Fig. 3.3(a), representing two parallel roads subject to a constant inflow of vehicles* $\bar{\lambda} \in \mathbb{R}_{>0}$*. We assume that the travel costs are linear*

$$\tau_\ell(x_\ell) = x_\ell,$$

and that all outflows are identical and piecewise-affine:

$$f_\ell^{\text{out}}(x_\ell) = \min\{vx_\ell, C\},$$

for all $\ell \in \mathcal{L} = \{1, \dots, 4\}$*, where* $v \in \mathbb{R}_{>0}$*.*

We distinguish among two cases: (a) the network is operating in congested regimes, that is, at all times $x_1 > C/v$ *and* $x_2 > C/v$*, and (b) the network is operating in regimes of free-flow, that is, at all times* $x_1 \leq C/v$ *and* $x_2 \leq C/v$*. Fig. 3.4 (a) and (b) show the phase portrait of the system trajectories in case (a) and case (b), respectively. As illustrated by the plots: in case (a) the trajectories of the system are oscillating periodic orbits; in contrast, in case (b) the trajectories converge asymptotically to an equilibrium point. The presence of periodic orbits implies that the equilibrium points are stable, but not asymptotically stable, thus supporting Theorem 3.16.*

The existence of periodic orbits in case (a) can be further formalized. To this aim, we recall the dynamical equations governing the system in this regime:

$$\dot{x}_2 = -C + r_{12}\bar{\lambda},$$

$$\dot{x}_3 = -C + r_{13}\bar{\lambda},$$

$$\dot{r}_{12} = r_{12}(1 - r_{12})(x_3 - x_2),$$

where we used the fact that $f_1^{\text{out}} = \bar{\lambda}$ *after an initial transient. This system admits an equilibrium point described by* $r_{12} = 0.5$ *and* $x_3 = x_2$*. We adopt the change of variables* $z := x_3 - x_2$*, and rewrite the dynamical equations describing the new state* $[z,\ r_{12}]^{\mathsf{T}}$*:*

$$\dot{z} = (1 - 2r_{12})\bar{\lambda},$$

$$\dot{r}_{12} = r_{12}(1 - r_{12})z.$$

Next, we show that the following quantity:

$$U(z, r_{12}) := \frac{1}{2}z^2 - \bar{\lambda}\left(\ln r_{12} - \ln(1 - r_{12})\right),$$

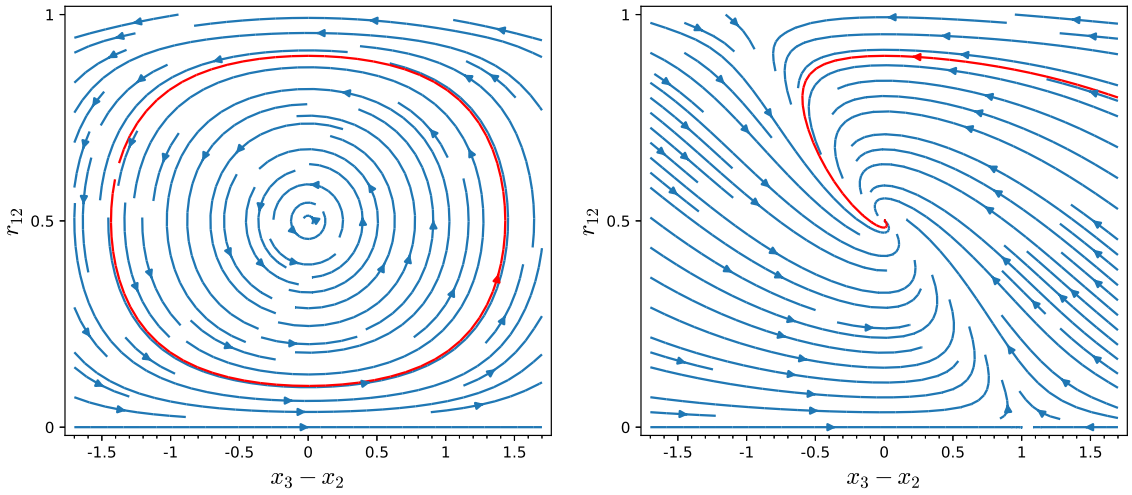

Figure 3.4: Phase portrait: (a) oscillatory trajectories, (b) stable trajectories. The red curve illustrates an example of trajectories passing through the conditions $x_3 = x_2$ and $r_{12} = 0.9$.

is conserved along the trajectories of the system. To this aim, we compute its time derivative to obtain

$$\begin{aligned}\dot{U}(z, r_{12}) &= z\dot{z} - \bar{\lambda}\left(\frac{1}{r_{12}} + \frac{1}{1 - r_{12}}\right)\dot{r}_{12} \\ &= z(1 - 2r_{12})\bar{\lambda} - \bar{\lambda}((1 - r_{12})z - r_{12}z)) \\ &= z(1 - 2r_{12})\bar{\lambda} - z(1 - 2r_{12})\bar{\lambda} = 0,\end{aligned}$$

which shows that the quantity $U(z, r_{12})$ is a constant of motion, and proves the existence of periodic orbits. □

In the remainder of this section, we illustrate the key technical results that prove Theorem 3.16. In short, the stability of the fixed points of (3.7) follows from interpreting the system as a negative feedback interconnection between the traffic dynamics and the

routing dynamics (see Fig. 3.2), and from showing that each open-loop component is a passive dynamical system. We refer to Chapter 2 for a summary of the notions of passivity utilized in the remainder.

We next show that the routing dynamics satisfy the passivity property. To this aim, we first prove that the group of routing equations at a single junction are passive. For every link $\ell \in \mathcal{L}$, recall that $\mathcal{A}_\ell$ is the set of links available at the downstream junction, and let $|\mathcal{A}_\ell| := \alpha$ be its cardinality. We interpret the set of α dynamical equations

$$\dot{r}_{\ell m} = r_{\ell m}(\sum_q r_{\ell q}\pi_q - \pi_m), \text{ for all } m \in \mathcal{A}_\ell, \tag{3.15}$$

as a dynamical system with input and output, respectively,

$$\begin{aligned} u_\ell &= [\pi_{m_1}, \dots, \pi_{m_\alpha}]^\mathsf{T}, \\ y_\ell &= [r_{\ell m_1}, \dots, r_{\ell m_\alpha}]^\mathsf{T}. \end{aligned} \tag{3.16}$$

The following result formalizes the passivity of equations (3.15).

Lemma 3.18. ***(Passivity of Single-Junction Routing Dynamics)*** *The single-junction routing dynamics* (3.15) *is passive with respect to the input-output pair* $(-u_\ell, y_\ell)$.

Proof. We let $[r^*_{\ell m_1}, \dots, r^*_{\ell m_p}]$ denote a fixed point of (3.15), and we show that

$$V_\ell(r) = \sum_{m \in \mathcal{A}_\ell} r^*_{\ell m} \ln\left(\frac{r^*_{\ell m}}{r_{\ell m}}\right), \tag{3.17}$$

is a storage function for the dynamical system defined by (3.15). We begin by observing that V_ℓ is differentiable because it is a linear combination of natural logarithm functions. Moreover, by using the log-sum inequality, we have

$$\begin{aligned} V_\ell(r) &= \sum_m r^*_{\ell m} \ln\left(\frac{r^*_{\ell m}}{r_{\ell m}}\right) \\ &\geq \sum_m r^*_{\ell m} \ln\left(\frac{\sum_m r^*_{\ell m}}{\sum_m r_{\ell m}}\right) \\ &= \ln(1) = 0, \end{aligned}$$

where we used the fact that $\sum_m r^*_{\ell m} = \sum_m r_{\ell m} = 1$, which shows that V_ℓ is an appropriate choice of storage function.

To show the passivity property, we first incorporate the negative sign of the input vector into the dynamical equation, and we rewrite (3.15) as

$$\dot{r}_{\ell m} = r_{\ell m}(\pi_m - \sum_q r_{\ell q}\pi_q), \text{ for all } m \in \mathcal{A}_\ell,$$

and we next show passivity of the above equation with respect to the input-output pair (u_ℓ, y_ℓ). The derivative of the storage function is

$$\begin{aligned}
\dot{V}_\ell(r) &= -\sum_m r^*_{\ell m} \frac{\dot{r}_{\ell m}}{r_{\ell m}} = -\sum_m r^*_{\ell m}(\pi_m - \sum_q r_{\ell q}\pi_q) \\
&= -\sum_m r^*_{\ell m}\pi_m + \underbrace{\sum_m r^*_{\ell m}}_{=1} \sum_q r_{\ell q}\pi_q \\
&= -\sum_m r^*_{\ell m}\pi_m + \sum_q r_{\ell q}\pi_q \\
&\leq \sum_q r_{\ell q}\pi_q = u_\ell^\mathsf{T} y_\ell,
\end{aligned}$$

where for the last inequality we used the fact that $r_{\ell q} \geq 0$ and $\pi_q \geq 0$, which shows the claim and concludes the proof. ■

Next, we leverage the above lemma to show that the overall routing dynamics (3.5) also satisfy the passivity property. To this aim, we consider (3.5) as a dynamical system with input and output vectors, respectively,

$$\begin{aligned}
u_r &= [u_{\ell_1}, \ldots, u_{\ell_n}]^\mathsf{T}, \\
y_r &= [y_{\ell_1}, \ldots, y_{\ell_n}]^\mathsf{T},
\end{aligned} \tag{3.18}$$

where u_{ℓ_i} and y_{ℓ_i}, $i \in \{1, \ldots, n\}$, are defined in (3.16). Passivity of the overall routing dynamics is formalized next.

Lemma 3.19. ***(Passivity of Overall Routing Dynamics)*** *Let the perceived travel costs be modeled as in* (3.3)*. Then, the overall routing dynamics* (3.5) *is passive with respect to the input-output pair* $(-u_r, y_r)$*.*

Proof. The proof of this statement consists of two parts. First, we show that the dynamical equations at every pair of junctions are independent, and thus the overall routing dynamics (3.5) can be studied as a composition of independent subsystems. To this aim, we will show that u_ℓ is independent of y_m in (3.16), for all $\ell \neq m$. This fact immediately follows by observing that, when the perceived travel costs follow the model (3.3), the perceived cost $\pi_\ell(x)$ is a function that only depends on x, and it is independent of the routing r.

Second, we show that passivity of all the individual junctions implies passivity of the overall routing dynamics (3.5). To this aim, we consider the following storage function for (3.5):

$$V_r(r) = \sum_{\ell \in \mathcal{L}} V_\ell(r), \tag{3.19}$$

where V_ℓ denotes the storage function associated to junction ℓ. By taking the time derivative of the above storage function:

$$\dot{V}_r(r) = \sum_{\ell \in \mathcal{L}} \dot{V}_\ell(r) \leq \sum_{\ell \in \mathcal{L}} u_\ell^\mathsf{T} y_\ell = u_r^\mathsf{T} y_r,$$

where the inequality follows from the passivity of the individual junctions, which proves the passivity of (3.5). ■

Next, we show that the traffic dynamics (5.6) satisfy the passivity property. To this aim, we interpret (5.6) as an input-output dynamical system with input described by the set of routing ratios, and output described by the set of perceived link costs. Formally, to the scalar input $r_{\ell m}$ we associate the scalar output π_m or, equivalently, in vector form we consider the following input and output vectors:

$$\begin{aligned} u_x &= [r_{11}, r_{12}, \dots, r_{1n}, r_{21}, \dots, r_{nn}]^{\mathsf{T}}, \\ y_x &= [\ \pi_1,\ \pi_2, \dots,\ \pi_n,\ \pi_1, \dots,\ \pi_n]. \end{aligned} \tag{3.20}$$

The following result formalizes the passivity of (5.6).

Lemma 3.20. ***(Passivity of the Traffic Dynamics)*** *Assume that all links $\ell \in \mathcal{L}$ have finite flow capacity $C_\ell < \infty$. Then, the traffic network* (5.6) *is a passive dynamical system with respect to the input-output pair (u_x, y_x).*

Moreover, if for all ℓ there exists $\rho_\ell \in \mathbb{R}_{>0}$ such that

$$f_\ell(x_\ell) \geq \rho_\ell \pi_\ell(x_\ell), \tag{3.21}$$

then the traffic dynamics (5.6) *are output strictly passive.*

Proof. We show that the following function

$$V_x(x) = \frac{1}{h} \sum_{\ell \in \mathcal{L}} \int_0^{x_\ell} \pi_\ell(\sigma)\ d\sigma, \tag{3.22}$$

is a storage function for (5.6), where the constant $h \in \mathbb{R}_{>0}$ is chosen as follows:

$$h = \max_{\ell \in \mathcal{L}} \; C_\ell.$$

We note that V_x is non-negative and it is differentiable, because it is the combination of integral functions, and thus it is an appropriate choice of storage function. By taking the time derivative of the storage function we obtain

$$\begin{aligned}
\dot{V}_x(x) &= \frac{1}{h} \sum_{\ell \in \mathcal{L}} \pi_\ell(x_\ell) \dot{x}_\ell \\
&= \frac{1}{h} \sum_{\ell \in \mathcal{L}} \pi_\ell(x_\ell) \left(-f_\ell^{\text{out}}(x_\ell) + \sum_{m \in \mathcal{A}_\ell} r_{m\ell} f_m^{\text{out}}(x_m) \right) \\
&= -\frac{1}{h} \sum_{\ell \in \mathcal{L}} \pi_\ell(x_\ell) f_\ell^{\text{out}}(x_\ell) \\
&\qquad\qquad + \frac{1}{h} \sum_{\ell \in \mathcal{L}} \pi_\ell(x_\ell) \sum_{m \in \mathcal{A}_\ell} r_{m\ell} f_m^{\text{out}}(x_m) \\
&\leq \frac{1}{h} \sum_{\ell \in \mathcal{L}} \pi_\ell(x_\ell) \sum_{m \in \mathcal{A}_\ell} r_{m\ell} f_m^{\text{out}}(x_m) \\
&\leq \sum_{\ell \in \mathcal{L}} \sum_{m \in \mathcal{A}_\ell} \pi_\ell(x_\ell) r_{m\ell} = u_x^{\mathsf{T}} y_x,
\end{aligned}$$

where for the first inequality we used the fact that $\pi_\ell(x_\ell) f_\ell(x_\ell) \geq 0$ for all $\ell \in \mathcal{L}$, and the last inequality follows from the above choice of h (which implies $f_m/h < 1$, for all $m \in \mathcal{L}$). Hence, the bound proves the passivity of (5.6).

To show output-strict passivity, we substitute the inequality (3.21) into the time-derivative of the storage function to obtain:

$$\begin{aligned}
\dot{V}_x(x) = & -\frac{1}{h}\sum_{\ell\in\mathcal{L}}\pi_\ell(x_\ell)f_\ell^{\text{out}}(x_\ell) \\
& \qquad + \frac{1}{h}\sum_{\ell\in\mathcal{L}}\pi_\ell(x_\ell)\sum_{m\in\mathcal{A}_\ell} r_{m\ell}f_m^{\text{out}}(x_m) \\
\leq & -\frac{1}{h}\sum_{\ell\in\mathcal{L}}\rho_\ell\pi_\ell(x_\ell)^2 + \frac{1}{h}\sum_{\ell\in\mathcal{L}}\pi_\ell(x_\ell)\sum_{m\in\mathcal{A}_\ell} r_{m\ell}f_m^{\text{out}}(x_m) \\
\leq & -\sum_{\ell\in\mathcal{L}}\rho_\ell\pi_\ell(x_\ell)^2 + \sum_{\ell\in\mathcal{L}}\sum_{m\in\mathcal{A}_\ell}\pi_\ell(x_\ell)r_{m\ell} \\
\leq & -y_x^{\mathsf{T}}y_x + u_x^{\mathsf{T}}y_x,
\end{aligned}$$

where the last inequality follows from $\rho_\ell > 0$, which shows that (5.6) is output strictly passive and concludes the proof. ■

The additional assumption (3.21) needed to ensure output strict passivity can be interpreted as follows. By using the fact that for every $x_\ell \in \mathcal{X}$, $\pi_\ell(x_\ell) > 0$, the inequality (3.21) can be rewritten as follows:

$$\frac{f_\ell(x_\ell)}{\pi_\ell(x_\ell)} \geq \rho_\ell,$$

and, by deriving both quantities with respect to x_ℓ we obtain

$$\frac{df_\ell(x_\ell)}{d\pi_\ell(x_\ell)} > 0,$$

where we used the fact that $\rho_\ell > 0$. Hence, in order to achieve output strict passivity, an increase in travel cost of a link must imply an increase in traffic flow in the link.

We are now ready to formally prove Theorem 3.16.

Proof of Theorem 3.16: To prove the stability of the fixed points, we interpret (3.7) as a negative feedback interconnection between the traffic dynamics and the routing dynamics, and we leverage the Passivity Theorem [32] to infer the Lyapunov stability of the system. We refer to Theorem 2.1 in Chapter 2 for a concise statement of the Passivity Theorem.

We begin by observing that the lemmas 3.19 and 3.20 ensure passivity of the open loop systems. Next, we show that the equilibrium points are local minima for the storage function of routing (3.19) and for the storage function of traffic (3.22). First, we observe that the routing storage function $V_r(r)$ in (3.19) is the summation of the storage functions at the junctions (3.17), which are non-negative quantities that are identically zero at the equilibrium points $V_\ell(r^*) = 0$. Hence, the equilibrium points are local minima of the function $V_r(r)$.

Second, we show that $V_x(x)$ attains a minimum at the equilibrium points. To this aim, we first let $\bar{\lambda} = 0$ and we study the equilibrium points of (5.6). Every equilibrium point x^* satisfies the following identity

$$0 = (R^\mathsf{T} - I) f(x^*).$$

By observing that $(R^\mathsf{T} - I)$ is invertible (see e.g. [4, Theorem 1]), and that $f(x^*) = 0$ only if $x^* = 0$ (see Assumption (A1)), the above equation implies that the unique equilibrium point of the system satisfies $x^* = 0$. The choice of $V_x(x)$ in (3.22) implies that $V_x(x)$ is

non-negative and that $V_x(x^*) = 0$, which shows that x^* is a local minima of the storage function. Lastly, we observe that any nonzero $\bar{\lambda}$ has the effect of shifting the equilibrium point, and thus it does not change the properties of the storage function.

Finally, the stability of the equilibrium points follows by application of condition (i) in Theorem 2.1. ■

3.5 Robust Information Design

In this section, we propose a control technique to guarantee the asymptotic stability the equilibrium points, and thus strengthen the robustness of the system. The method relies on regulating the rate at which travelers react to congestion by properly modifying the reaction rates. To this aim, we next introduce the notion of congestion-aware reaction rates.

Definition 3.21. ***(Congestion-Aware Reaction Rates)*** *A set of reaction rates for the dynamics* (3.5) *is congestion-aware if, for all* $\ell \in \mathcal{L}$*,*

$$\delta_\ell : \mathcal{T}^n \to (0, +\infty).$$

Moreover, let $\mathcal{T}_\ell := \{\pi_m\}_{m \in \mathcal{A}_\ell} \subseteq \mathcal{T}^n$ *be the set of perceived costs at the links downstream of* ℓ*. A set of congestion-aware reaction rates is local if, for all* $\ell \in \mathcal{L}$*,*

$$\delta_\ell : \mathcal{T}_\ell \to (0, +\infty). \tag{3.23}$$

□

The class of congestion-aware reaction rates conceptualizes a setting where the rate at which travelers react to changes in traffic congestion is a function of the instantaneous perceived costs. We observe that this control scheme can be achieved, for instance, by appropriately designing the rate at which navigation apps update their routing suggestions. Similarly, local congestion-aware reaction rates model a setting where, at every node of the network, the reaction rates at the incoming links only depend on the perceived costs at the outgoing links.

We observe that the adoption of congestion-aware reactions does not alter the equilibrium points of the interconnected system (3.7). In fact, reaction rates are positive multiplicative quantities in the dynamical equation (3.4), and thus the properties of the equilibrium points discussed in Section 3.3 remain unchanged. The following result characterizes the stability of the equilibrium points under congestion-aware reaction rates.

Theorem 3.22. ***(Asymptotic Stability Under Congestion-Aware Reaction Rates)*** *Consider the interconnected system* (3.7) *where the routing dynamics adopt the class of local congestion-aware reaction rates* (3.23)*. Moreover, assume that for every link* $\ell \in \mathcal{L}$ *there exists a scalar* $\rho_\ell \in \mathbb{R}_{>0}$ *such that*

$$f_\ell(x_\ell) \geq \rho_\ell \pi_\ell(x_\ell).$$

Then, every equilibrium point (x^*, r^*) *that satisfies* (3.10) *is asymptotically stable.*

The proof of this theorem is postponed to later in this section.

The above theorem shows that the class of local congestion-aware reaction rates ensures the asymptotic stability of the equilibrium points of the interconnected traffic-routing system.

The result has an important practical interpretation that we illustrate next. Let $p = (\{v_1, \ldots, v_k\}, \{\ell_1, \ldots, \ell_k\})$ be an origin-destination path in the graph, that is, $\ell_1 = s$ and $\ell_k = d$. It follows from the recursive definition of perceived costs (3.3) that the perceived costs are non-increasing along a path, that is, for all $i \in \{1, \ldots, n-1\}$,

$$\pi_{\ell_i} \geq \pi_{\ell_{i+1}}.$$

By combining this observation with the definition of local reactions (3.23), it follows that the magnitude of the reaction rates is non-increasing along a path, that is,

$$\delta_{\ell_i} \geq \delta_{\ell_{i+1}}.$$

Hence, Theorem 3.22 states that in order to achieve asymptotic stability of the equilibrium points, travelers that are closer to the network origin must react faster to changes in traffic congestion as compared to travelers that are in the proximity of the network destination.

In the remainder of this section, we present the key technical results that formally prove Theorem 3.22. Loosely speaking, the asymptotic stability of the equilibrium points follows by ensuring that the open loop components of the negative feedback interconnection (3.7) satisfy a strong passivity notion. We begin by proving this property for the routing dynamics.

Lemma 3.23. ***(Input Strict Passivity of Routing Dynamics)*** *Assume the routing dynamics* (3.5) *adopt the class of local congestion-aware reaction rates* (3.23)*. Then, the overall routing dynamics* (3.5) *is input strictly passive.*

Proof. The proof of this statement consists of two parts. First, we show that the single-junction routing dynamics (3.15) are input strictly passive. To this aim, similarly to the proof of Lemma 3.18, we reverse the sign of the dynamical equation to take into account the negative sign in the input. Moreover, we consider the following storage function

$$V_\ell(r) = \frac{1}{h} \sum_{m \in \mathcal{A}_\ell} r^*_{\ell m} \ln \left(\frac{r^*_{\ell m}}{r_{\ell m}} \right),$$

where $[r^*_{\ell m_1}, \ldots, r^*_{\ell m_p}]$ is a fixed point of (3.15), and the scalar $h_\ell > 0$ is chosen so that

$$h = \max_{\ell \in \mathcal{L}} \delta_\ell.$$

We observe (3.23) implies $h < \infty$, and that $V_\ell(r)$ is an appropriate choice of storage function (see proof of Lemma 3.18). By computing the time derivative of the storage we obtain

$$\begin{aligned}
\dot{V}_\ell(r) &= -\frac{1}{h}\sum_m r^*_{\ell m}\frac{\dot{r}_{\ell m}}{r_{\ell m}} = -\frac{1}{h}\sum_m r^*_{\ell m}(\pi_m - \sum_q r_{\ell q}\pi_q)\delta_\ell \\
&= -\frac{1}{h}\sum_m r^*_{\ell m}\pi_m\delta_\ell + \frac{1}{h}\underbrace{\sum_m r^*_{\ell m}}_{=1}\sum_q r_{\ell q}\pi_q\delta_\ell \\
&= -\frac{1}{h}\sum_m r^*_{\ell m}\pi_m\delta_\ell + \frac{1}{h}\sum_q r_{\ell q}\pi_q\delta_\ell \\
&= -\frac{1}{h}\sum_m r^*_{\ell m}\pi_m\tilde{\delta}_m(\pi_m) + \frac{1}{h}\sum_q r_{\ell q}\pi_q\delta_\ell \\
&\leq -\sum_m \pi_m\tilde{\delta}_m(\pi_m) + \sum_q r_{\ell q}\pi_q \\
&= -u_\ell^\mathsf{T}\varphi(u_\ell) + u_\ell^\mathsf{T} y_\ell,
\end{aligned}$$

where for the fourth identity we used the fact that δ_ℓ is a function of π_m, namely, $\delta_\ell = \tilde{\delta}_m(\pi_m)$, the inequality follows from our choice of h (which implies $\delta_\ell/h < 1$), and $\varphi(u_\ell) = [\tilde{\delta}_{m_1}(\pi_{m_1}), \ldots, \tilde{\delta}_{m_p}(\pi_{m_p})]^\mathsf{T}$. The above inequality shows that the single-junction routing (3.15) is input strictly passive.

Finally, input strict passivity of the overall routing dynamics follows by combining input strict passivity of the junction dynamics with the choice of storage function $V_r(r) = \sum_{\ell\in\mathcal{L}} V_\ell(r)$ for (3.5), and by adopting a reasoning similar to the one used in the proof of Lemma 3.19. ■

We are now ready to formally prove Theorem 3.22.

Proof of Theorem 3.22: To prove the asymptotic stability of the fixed points, interpret (3.7) as a negative feedback interconnection between the traffic dynamics and the routing dynamics, and we leverage the stronger version of the Passivity Theorem [32] for Lyapunov stability. We refer to condition (ii) of Theorem 2.1 in Chapter 2 for a concise description of the assumptions required to prove this result.

The proof of this claim is organized into three main parts, and leverages the fact that the open loop components are passive dynamical systems with storage functions defined in the proofs of lemmas 3.20 and 3.23. First, we observe that Theorem 3.16 immediately implies that the equilibrium points are local minima for the storage functions.

Second, we show that each open loop systems is zero-state detectable [32]. Zero-state detectability of the routing dynamics immediately follows from the choice of input and output (3.16), and by observing that the state of the system coincides with its output. Zero-state detectability of the traffic dynamics immediately follows from the choice of input and output (3.20), and by observing that if the output of the system is identically zero then its state is identically zero.

Third, we show that the inequalities (2.4) are satisfied. We begin by observing that input strict passivity of the routing dynamics, proved in Lemma 3.23, ensures the existence of a function $\varphi_{\text{routing}} : \mathcal{T} \to \mathbb{R}^n_{>0}$, such that

$$v^{\mathsf{T}} \varphi_{\text{routing}}(v) > 0, \text{ for all } v \neq 0.$$

Moreover, output strict passivity of the traffic dynamics, proved in Lemma 3.20, ensures the existence of a function $\rho_{\text{traffic}} : \mathcal{T} \to \mathbb{R}^n_{>0}$, such that

$$v^\mathsf{T} \rho_{\text{traffic}}(v) > 0, \text{ for all } v \neq 0.$$

Finally, the statement of the result follows by combining the above observations, and by application of condition (ii) in the passivity theorem 2.1. ■

3.6 Simulation Results

This section presents two sets of numerical simulations that illustrate our findings.

Data From SR60-W and I10-W in Southern California. Consider the traffic network in Fig. 3.5(a), which schematizes the west bounds of the freeways SR60-W and I10-W in Southern California. Let x_{60} and x_{10} be the average traffic density in the examined sections of SR60-W (absolute miles $13.1 - 22.4$) and in the section of I10-W (absolute miles $24.4 - 36.02$), respectively. Moreover, let r_{60} (resp. $r_{10} = 1 - r_{60}$) be the fraction of travelers choosing freeway SR60-W over I10-W (resp. choosing freeway I10-W over SR60-W) for their commute. Fig. 3.5(b) illustrates the time-evolution of the recorded traffic density[1] for the two freeways on Friday, March 6, 2020. The figure also illustrates an estimation of the densities and of the routing fraction as predicted by our models, demonstrating that our dynamical framework can predict the complex dynamical behaviors observed in practice.

[1]Source: Caltrans Freeway Performance Measurement System (PeMS).

Table 3.1: Choice of Affine Travel Costs

ℓ	1	2	3	4	5	6	7
a_ℓ	1	10	1	1	1	10	1
b_ℓ	0	0	50	10	50	0	0

Oscillating Trajectories in Seven-Link Network. Consider the seven-link network discussed in Example 3.2 and reported in Fig. 3.6(a), assume that the outflows are linear

$$f_\ell(x_i) = x_i, \text{ for all } i \in \{1, \dots, 7\},$$

and that the travel costs are affine:

$$\tau_\ell(x_\ell) = a_\ell x_\ell + b_\ell, \text{ for all } i \in \{1, \dots, 7\},$$

where the parameters a_ℓ and b_ℓ are summarized in Table 3.1. Since the flow capacities of the links are unbounded, Theorem 3.13 ensures the existence of an equilibrium point (x^*, r^*). It can be verified that an equilibrium point that satisfies (3.10) is:

$$x_1^* = 6,\ x_2^* = 4,\ x_3^* = 2,\ x_4^* = 2,\ x_5^* = 2,\ x_6^* = 4,\ x_7^* = 6,$$
$$r_{12} = 2/3,\ r_{13} = 1/3,\ r_{24} = 1/2,\ r_{25} = 1/2.$$

Fig. 3.6 shows an example of trajectories, demonstrating that the system admits a periodic orbit, which prevents the state from converging to the equilibrium points asymptotically.

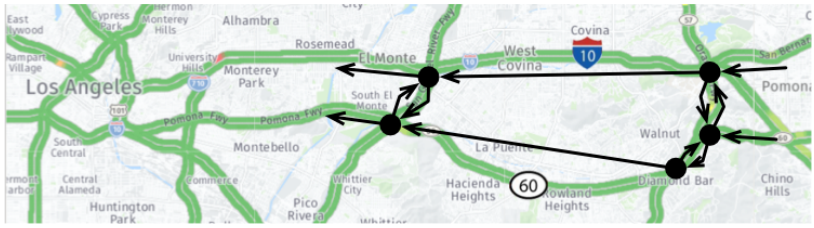

(a)

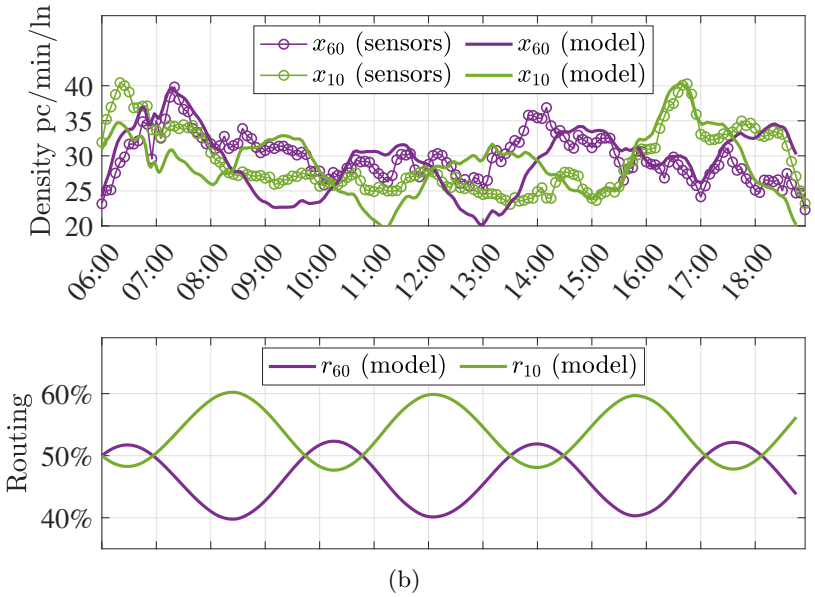

(b)

Figure 3.5: Time series data for SR60-W and I10-W on March 6, 2020. (a) schematic of traffic network. (b) Sensory data (continuous lines with circles) and trajectories predicted by our models (continuous lines). (c) Routing predicted by our models. Simulation uses constant inflow $\bar{\lambda} = 3340$ veh/hr/ln.

Fig. 3.7 shows the trajectories of the same network when the routing apps use a set of local congestion-aware reaction rates, demonstrating that this class of control policies ensures the asymptotic stability of the equilibrium points.

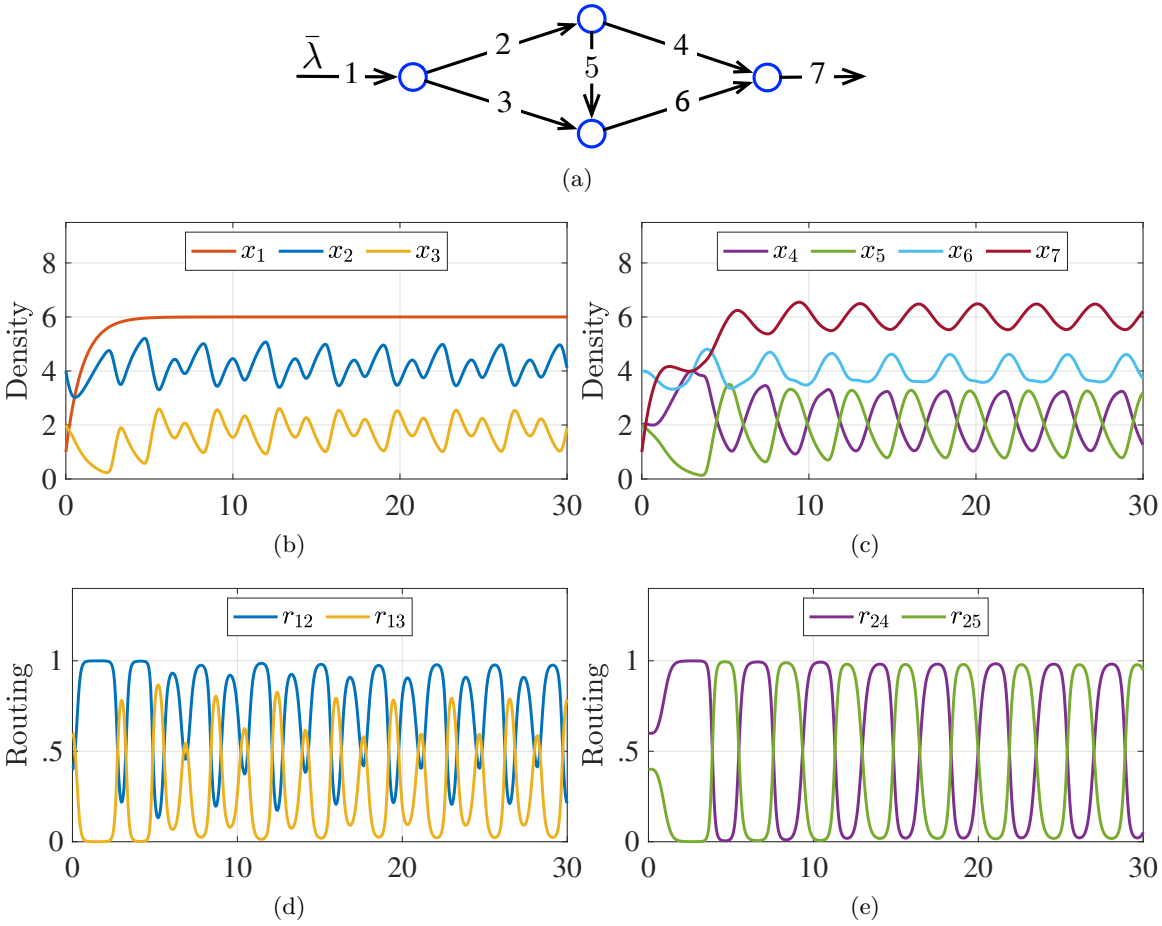

Figure 3.6: (a) Seven-link network. (b)-(c) Oscillating traffic state. (d)-(e) Oscillating routing state.

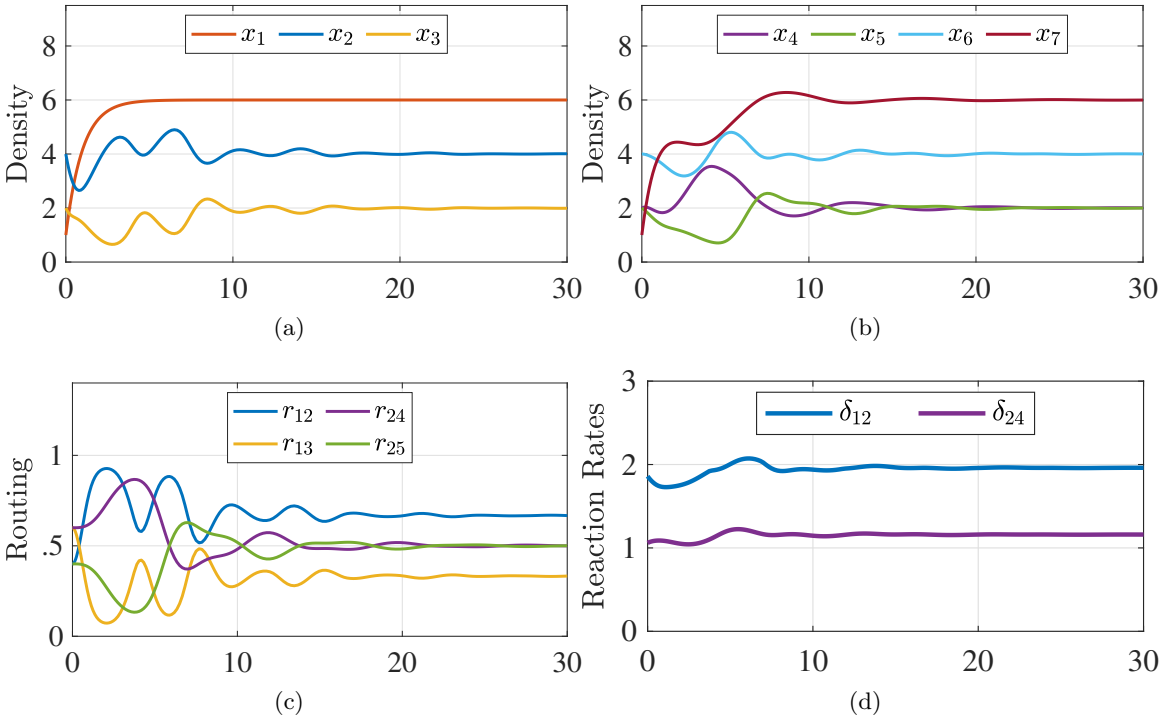

Figure 3.7: Asymptotic stability under congestion-aware reaction rates.

Chapter 4

Robust Network Optimization: Application to Traffic Intersections

In this chapter, we tackle the topic of network robustness by focusing on applications to urban traffic networks. Specifically, we consider the problem of controlling signalized traffic intersections in a robust fashion, with the goal of ensuring system-level optimality. We refer the reader to [4, 8] for a complete discussion of the technical results presented in this chapter.

4.1 Introduction

The design of feedback policies for the control of traffic infrastructures is an intensively-studied topic, and the available techniques can mainly be divided into three categories: routing policies, flow control, and intersections control. Routing policies rely on game-theoretic models to capture the behavior of the drivers and to influence their turning

preferences in order to optimize congestion objectives, and have been studied both in a centralized [47] and distributed [48] framework. Flow control uses a combination of speed limits and gating techniques to regulate the road flows and network inflows, respectively [49, 50]. Conversely, intersection control refers to the design of the scheduling of the (automated) intersections so that the flow through intersections is maximized, and can be achieved: (i) by controlling the signaling sequence and offset, and/or (ii) by designing the durations of the signaling phases. The control of signaling offsets typically aims at tuning the synchronization of green lights between adjacent intersections in order to produce green-wave effects [51], and consists of solving a group of optimization problems that take into account certain subparts of the infrastructure, while minimizing metrics such as the number of stops experienced by the vehicles. In contrast, the durations of green times at intersections affects the average behavior of the traffic flows in the network, and plays a significant role in the efficiency of large-scale networks [52].

Widely-used distributed signaling control programs include SCOOT [53], RHODES [54], OPAC [55], SCATS [56], and emerge as the most common techniques currently employed in major cities. The sub-optimal performance of these methods has recently motivated the development of Max-Pressure techniques [57]. The Max-Pressure controller is based on a store-and-forward model, where queues at intersections have unlimited capacity and, under this assumption, Max-Pressure is guaranteed to maximize the network throughput by stabilizing the network. Centralized policies require higher modeling efforts but, in general, have better performance guarantees [58]. Among the centralized policies, the Traffic-Responsive Urban Control [52] has received considerable interest for its simplicity

and good performance. Based on a store-and-forward modeling paradigm, the method consists in minimizing the network queue lengths through a linear-quadratic regulator that uses a relaxation of the physical constraints to abide with the high complexity. Variations of these techniques to incorporate physical constraints have been studied in [59, 60].

The tremendous complexity of urban traffic networks has recently motivated the adoption of model-free control methods that rely only on historical data [61] and, concurrently, the development of simplified models to deal with the switching nature of the traffic signals [62]. However, the highly-nonlinear behavior of these dynamical systems still limits our capability to consider adequate optimization and prediction horizons, and the development of tractable models capable of capturing all the relevant network dynamics is still an open problem.

Motivated by the considerable complexity of urban transportation systems, in this work we propose a simplified framework to capture the behavior of traffic networks operating in free-flow regimes with arbitrary travel speeds. In this model, each road is modeled through multiple state variables, representing the spatial evolution of traffic densities within the road. This assumption allows us to capture the non-uniform spatial displacement of traffic within each road, and to construct a simplified network model that results in a more-tractable framework for optimization.

We employ the proposed model to design the durations of the green times at the intersections, and we relate congestion objectives with the optimization of a metric of controllability of the dynamical system associated with the traffic network. To the best of the authors' knowledge, this work represents a novel, computationally-tractable, method

to perform network-wide optimization of the green-splits durations at intersections. We provide conditions that guarantee stability of the system, and we characterize the performance of the control policy in relation to the network congestion. We use the concept of smoothed spectral abscissa [22] to solve the optimization, and we demonstrate the benefits of our methods through a microscopic simulation on the urban interconnection of Manhattan, NY. We characterize the complexity of our algorithms, and propose a method to parallelize the computation so that it can be solved efficiently by a group of cooperating distributed agents. Our results and simulations suggest that the increased system performance obtained by our control method justifies the increment in complexity deriving from the adoption of a global system description.

The rest of this chapter is organized as follows. Section 4.2 illustrates our model of traffic network, and formalizes the problem of designing the durations of the green times at the intersections with the goal of optimizing vehicle evacuation. The section includes a discussion of the benefits in adopting a simplified model, and presents a comparison with more-established macroscopic models. Section 4.3 illustrates the proposed centralized approach to numerically solve the optimization problem, while Section 4.4 presents a technique to parallelize the computation among a set of distributed agents for more efficient computation. Section 4.5 is devoted to macroscopic and microscopic simulations to validate our modeling assumptions and optimization techniques.

4.2 Dynamical Model of Traffic Networks and Problem Formulation

We model urban traffic networks as a group of one-way roads interconnected through signalized intersections. Within each road, vehicles move at uniform velocity, while traffic flows are exchanged between adjacent roads by means of the signalized intersection connecting them. In this section, we discuss a concise dynamical model for traffic networks in certain regimes, that will be employed for the analysis.

4.2.1 Model of Road and Traffic Flow

Let $\mathcal{N} = (\mathcal{R}, \mathcal{I})$ denote a traffic network with roads $\mathcal{R} = \{r_1, \dots, r_{n_r}\}$ and intersections $\mathcal{I} = \{\mathcal{I}_1, \dots, \mathcal{I}_{n_\mathcal{I}}\}$. Each element in the set $\mathcal{R}$ models a one way link interconnecting two signalized intersections, whereas intersections regulate conflicting flows of traffic among adjacent roads (see Section 4.2.2). We assume that exogenous inflows enter the network at (source) roads $\mathcal{S} \subseteq \mathcal{R}$ and, similarly, vehicles exit the network at (destination) roads $\mathcal{D} \subseteq \mathcal{R}$, with $\mathcal{S} \cap \mathcal{D} = \varnothing$. The following standard connectivity assumption ensures that vehicles are allowed to leave the network.

Assumption 4.1. *For every road $r_i \in \mathcal{R}$ there exists at least one path in $\mathcal{N}$ from r_i to a road $r_j \in \mathcal{D}$.*

We denote by $\ell_i \in \mathbb{R}_{>0}$ the length of road r_i, and we model each road r_i by discretizing it into $\sigma_i = \lceil \ell_i / h \rceil$ segments of uniform length $h \in \mathbb{R}_{\geq 0}$ (see Fig. 4.1). We denote by $x_i^k \in \mathbb{R}$ the traffic density associated with the k-th segment of road r_i, $k \in \{1, \dots, \sigma_i\}$. We

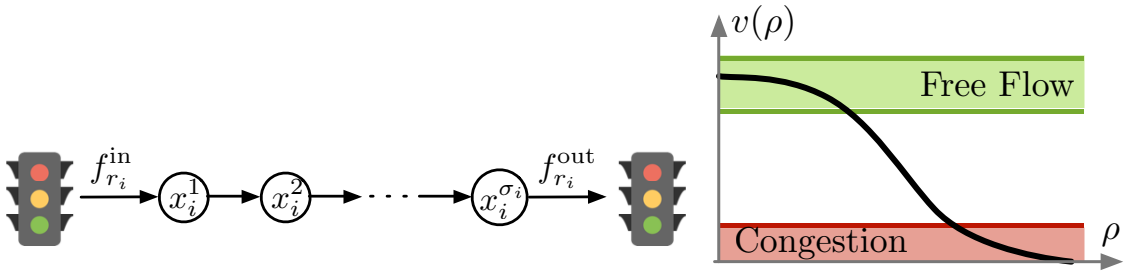

(a) (b)

Figure 4.1: (a) The portion of road comprised between two signalized intersections is modeled with a set of σ_i variables. (b) The almost-flat behavior in regimes of free-flow or congestion motivates our approximation $\gamma(\rho_i) \approx \gamma_i$.

assume that inflows of vehicles $f_{r_i}^{\text{in}}$ enter the road in correspondence of its upstream segment (i.e. $k = 1$); accordingly, outflows $f_{r_i}^{\text{out}}$ leave the road in correspondence of its downstream segment (i.e. $k = \sigma_i$). We approximate the relationship between traffic flows and densities by assuming that vehicles move from upstream to downstream with uniform velocity γ_i. Then, the dynamics of the road state $x_i = [x_i^1 \cdots x_i^{\sigma_i}]^\mathsf{T}$ are described by:

$$\begin{bmatrix} \dot{x}_i^1 \\ \dot{x}_i^2 \\ \vdots \\ \dot{x}_i^{\sigma_i} \end{bmatrix} = \underbrace{\frac{\gamma_i}{h} \begin{bmatrix} -1 & & & \\ 1 & -1 & & \\ & \ddots & \ddots & \\ & & 1 & 0 \end{bmatrix}}_{D_i} \begin{bmatrix} x_i^1 \\ x_i^2 \\ \vdots \\ x_i^{\sigma_i} \end{bmatrix} + \begin{bmatrix} f_{r_i}^{\text{in}} \\ 0 \\ \vdots \\ -f_{r_i}^{\text{out}} \end{bmatrix}. \tag{4.1}$$

Differently from more-established network models where a single state variable is associated to a uniform road segment (e.g., [57, 34]), the choice of a constant space-discretization step allows us to capture the fact that the density of vehicles may not be uniform along the road.

Remark 4.2. ***(Equivalence with Hydrodynamic Models)*** *The dynamical model* (4.1) *derives from the mass-conservation continuity equation [63] in certain traffic regimes, as we explain next. Let* $\rho_i = \rho_i(s,t) \geq 0$ *denote the (continuous) density of vehicles within road* r_i *at the spatial coordinate* $s \in [0, \ell_i]$ *and time* $t \in \mathbb{R}_{\geq 0}$*. Let* $f_i = f_i(s,t) \geq 0$ *denote the (continuous) flow of vehicles along the road, and let traffic densities and traffic flows follow the hydrodynamic relation*

$$\frac{\partial \rho_i}{\partial t} + \frac{\partial f_i}{\partial s} = 0.$$

We complement the above equation with the Lighthill-Whitham-Richards relation $f_i = f_i(\rho_i)$*, where flows instantaneously change with the density. Then, we include the speed-density fundamental relationship* $f_i = \rho_i v(\rho_i)$*, where* $v : \mathbb{R}_{\geq 0} \to \mathbb{R}_{\geq 0}$ *represents the speed of flow, to obtain*

$$\frac{\partial \rho_i}{\partial t} + \left(v(\rho_i) + \rho_i \frac{d\ v(\rho_i)}{d\rho_i} \right) \frac{\partial \rho_i}{\partial s} = 0.$$

Solutions to the above relation are kinematic waves [64], moving at speed $\gamma(\rho_i) = v(\rho_i) + \rho_i \frac{dv(\rho_i)}{d\rho_i}$*. We consider regimes where the speed of the kinematic wave can be approximated as* $\gamma(\rho_i) \approx \gamma_i$*. As illustrated in Fig. 4.1(b), this approximation is accurate in regimes of free flow or congestion, characterized by* $\frac{dv(\rho_i)}{d\rho_i} \approx 0$*. By letting* γ_i *denote the average speed of flow, the approximated continuity equation reads*

$$\frac{\partial \rho_i}{\partial t} + \gamma_i\ \frac{\partial \rho_i}{\partial s} = 0.$$

We then discretize in space the above relation by defining the discrete spatial coordinate

$$s_k = kh, \qquad\qquad k \in \{0, \ldots, \sigma_i\},$$

and by replacing the partial derivative with respect to s with the difference quotient

$$\frac{\partial \rho_i(s_k, t)}{\partial t} = -\gamma_i \, \frac{\rho_i(s_k, t) - \rho_i(s_{k-1}, t)}{h}.$$

This discretization leads to the dynamical model (4.1)*, by introducing the boundaries inflows $f_{r_i}^{\text{in}}$ and outflows $f_{r_i}^{\text{out}}$, and by replacing $\rho_i(s_k, t)$ with the compact notation x_i^k.* □

4.2.2 Model of Intersection and Interconnection Flow

Signalized intersections alternate the right-of-way of vehicles to coordinate and secure conflicting flows between adjacent roads. Every signalized intersection $\mathcal{I}_j \in \mathcal{I}$, $j \in \{1, \ldots, n_{\mathcal{I}}\}$, is modeled as a set $\mathcal{I}_j \subseteq \mathcal{R} \times \mathcal{R}$, consisting of all allowed movements between the intersecting roads. For road $r_i \in \mathcal{R}$, let $\mathcal{I}_{\text{in}}^{r_i}$ denote the (unique) intersection at road upstream; similarly, let $\mathcal{I}_{\text{out}}^{r_i}$ denote the (unique) intersection at road downstream. We model the switching behavior of a signalized intersection through the green split function $s : \mathcal{R} \times \mathcal{R} \times \mathbb{R}_{\geq 0} \to \{0, 1\}$ that assumes boolean values 1 (green phase) or 0 (red phase),

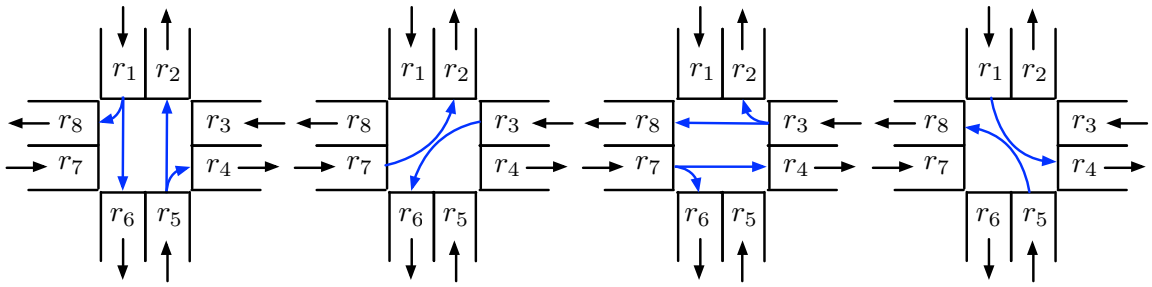

Figure 4.2: Typical set of phases at a four-ways intersection.

and let the interconnection flows be

$$f_{r_i}^{\text{in}} = \sum_{(r_i,r_k)\in\mathcal{I}_{\text{in}}^{r_i}} s(r_i, r_k, t)\, f(r_i, r_k) + u_{r_i},$$
$$f_{r_i}^{\text{out}} = \sum_{(r_k,r_i)\in\mathcal{I}_{\text{out}}^{r_i}} s(r_k, r_i, t)\, f(r_k, r_i) + w_{r_i}, \tag{4.2}$$

where $f : \mathcal{R} \times \mathcal{R} \to \mathbb{R}_{\geq 0}$ denotes the intersection transmission rate. We remark that the notation $f(r_i, r_k)$ represents the transmission rate from road r_k to r_i and, similarly, $s(r_i, r_k, t)$ denotes the green split function that controls traffic flows from r_k and directed to r_i. We note that equation (4.2) incorporates the exogenous inflows and outflows to each road (flows of traffic that are not originated or merge to modeled intersections or roads) through the terms $u_{r_i} : \mathbb{R}_{\geq 0} \to \mathbb{R}_{\geq 0}$ and $w_{r_i} : \mathbb{R}_{\geq 0} \to \mathbb{R}_{\geq 0}$, respectively. We note that $u_{r_i} \neq 0$ if and only if r_i is a source road (that is, $r_i \in \mathcal{S}$), and $w_{r_i} \neq 0$ if and only if r_i is a destination road (that is, $r_i \in \mathcal{D}$).

Example 4.3. ***(Intersections and Scheduling Functions)*** *Consider the four-ways intersection $\mathcal{I}_1$ illustrated in Fig. 4.2. The intersection is modeled through the set of allowed*

movements

$$\mathcal{I}_1 = \{(r_1, r_6), (r_1, r_8), (r_5, r_2), (r_5, r_4), (r_7, r_2), (r_3, r_6),$$
$$(r_3, r_8), (r_3, r_2), (r_7, r_4), (r_7, r_6), (r_5, r_8), (r_1, r_4)\}.$$

Allowed movements at a certain intersections are typically grouped into sets of phases, where each phase represents a set of movements that can occur simultaneously. For $\mathcal{I}_1$*, a typical set of phases is* $\{\mathcal{P}_1, \mathcal{P}_2, \mathcal{P}_3, \mathcal{P}_4\}$*, where*

$$\mathcal{P}_1 = \{(r_1, r_6), (r_1, r_8), (r_5, r_2), (r_5, r_4)\},$$
$$\mathcal{P}_2 = \{(r_7, r_2), (r_3, r_6)\},$$
$$\mathcal{P}_3 = \{(r_3, r_8), (r_3, r_2), (r_7, r_4), (r_7, r_6)\},$$
$$\mathcal{P}_4 = \{(r_5, r_8), (r_1, r_4)\}.$$

The green split function alternates the set of available phases within the cycle time $T \in \mathbb{R}_{>0}$*, that is, for given scalars* t_0, t_1, t_2, t_3, t_4*, with* $0 = t_0 \leq t_1 \leq t_2 \leq t_3 \leq t_4 = T$*, denoting the switching instants, the green split function is*

$$s(r_i, r_k, t) = \begin{cases} 1 & \text{if } (r_i, r_k) \in \mathcal{P}_j \text{ and } t \in [t_{j-1}, t_j), \\ 0 & \text{otherwise,} \end{cases}$$

where $j \in \{1, \ldots, 4\}$. □

We model the transmission rate during a green-light phase as a function proportional to the density of vehicles "waiting" in the downstream section of the road, that is,

$$f(r_i, r_k) = c(r_i, r_k) x_k^{\sigma_k}, \tag{4.3}$$

where $c : \mathcal{R} \times \mathcal{R} \to \mathbb{R}_{\geq 0}$. In particular, $c(r_i, r_k)$ incorporates the turning preferences of the drivers when decomposing $c(r_i, r_k) = \varphi(r_i, r_k)\phi(r_i, r_k)$, where $\varphi : \mathcal{R} \times \mathcal{R} \to [0, 1]$ represents the average routing ratio of vehicles entering road r_i after exiting r_k, $\sum_i \varphi(r_i, r_k) = 1$, and $\phi : \mathcal{R} \times \mathcal{R} \to \mathbb{R}_{\geq 0}$ captures the speed of the outflow from the dedicated turn lane.

Differently from traditional traffic network models where a single state variable is typically used to model a uniform road segment [57, 34], our model associates multiple state variables to each road segment interconnecting two signalized intersections. This approach allows us to capture the fact that the density of vehicles may not be uniform along each link, and to model the outflows during a green-light phase as functions that depend only on the state of the section of road that is located in the proximity of the intersection. The precision of the illustrated model is demonstrated through a set of microscopic simulations in [65] for a small scale network.

Remark 4.4. ***(Model Validity and Limitations)*** *Two main limitations can be identified in the simplified modeling settings considered in this work with respect to more comprehensive models, such as [34]. First, our model assumes a constant speed of flow along each road segment connecting two signalized intersections. Second, the linear approximation does not allow to limit the inflow to a certain road when that road is congested, which corresponds to the assumption that roads have infinite capacity. We remark, however, that these*

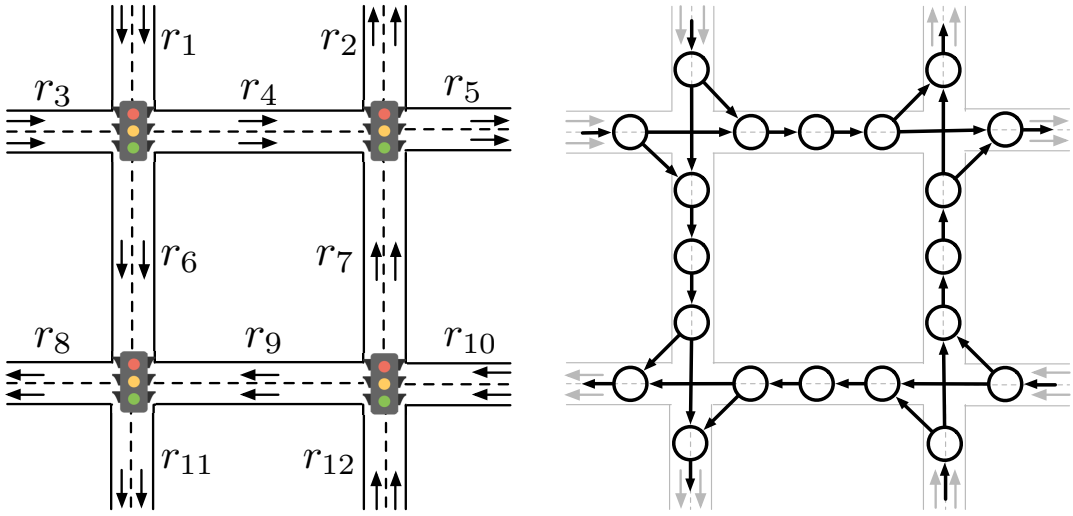

(a) (b)

Figure 4.3: Network model associated with a traffic network composed of $n_{\mathcal{I}} = 4$ intersections and $n_{\mathrm{r}} = 12$ roads. Each road is associated with a set of states that represent the density of the cells within the roads.

two phenomena can be captured by appropriately tuning the parameters γ_i and $\phi(r_i, r_k)$, respectively, when these situations occur. Thus, if the network conditions do not change significantly fast with respect to the network dynamics, one can tune the parameters γ_i and $\phi(r_i, r_k)$ and occasionally re-update the model to capture the current network conditions. We anticipate that, although this approach implies that the model is accurate only in the current network regime, the approach is well-suited for the receding horizon technique that will be later adopted in this chapter (see Section 4.2.4). □

4.2.3 Switching and Time-Invariant Traffic Network Dynamics

Individual road dynamics can be combined into a joint network model that captures the interactions among all modeled routes and intersections. To this aim, we adopt

an approach similar to [60], and assume that exogenous outflows are proportional to the number of vehicles in the road, that is, $w_{r_i} = \bar{w}_{r_i} x_i^{\sigma_i}$, $\bar{w}_{r_i} \in [0, 1]$. By combining Equations (4.1), (4.2) and (4.3), we obtain

$$\underbrace{\begin{bmatrix} \dot{x}_1 \\ \dot{x}_2 \\ \vdots \\ \dot{x}_{n_\mathrm{r}} \end{bmatrix}}_{\dot{x}} = \underbrace{\begin{bmatrix} A_{11} & A_{12} & \cdots & A_{1n_\mathrm{r}} \\ A_{21} & A_{22} & \ddots & A_{2n_\mathrm{r}} \\ \vdots & \ddots & \ddots & \vdots \\ A_{n_\mathrm{r}1} & A_{n_\mathrm{r}2} & \cdots & A_{n_\mathrm{r}n_\mathrm{r}} \end{bmatrix}}_{A} \underbrace{\begin{bmatrix} x_1 \\ x_2 \\ \vdots \\ x_{n_\mathrm{r}} \end{bmatrix}}_{x} + \underbrace{\begin{bmatrix} I_{n_1} & 0 & \cdots & 0 \\ 0 & I_{n_2} & \ddots & 0 \\ \vdots & \ddots & \ddots & \vdots \\ 0 & 0 & \cdots & I_{n_\mathrm{r}} \end{bmatrix}}_{B} \underbrace{\begin{bmatrix} u_1 \\ u_2 \\ \vdots \\ u_{n_\mathrm{r}} \end{bmatrix}}_{u}, \tag{4.4}$$

where $A \in \mathbb{R}^{n \times n}$, $n = \sum_{i=1}^{n_\mathrm{r}} \sigma_i$ is the overall number of states, u derives from (4.2), and

$$A_{ik} = \begin{cases} s(r_i, r_k, t) c(r_i, r_k) e_1 e_{\sigma_k}^\mathsf{T}, & \text{if } i \neq k, \\ D_i - \left(\sum_\ell s(r_\ell, r_i, t) c(r_\ell, r_i) + \bar{w}_{r_i}\right) e_{\sigma_i} e_{\sigma_i}^\mathsf{T}, & \text{if } i = k, \end{cases}$$

where $e_i = [0 \ldots 1 \ldots 0]^\mathsf{T}$ is a vector with a single nonzero entry with value 1 in position i and of appropriate dimension.

We note that the matrix A in (4.4) is typically sparse because not all roads are adjacent in the interconnection, and its sparsity pattern varies over time as determined by the splits $s(r_i, r_k, t)$. Thus, the network model (4.4) is a linear switching system, where the switching signals are the split functions.

Example 4.5. ***(Traffic Network Interconnection)*** *Consider the network illustrated in Fig. 4.3, with $\mathcal{R} = \{r_1, \ldots, r_{12}\}$ and $\mathcal{I} = \{\mathcal{I}_1, \ldots, \mathcal{I}_4\}$. The network comprises four destination roads $\mathcal{D} = \{r_2, r_5, r_8, r_{11}\}$ ($\bar{w}_{r_i} = 1$ for all $r_i \in \mathcal{D}$, and $\bar{w}_{r_i} = 0$ otherwise), and*

four source roads ($\mathcal{S} = \{r_1, r_3, r_{10}, r_{12}\}$, with $u_{r_i} \neq 0$ only if $r_i \in \mathcal{S}$). Let $\ell_i/h = 3$ and $\gamma_i/h = 3$ for all $i \in \{1, \ldots, n_r\}$. Then, the matrices in (4.4) read as

$$A_{ii} = \begin{bmatrix} -1 & & \\ 1 & -1 & \\ & 1 & -\left(\sum_\ell s(r_\ell, r_i, t)c(r_\ell, r_i) + \bar{w}_{r_i}\right) \end{bmatrix},$$

$$A_{ij} = \begin{bmatrix} 0 & 0 & s(r_i, r_j, t)c(r_i, r_j) \\ 0 & 0 & 0 \\ 0 & 0 & 0 \end{bmatrix},$$

for all $i, j \in \{1, \ldots, n_{\mathrm{r}}\}$. Notice that $s(r_i, r_j, t) = 0$ for all times if $(r_j, r_k) \notin \mathcal{I}_k$ for all $k \in \{1, \ldots, n_{\mathcal{I}}\}$. □

Next, we make the classical assumption that scheduling functions are periodic, with period $T \in \mathbb{R}_{>0}$. That is, for all $(r_i, r_k) \in \mathcal{I}_j$, $j \in \{1, \ldots, n_{\mathcal{I}}\}$, and for all times t:

$$s(r_i, r_k, t) = s(r_i, r_k, t + T).$$

Let $\mathcal{T} = \{\tau_1, \ldots, \tau_m\}$ denote the set of time instants when a scheduling function changes its value, that is,

$$\mathcal{T} = \{\tau \in [0, T] \ : \ \exists (r_i, r_k) \in \mathcal{I}, \lim_{t \to \tau^-} s(r_i, r_k, t) \neq \lim_{t \to \tau^+} s(r_i, r_k, t)\}.$$

Notice that the matrix A in (4.4) remains constant between consecutive time instants τ_{i-1} and τ_i. We denote each constant matrix by A_i, and refer to it as to the i-th *network mode*. Further, let $d_i = \tau_i - \tau_{i-1}$, with $i \in \{1, \ldots, m\}$ and $\tau_0 = 0$, denote the duration of the i-th network mode. We employ a state-space averaging technique [66] and define a linear, time-invariant, approximation of the switching network model (4.4):

$$\dot{x}_{\text{av}} = A_{\text{av}} x_{\text{av}} + B u_{\text{av}}, \tag{4.5}$$

where $A_{\text{av}} = \frac{1}{T} \sum_{i=1}^{m} d_i A_i$, and $u_{\text{av}} = [u_{\text{av},1} \ldots u_{\text{av},n_{\text{r}}}]$, $u_{\text{av},i} = (1/T) \int_0^T u_i(\tau)\ d\tau$. We note that the averaging technique preserves the sparsity pattern of the network, that is, $A_{\text{av}}(i,j) \neq 0$ if and only if $A_k(i,j) \neq 0$ for some k.

In general, the approximation of the behavior of the switching system (4.4) with the average dynamics (4.5) is accurate if the operating period T is short in comparison to the underlying system dynamics. Under suitable technical assumptions, a bound on the deviation of average models with respect to the network instantaneous state has been characterized in [66]. In particular, the bound becomes tighter for decreasing values of T and increasing values of road lengths. A numerical validation of the averaging technique and its validity in relation to T is discussed in Section 4.5 (see Fig. 4.5).

4.2.4 Problem Formulation

In this chapter, we consider the average model (4.5) and focus on the problem of designing the durations of the green split functions so that a measure of network efficiency is optimized. Motivated by the relationship $A_{\text{av}} = \frac{1}{T} \sum_{i=1}^{m} d_i A_i$ (see (4.5)), the average

model allows us to design the durations of the network modes, rather than their exact sequence. This approach motivates the adoption of a two-stage optimization process. First, the durations of the modes is optimized by considering a global model that captures the dynamics of the entire interconnection. Second, offset optimization techniques (e.g. [51]) can be employed to decide the specific sequence of phases given the durations of the splits, and by considering reduced or local interconnection models. This chapter is devoted to the former. To formalize our optimization problem, we denote by y_{av} the vector of the queue lengths originated by the signalized intersections, and model y_{av} as the density of vehicles "waiting" at the downstream section of each road:

$$y_{\text{av}} = C_{\text{av}} x_{\text{av}}, \qquad C_{\text{av}} = \begin{bmatrix} e_{\sigma_1}^{\mathsf{T}} & \dots & 0 \\ \vdots & \ddots & \\ 0 & \dots & e_{\sigma_{n_{\text{r}}}}^{\mathsf{T}} \end{bmatrix}. \tag{4.6}$$

We assume the network is initially at a certain initial state x_0, and focus on the problem of optimally designing the mode durations $\{d_1, \dots d_m\}$ that minimize the $\mathcal{H}_2$-norm

of the vector of queue lengths y_{av}, formalized as follows

$$\min_{d_1,\ldots,d_m} \quad \int_0^\infty \|y_{\text{av}}\|_2^2 \, dt,$$

$$\text{subject to} \quad \dot{x}_{\text{av}} = A_{\text{av}} x_{\text{av}}, \tag{4.7a}$$

$$y_{\text{av}} = C_{\text{av}} x_{\text{av}}, \tag{4.7b}$$

$$x_{\text{av}}(0) = x_0, \tag{4.7c}$$

$$A_{\text{av}} = \frac{1}{T}\left(d_1 A_1 + \cdots + d_m A_m\right), \tag{4.7d}$$

$$T = d_1 + \cdots + d_m, \tag{4.7e}$$

$$d_i \geq 0 \quad i \in \{1, \ldots, m\}. \tag{4.7f}$$

Loosely speaking, the optimization problem (4.7) seeks for an optimal set of split durations that minimize the $\mathcal{L}_2$-norm of the impulse-response of the system to the initial conditions. Thus, similarly to [50], our framework considers the "cool down" period, where exogenous inflows and outflows are not known a priori, and the goal is to evacuate the network as fast as possible where the final condition is an empty system. In order to take into account for the model inaccuracies due to linearization and time-averaging, the matrix A_{av} and the initial state x_0 shall be updated when the network conditions have significantly changed, and the solution to (4.7) shall be recomputed with the updated parameters. In particular, we denote by T_{update} the time interval between two updates, and note that T_{update} is a fundamental design parameter that should be accurately chosen. Finally, we note that constraint (4.7e) implies that for any solution to (4.7) there exists a set of split with the selected green durations, and thus ensures feasibility of the solutions.

4.3 Design of Optimal Network Mode Durations

In this section we propose a method to determine solutions to the optimization problem (4.7). The approach we discuss is centralized, namely, it requires full knowledge of the network dynamics and initial state. An extension of the framework to fit a distributed implementations is proposed in Section 4.4. Our approach consists in rewriting the cost function in (4.7) in terms of the controllability Gramian of the associated dynamical system, and is formalized next.

Lemma 4.6. ***(Controllability Gramian Cost Function)*** *Let*

$$\mathcal{W}(A_{\text{av}}, x_0) = \int_0^\infty e^{A_{\text{av}}t} x_0 x_0^{\mathsf{T}} e^{A_{\text{av}}^{\mathsf{T}}t} \ \ dt.$$

The following minimization problem is equivalent to (4.7)*:*

$$\begin{aligned} \underset{d_1,\dots,d_m}{min} \quad & \text{Trace}\left(C_{\text{av}}\ \mathcal{W}(A_{\text{av}}, x_0)\ C_{\text{av}}^{\mathsf{T}}\right), \\ \textit{subject to} \quad & A_{\text{av}} = \frac{1}{T}\left(d_1 A_1 + \cdots + d_m A_m\right), \\ & T = d_1 + \cdots + d_m, \\ & d_i \geq 0, \quad i \in \{1, \dots, m\}. \end{aligned} \tag{4.8}$$

Proof. By incorporating (4.7a), (4.7b), and (4.7c) into the cost function of optimization problem (4.7), we can rewrite:

$$\begin{aligned}\int_0^\infty \|y_{\text{av}}\|_2^2 \, dt &= \int_0^\infty x_0^\mathsf{T} e^{A_{\text{av}}^\mathsf{T} t} C_{\text{av}}^\mathsf{T} C_{\text{av}} e^{A_{\text{av}} t} x_0 \, dt \\ &= \text{Trace}\left(\int_0^\infty x_0^\mathsf{T} e^{A_{\text{av}}^\mathsf{T} t} C_{\text{av}}^\mathsf{T} C_{\text{av}} e^{A_{\text{av}} t} x_0 \, dt \right) \\ &= \int_0^\infty \text{Trace}\left(C_{\text{av}} e^{A_{\text{av}} t} x_0 x_0^\mathsf{T} e^{A_{\text{av}}^\mathsf{T} t} C_{\text{av}}^\mathsf{T} \right) dt \\ &= \text{Trace}\left(C_{\text{av}} \int_0^\infty e^{A_{\text{av}} t} x_0 x_0^\mathsf{T} e^{A_{\text{av}}^\mathsf{T} t} dt \; C_{\text{av}}^\mathsf{T} \right),\end{aligned}$$

from which the claimed statement follows. ■

We now use the above result to characterize the stability of the proposed control policy. To this aim, we note that the cost function in (4.7) is finite only if the choice of parameters $\{d_1, \ldots, d_m\}$ leads to a matrix A_{av} that is Hurwitz-stable. Requiring Hurwitz stability of A_{av} corresponds to imposing that all real parts of the eigenvalues of A_{av} are strictly negative. Formally, we require $\alpha(A_{\text{av}}) < 0$, where $\alpha(A_{\text{av}}) := \sup\{\Re(s) : s \in \mathbb{C}, \det(sI - A_{\text{av}}) = 0\}$ denotes the spectral abscissa of A_{av}. The following result proves stability of the system under optimal green time durations.

Theorem 4.7. ***(Stability of Optimal Solutions)*** *Let Assumption 4.1 be satisfied and let $s(r_i, r_k, \bar{t}) \neq 0$ for all $(r_i, r_k) \in \mathcal{I}$, and for some $\bar{t} \in [0, T]$. Then,*

$$\alpha(A_{\text{av}}) < 0.$$

Proof. From the structure of (4.4) and from the assumption $s(r_i, r_k, \bar{t}) \neq 0$ follows that $A_{\text{av}}(i,i) < 0$ for all $i \in \{1, \ldots, n\}$, while $A_{\text{av}}(i,j) \geq 0$ for all $j \in \{1, \ldots, n\}$, $j \neq i$. Moreover, all columns of A_{av} have nonpositive sum. In particular, the columns corresponding to destination cells have strictly negative sum, that is, $\sum_{i=1}^{n} A_{\text{av}}(i,j) \leq 0$ for all $j \in \{1, \ldots, n\}$, and $\sum_{i=1}^{n} A_{\text{av}}(i,j) < 0$ for all j such that $r_j \in \mathcal{D}$. To show $\alpha(A_{\text{av}}) < 0$, we use the fact that destination cells in $\mathcal{D}$ have no departing edges, and re-order the states so that

$$A_{\text{av}} = \begin{bmatrix} A_{11} & 0 \\ A_{21} & A_{22} \end{bmatrix},$$

where $A_{22} \in \mathbb{R}^{n_d \times n_d}$, $n_d = |\mathcal{D}|$, is the submatrix that describes the dynamics of the destination cells, $A_{11} \in \mathbb{R}^{(n-n_d)\times(n-nd)}$, and $A_{21} \in \mathbb{R}^{n_d \times (n-nd)}$. The fact $\alpha(A_{22}) < 0$ immediately follows from (4.2). The stability of A_{11} follows from the connectivity assumption in the original network, and from the analysis of grounded Laplacian matrices (see e.g. [67, Theorem 1]). ■

Next, we discuss a method to determine solutions to the optimization problem (4.8). Our technique relies on constructing a new optimization problem that constitutes a relaxation of (4.8), and that builds upon the concept of smoothed spectral abscissa. The smoothed spectral abscissa is a generalization of the spectral abscissa [22] and, for a dynamical system of the form (4.5)-(4.6), it is defined as the root $\tilde{\alpha} \in \mathbb{R}$ of the implicit equation

$$\text{Trace}\left(C_{\text{av}}\ \mathcal{W}(A_{\text{av}} - \tilde{\alpha} I, B)\ C_{\text{av}}^{\mathsf{T}}\right) = \epsilon^{-1}, \tag{4.9}$$

where $\epsilon \in \mathbb{R}_{\geq 0}$. It is worth noting that the root $\tilde{\alpha}$ is unique [22], and for fixed B and C_{av} it is a function of both ϵ and A_{av}. Formally, we shall denote $\tilde{\alpha} = \tilde{\alpha}(\epsilon, A_{\text{av}})$.

Remark 4.8. ***(Properties of the Smoothed Spectral Abscissa)*** *For any $\epsilon > 0$, the smoothed spectral abscissa is an upper bound to $\alpha(A)$, and this bound becomes exact as $\epsilon \to 0$. To see this, we first observe that the integral $\int_0^\infty e^{(A_{\text{av}}-\tilde{\alpha}I)t} B B^{\mathsf{T}} e^{(A_{\text{av}}-\tilde{\alpha}I)^{\mathsf{T}} t} dt$ exists and is finite for any $\tilde{\alpha} > \alpha(A_{\text{av}})$, as the function $e^{(A_{\text{av}}-\tilde{\alpha}I)t}$ is bounded and convergent as $t \to +\infty$. On the other hand, for any $\tilde{\alpha} < \alpha(A_{\text{av}})$ the function $e^{(A_{\text{av}}-\tilde{\alpha}I)t}$ becomes unbounded for $t \to +\infty$ and the above integral is infinite. It follows that, the left-hand side of* (4.9) *is finite only if $\tilde{\alpha} > \alpha(A)$ or, in other words, for any finite ϵ, $\tilde{\alpha}$ satisfies $\tilde{\alpha} > \alpha(A)$.* □

By letting $\tilde{\alpha} = 0$ in (4.9), we recast the optimization problem (4.8) in terms of the smoothed spectral abscissa as follows:

$$\begin{aligned} \min_{d_1,\ldots,d_m,\epsilon} \quad & \epsilon^{-1}, \\ \text{subject to} \quad & A_{\text{av}} = \frac{1}{T}\left(d_1 A_1 + \cdots + d_m A_m\right), \\ & T = d_1 + \cdots + d_m, \\ & d_i \geq 0, \quad i \in \{1, \ldots, m\}, \\ & \tilde{\alpha}(\epsilon, A_{\text{av}}) = 0, \end{aligned} \tag{4.10}$$

where the parameter ϵ is now an optimization variable. In what follows, we denote by $\{d_1^*, \ldots, d_m^*, \epsilon^*\}$ the value of the optimization parameters at optimality of (4.10). Problem (4.10) is a nonlinear optimization problem [22], because the optimization variables $\{d_1, \ldots, d_m\}$ and ϵ are related by means of the nonlinear equation (4.9).

For the solution of (4.10), we propose an iterative two-stages numerical optimization process. In the first stage, we fix the value of ϵ and seek for a choice of $\{d_1, \dots d_m\}$ that leads to a smoothed spectral abscissa that is identically zero. In other words, we let $\epsilon = \bar{\epsilon}$ (fixed), and solve the following minimization problem:

$$\begin{aligned} \min_{d_1,\dots,d_m} \quad & |\tilde{\alpha}(\bar{\epsilon}, A_{\text{av}})| \\ \text{subject to} \quad & A_{\text{av}} = \frac{1}{T}\left(d_1 A_1 + \cdots + d_m A_m\right), \\ & T = d_1 + \cdots + d_m, \\ & d_i \geq 0, \quad i \in \{1, \dots, m\}. \end{aligned} \tag{4.11}$$

We note that every a solution to (4.11), namely $\bar{A}_{\text{av}}$, which satisfies $\tilde{\alpha}(\bar{\epsilon}, \bar{A}_{\text{av}}) = 0$, is a point in the feasible set of (4.10) that corresponds to a cost of congestion $\int_0^\infty \|y_{\text{av}}\|_2^2 \, dt = 1/\bar{\epsilon}$.

In the second stage of the optimization, we perform a line-search over the parameter ϵ. In particular, the value of ϵ is iteratively increased until the minimizer ϵ^* is achieved. This approach is motivated by the fact that the optimizer of (4.11) with ϵ set to $\epsilon = \epsilon^*$ is $\{d_1^*, \dots, d_m^*\}$, that is, the optimal solution to (4.10). Finally, the iterative process is concluded when $\tilde{\alpha}(\bar{\epsilon}, A_{\text{av}}) = 0$ is no longer achievable in (4.11).

The benefit of considering a two-stage optimization process and of solving (4.11) as opposed to (4.10) is that we can derive an expression for the gradient of the cost function $\tilde{\alpha}(\bar{\epsilon}, A_{\text{av}})$ with respect to the parameters $\{d_1, \dots, d_m\}$. The derivation of the descent direction is the focus of the remaining part of this section. In the remainder, with a slight abuse

of notation, we use the compact form $\tilde{\alpha}(\bar{\epsilon}, A_{\rm av}) = \tilde{\alpha}_{\bar{\epsilon}}$ and,for a matrix $M = [m_{ij}] \in \mathbb{R}^{m\times n}$, we denote its vectorization by $M^{\rm vec} = [m_{11} \dots m_{m1}, m_{12} \dots m_{mn}]^{\mathsf{T}}$.

Lemma 4.9. (*Descent Direction*) *Let $\tilde{\alpha}_{\bar{\epsilon}}$ denote the unique root of* (4.9) *with $\bar{\epsilon} \in \mathbb{R}_{>0}$. Let $d = [d_1, \dots, d_m]^{\mathsf{T}}$, and let $K = \frac{1}{T}[A_1^{\rm vec}\ A_2^{\rm vec}\ \dots\ A_m^{\rm vec}]$. Then,*

$$\frac{\partial \tilde{\alpha}_{\bar{\epsilon}}}{\partial d} = K^{\mathsf{T}} \left(\frac{QP}{\mathrm{Trace}\,(QP)} \right)^{\rm vec}$$

where $P \in \mathbb{R}^{n\times n}$ and $Q \in \mathbb{R}^{n\times n}$ are the unique solution to the two Lyapunov equations

$$\begin{aligned} (A_{\rm av} - \tilde{\alpha}_{\bar{\epsilon}} I)\ P + P(A_{\rm av} - \tilde{\alpha}_{\bar{\epsilon}} I)^{\mathsf{T}} + x_0 x_0^{\mathsf{T}}\ &= 0, \\ (A_{\rm av} - \tilde{\alpha}_{\bar{\epsilon}} I)^{\mathsf{T}} Q + Q(A_{\rm av} - \tilde{\alpha}_{\bar{\epsilon}} I)\ + C_{\rm av} C_{\rm av}^{\mathsf{T}} &= 0, \end{aligned} \tag{4.12}$$

and $I \in \mathbb{R}^{n\times n}$ denotes the identity matrix.

Proof. The expression for the partial derivative of the smoothed spectral abscissa with respect to d can be obtained from the composite function

$$\frac{\partial \tilde{\alpha}_{\bar{\epsilon}}}{\partial d} = \frac{\partial A_{\rm av}}{\partial d}\ \frac{\partial \tilde{\alpha}_{\bar{\epsilon}}}{\partial A_{\rm av}},$$

where $\frac{\partial A_{\rm av}}{\partial d}$ follows immediately from (4.7d), and the expression for the derivative of $\tilde{\alpha}_{\bar{\epsilon}}$ with respect to $A_{\rm av}$ is given in [22, Theorem 3.2]. ■

We remark that the equations (4.12) always admit a unique solution. To see this, we use the fact that $\tilde{\alpha}$ is an upper bound to $\alpha(A_{\rm av})$, and observe that $(A_{\rm av} - \tilde{\alpha}_{\bar{\epsilon}} I)$ is

Algorithm 1: Centralized solution to (4.7).

Input: Matrix C_{av}, vector x_0, scalars ξ, μ
Output: $\{d_1^*, \dots d_m^*, \epsilon^*\}$ solution to (4.7)

1 Initialize: $d^{(0)}$, $\bar{\epsilon} = 0$, $k = 1$
2 **while** $\tilde{\alpha}_{\bar{\epsilon}}^{(k)} = 0$ **do**
3 **repeat**
4 Compute $\tilde{\alpha}_{\bar{\epsilon}}^{(k)}$ by solving (4.9);
5 Solve for P and Q: $(A_{\text{av}}^{(k)} - \alpha_{\bar{\epsilon}}^{(k)} I)P + P(A_{\text{av}}^{(k)} - \alpha_{\bar{\epsilon}}^{(k)} I)^{\mathsf{T}} + x_0 x_0^{\mathsf{T}} = 0$;
  $(A_{\text{av}}^{(k)} - \alpha_{\bar{\epsilon}}^{(k)} I)^{\mathsf{T}} Q + Q(A_{\text{av}}^{(k)} - \alpha_{\bar{\epsilon}}^{(k)} I) + C_{\text{av}} C_{\text{av}}^{\mathsf{T}} = 0$;
6 $\nabla \leftarrow K^{\mathsf{T}} \left(\frac{QP}{\text{Trace}(QP)} \right)^{\text{vec}}$;
7 Compute projection matrix $\mathcal{P}^{(k)}$;
8 $d^{(k)} \leftarrow d^{(k)} - \mu \, \mathcal{P}^{(k)} \nabla$;
9 $A_{\text{av}}^{(k)} \leftarrow \frac{1}{T} (d_1 A_1 + \cdots + d_m A_m)$;
10 $k \leftarrow k + 1$;
11 **until** $\mathcal{P}^{(k)} \nabla = 0$;
12 $\bar{\epsilon} \leftarrow \bar{\epsilon} + \xi$;
13 **end**
14 **return** d;

Hurwitz-stable for every A_{av}. A gradient descent method based on Lemma 4.9 is illustrated in Algorithm 1. Each iteration of the algorithm comprises the following steps. First, (lines $4-6$) a (possibly non feasible) descent direction ∇ is derived as illustrated in Lemma 4.9. Second, (line $7-8$) a gradient-projection technique [68] is used to enforce constraints (4.7d)-(4.7f). The update-step follows (line 9). Algorithm 1 employs a fixed stepsize $\mu \in (0, 1)$, and a terminating criterion (line 11) based on the Karush-Kuhn-Tucker conditions for projection methods [68]. The ϵ-update step, which constitutes the outer while-loop (line $2-13$), is then performed at each iteration of the gradient descent phase, and the line-search is terminated when $|\tilde{\alpha}_\epsilon| = 0$ cannot be achieved. To prevent the algorithm from stopping at local minima, the gradient descent algorithm can be repeated over multiple feasible initial conditions $d^{(0)}$.

Table 4.1: Execution time of Algorithm 1 on a 2.7 GHz Intel Core i5.

n	23	113	265	309	431	665	852
Exec. Time [sec]	0.5	4.5	33.4	59.3	142.9	409	893

Finally, we illustrate in Table 4.1 typical execution times of Algorithm 1 on a commercial (laptop) processor.

Remark 4.10. (*Complexity of Algorithm 1*) *The computational complexity of Algorithm 1 can be derived as follows. First, solving* (4.9) *to determine the value of the smoothed spectral abscissa can be performed via a root-finding algorithm (such as the bisection algorithm), whose complexity is a logarithmic function of the desired accuracy. Since computing the trace of a matrix has linear complexity in the matrix size, for given accuracy the complexity of this operation is* $\mathcal{O}(n)$*. Second, modern methods to solve Lyapunov equations (i.e.,* (4.12)*) rely on the Schur decomposition of the matrix* A_{av} *[69], whose complexity is* $\mathcal{O}(n^3)$*. It is worth noting that, given the Schur decomposition* $A_{\mathrm{av}} = UTU^{\mathsf{T}}$*, where* T *is upper triangular and* U *is unitary, a decomposition for* $(A_{\mathrm{av}} - \tilde{\alpha}I)$ *follows immediately by shifting* T *to* $(T - \tilde{\alpha}I)$*. Therefore, a single decomposition is required at each iteration of the gradient descent and the complexity of Algorithm 1 is therefore* $\mathcal{O}(n^3)$*.*

The space complexity of the algorithm can be derived as follows. Storing each matrix $A_{\mathrm{av}}^{(k)}, Q, P$ *requires* n^2 *units of space, while each vector* Δ *and* d *require* m *units of space. Thus, the space complexity of Algorithm 1 is* $\mathcal{O}(n^2 + m)$*.*

Finally, we note that a constant-step discretization technique (4.1) *implies that the system size* n *scales linearly with* $1/h$*.* □

4.4 Distributed Gradient Descent

The centralized computation of $\{d_1^*, \ldots, d_m^*, \epsilon^*\}$ assumes the complete knowledge of matrices $A_1, \ldots A_m$, and requires to numerically solve the Lyapunov equations (4.12). For large-scale traffic networks, such computation imposes a limitation in the dimension of the matrix A_{av} and, consequently, on the number of signalized intersections that can be optimized simultaneously. Since the performance of the proposed optimization technique depends upon the possibility of modeling and optimizing large network interconnections, a limitation on the number of modeled roads and intersections constitutes a bottleneck toward the development of more efficient infrastructures. A possible solution to address this issue is to distribute the computation of the descent direction in Algorithm 1 among a group of agents, in a way that each agent is responsible for a subpart of the computation (e.g. see Fig. 4.4). In addition, certain model parameters describing the instantaneous state of network components (e.g. the current speed of flow in a certain road or the instantaneous value of the transmission rate at a certain intersection), may be readily measurable by an agent that is located in the proximity of that component, while they may be unknown to other agents that are remotely located in the network. In this case, the benefit of a distributed implementation is that it allows local agents to directly include these model parameters into the optimal solution, thus avoiding unnecessary overheads due to transmission. In particular, agents may represent geographically-distributed control centers or clusters in parallel computing, each responsible for the control of a subset of the network.

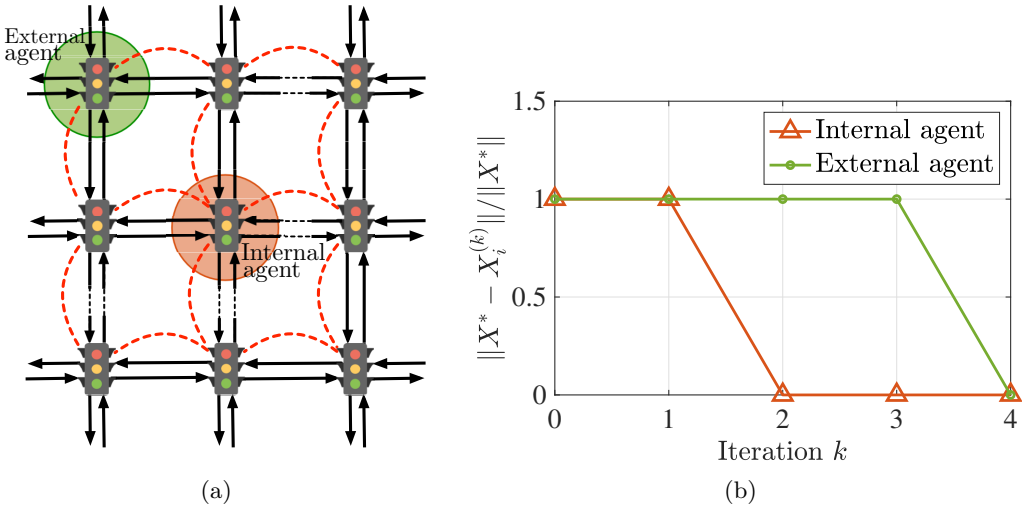

(a) (b)

Figure 4.4: (a) Manhattan-like traffic interconnection. In this example, agents are signalized intersections that have local knowledge of the road interconnection (attached black arrows) and can communicate with neighbors (dashed red lines). Colored circles illustrate the information available to each agent. (b) Error between distributed and centralized solution vs iterations. Internal agents experience faster convergence due to shorter longest paths in the graph.

In order to distribute the computation of solutions to (4.12), we focus on distributively solving equations of the form

$$\Lambda X + X\Lambda^{\mathsf{T}} + D = 0, \tag{4.13}$$

where $X = X^{\mathsf{T}} \in \mathbb{R}^{n\times n}$ is unknown, $D = D^{\mathsf{T}} \in \mathbb{R}^{n\times n}$ is a given matrix, and $\Lambda \in \mathbb{R}^{n\times n}$. Let Λ be partitioned as

$$\Lambda = \Lambda_1 + \cdots + \Lambda_\nu, \tag{4.14}$$

where $\Lambda_i \in \mathbb{R}^{n\times n}$, $i \in \{1, \ldots, \nu\}$. We assume that each agent i knows Λ_i only. Note that Λ_i are sparse matrices, and their sparsity pattern depends upon the subpart of infrastructure

associated with that agent. In addition, we assume that neighboring agents are allowed to exchange information by means of a communication interconnection. Let $\mathcal{G} = (\mathcal{V}, \mathcal{E})$ be the communication graph, where each vertex $i \in \{1, \ldots, \nu\}$ represents one agent, and $\mathcal{E} \subseteq \mathcal{V} \times \mathcal{V}$ represents the communication lines. The method we propose to distributively compute X relies on an equivalent decomposition of equation (4.13) as a set of ν independent linear equations, as discussed next.

Lemma 4.11. ***(Distributed Solutions to*** (4.13)***)*** *Let Λ be Hurwitz-stable. The following statements are equivalent:*

(i) X^* solves (4.13)*;*

(ii) For all $i \in \{1, \ldots, \nu\}$, there exists $D_i \in \mathbb{R}^{n \times n}$ s.t.

$$\Lambda_i X^* + X^* \Lambda_i^{\mathsf{T}} + D_i = 0, \text{ and } \sum_{i=1}^{\nu} D_i = D.$$

Proof. In order to prove the claim, we first observe that under the assumption of Hurwitz-stability for Λ, the solution X^* to (4.13) is unique.

$(i) \Rightarrow (ii)$. Let X^* denote the unique solution to (4.13). By expanding $\Lambda = \Lambda_1 + \cdots + \Lambda_\nu$, we obtain

$$\sum_{i=1}^{\nu} (\Lambda_i X^* + X^* A_i^{\mathsf{T}}) + D = 0.$$

Thus, by letting $D_i = -(\Lambda_i X^* + X^* A_i^{\mathsf{T}})$, (ii) immediately follows.

$(ii) \Rightarrow (i)$. Let $(\tilde{X}, \tilde{D}_1, \ldots, \tilde{D}_\nu)$ satisfy (ii), that is, for all $i \in \{1, \ldots, \nu\}$

$$\Lambda_i \tilde{X} + \tilde{X} \Lambda_i^{\mathsf{T}} + \tilde{D}_i = 0, \qquad \sum_{i=1}^{\nu} \tilde{D}_i = \tilde{D}.$$

Notice that the existence of the solution to (4.13) guarantees the existence of $(\tilde{X}, \tilde{D}_1, \ldots, \tilde{D}_\nu)$. By substitution, we obtain $-\sum_{i+1}^{\nu}(\Lambda_i \tilde{X} + \tilde{X} \Lambda_i^{\mathsf{T}}) = D$, or in other words, $\tilde{X}$ satisfies $\Lambda \tilde{X} + \tilde{X} \Lambda^{\mathsf{T}} + D = 0$. The uniqueness of the solution to (4.13) implies $\tilde{X} = X^*$ and concludes the proof. ■

Next, we show that the unknown matrices $X^*, D_1, \ldots, D_\nu$ can be reconstructed by the set of agents by cooperatively exchanging information. To this aim, for all $i \in \{1, \ldots, \nu\}$, we vectorize the set of Lyapunov equations in Lemma 4.11, and let $\bar{\Lambda}_i = \Lambda_i \otimes I + I \otimes \Lambda_i$. Then, from Lemma 4.11, we can restate (4.13) as a system of linear equations of the form

$$\underbrace{\begin{bmatrix} \bar{\Lambda}_1 & I & 0 & \cdots & 0 \\ \bar{\Lambda}_2 & 0 & I & & \vdots \\ \vdots & \vdots & \ddots & \ddots & \\ 0 & I & \cdots & I & I \end{bmatrix}}_{H} \underbrace{\begin{bmatrix} X^{\mathrm{vec}} \\ D_1^{\mathrm{vec}} \\ \vdots \\ D_\nu^{\mathrm{vec}} \end{bmatrix}}_{w} = \underbrace{\begin{bmatrix} 0 \\ 0 \\ \vdots \\ D^{\mathrm{vec}} \end{bmatrix}}_{z}, \tag{4.15}$$

where H is a given (known) matrix and w is an unknown parameter. In order to distribute the computation of vector w (and thus of X^*) among the ν distributed agents, we let

$$H_i = \begin{bmatrix} \bar{\Lambda}_i & 0 & \cdots & I & \cdots & 0 \\ 0 & I & \cdots & & \cdots & I \end{bmatrix}, \qquad z_i = \begin{bmatrix} 0 \\ D^{\text{vec}} \end{bmatrix},$$

for all $i \in \{1, \ldots, \nu\}$. At every iteration k, each agent i constructs a local estimate $\hat{w}_i^{(k+1)}$ by performing the following operations in order for all its neighbors:

(i) Receive $\hat{w}_j^{(k)}$ and $K_j^{(k)}$ from neighbor j;

(ii) $\hat{w}_i^{(k+1)} = \hat{w}_i^{(k)} + [K_i^{(k)}\ 0][K_i^{(k)}\ K_j^{(k)}]^{\dagger}(\hat{w}_i^{(k)} - \hat{w}_j^{(k)})$;

(iii) $K_i^{(k+1)} = \text{Basis}(\text{Im}(K_i^{(k)}) \cap \text{Im}(K_i^{(k)}))$;

(iv) Transmit $\hat{w}_i^{(k+1)}$ and $K_i^{(k+1)}$ to neighbor j;

where,

$$\hat{w}_i^{(0)} = H_i^{\dagger} z_i, \qquad K_i^{(0)} = \text{Basis}(\text{Ker}(H_i)).$$

The convergence of the procedure (i)-(iv) can be ensured by adopting an approach similar to the one discussed in [70].

Remark 4.12. ***(Communication Complexity)*** *To characterize the communication complexity of the distributed algorithm, we observe that at every iteration each agent is required to transmit a set of packets describing the vector $\hat{w}_i^{(k+1)}$ and the subspace $K_i^{(k+1)}$. From* (4.15)*, we note that each vector $\hat{w}_i^{(k+1)}$ has length νn^2, while the dimension of the sub-*

space $K_i^{(k+1)}$ *is variable at each iteration. In particular, the size of the subspace decreases at each iteration when the index* i *increases, with* $\dim(K_i^{(k+1)}) = 2n^2\nu$ *when* $i = 0$*, and* $\dim(K_i^{(k+1)}) = 0$ *at the final iteration. Thus, at each step (iv) of the algorithm a set of packets describing (at most)* $n^2\nu$ *variables is transmitted. Finally, we note that the number of iterations that each agent is required to perform depends on the cardinality of its neighbors and on the diameter of the network. We also note that, in order to reduce the communication burden of the algorithm, each agent can first perform operations (i)-(iii) sequentially for all its neighbors, and then re-transmit (i.e., perform step (iv)).* □

Next, we numerically validate the algorithm for a test-case traffic interconnection. To this aim, we consider the Manhattan-like network interconnection depicted in Fig. 4.4 [71], and assume that each signalized intersection is equipped with a computational unit that is responsible for a subpart of the computation of (4.12), and is allowed to exchange information with the neighboring intersections by means of a set of communication channels (dashed-red lines in Fig. 4.4). To decompose the system as in (4.14), we assume that each agent has the sole knowledge of: (i) the local structure of the traffic interconnection, that is, the layout of interconnection between roads that are adjacent to that intersection (colored areas in Fig. 4.4(a)), and (ii) the current values of the intersection outflow parameters $c(r_i, r_k)$, and of the speed of the flow γ_i in the adjacent roads. We illustrate in Fig.4.4(b) the convergence of the distributed procedure (i)-(iv), by comparing the accuracy of the local estimate $\hat{X}_i^{(k)}$ with respect to the centralized solution X^* as a function of the iteration step k. As discussed in [70], this class of procedures will compute $\hat{X}_i^{(k)} = X^*$ in at most $\mathrm{diam}(\mathcal{G})$ steps, where $\mathrm{diam}(\mathcal{G})$ denotes the diameter of $\mathcal{G}$.

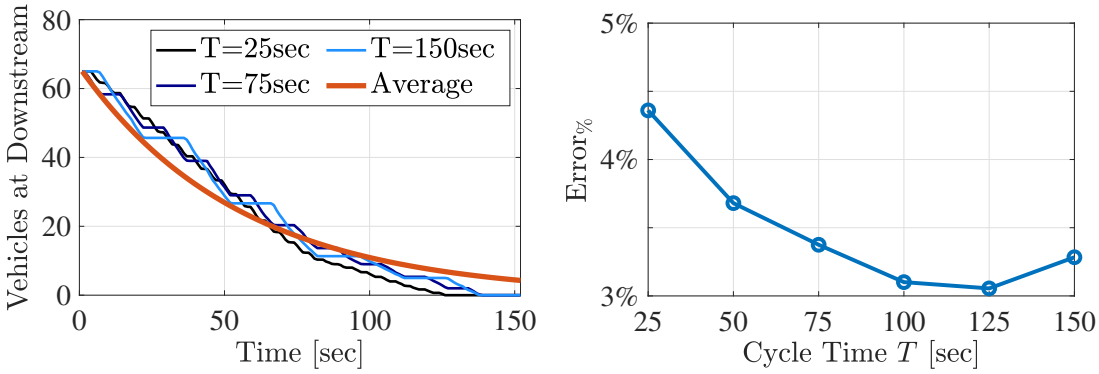

Figure 4.5: Accuracy of average dynamical model (4.5) with respect to microscopic simulations for a single signalized road. (a) Time evolution of the density at downstream for different intersection cycle time T. (b) Accuracy of the average dynamics in relation to the intersection cycle time T.

4.5 Simulations

This section provides numerical simulations in support to the methods presented in this chapter. We generate test cases using real-world traffic networks from the OpenStreet Map database and validate the techniques on a microscopic simulator based on *Sumo* [72]. A demo of the experimental setup adopted in this section is available online [14].

4.5.1 Averaging Technique

In order to validate our averaging technique, we first focus on a single road connected at downstream to a signalized intersection. To illustrate the discharging pattern emerging from the switching behavior of the signalized intersection, we assume the road has initially $x^{\sigma}(0) = 65$ vehicles in its downstream section, and zero inflows at all times. In all our simulations, we assume that each green phase is followed by a yellow phase, and we incorporate the durations of each yellow phase (clearance time) into the green times. We

illustrate in Fig. 4.5(a) a comparison between the road discharging patterns in the microscopic simulation and in the average model (4.5) for different choices of the cycle time T. The precision of the model is quantified in Fig. 4.5(b), where we illustrate the approximation error for different T, where

$$\text{Error}_{\%} = \frac{1}{H} \int_0^H \frac{\|x - x_{\text{av}}\|}{\|x_{\text{av}}\|} \, dt,$$

captures the deviation between the microscopic simulation and the average model, normalized over the time horizon $[0, H]$. As illustrated in the figure, inaccuracies due to linearization and time-averaging are lower than 5% for common cycle times.

4.5.2 Macroscopic Simulations

To validate our modeling assumptions and optimization techniques, we initially perform a set of macroscopic simulations based on the well-established Cell Transmission Model (CTM) [34]. We consider its averaged version discussed in [62, 66], with piecewise affine demand and supply functions, and adopt a proportional allocation rule to model congestion at the intersections [47]. The averaged Cell Transmission Model builds upon the traditional (non-averaged) version of the model by replacing the switching behavior of the signalized intersections with the average flow through the junction (see [62]). We stress that the Cell Transmission Model is adopted here to simulate the actual dynamics of the network, while model (4.5) is the system description used in the optimization.

We consider the Manhattan-like traffic network interconnection sketched in Fig. 4.4(a), with $n_{\text{r}} = 24$ roads of length $\ell = 0.1$mi. We construct the CTM by asso-

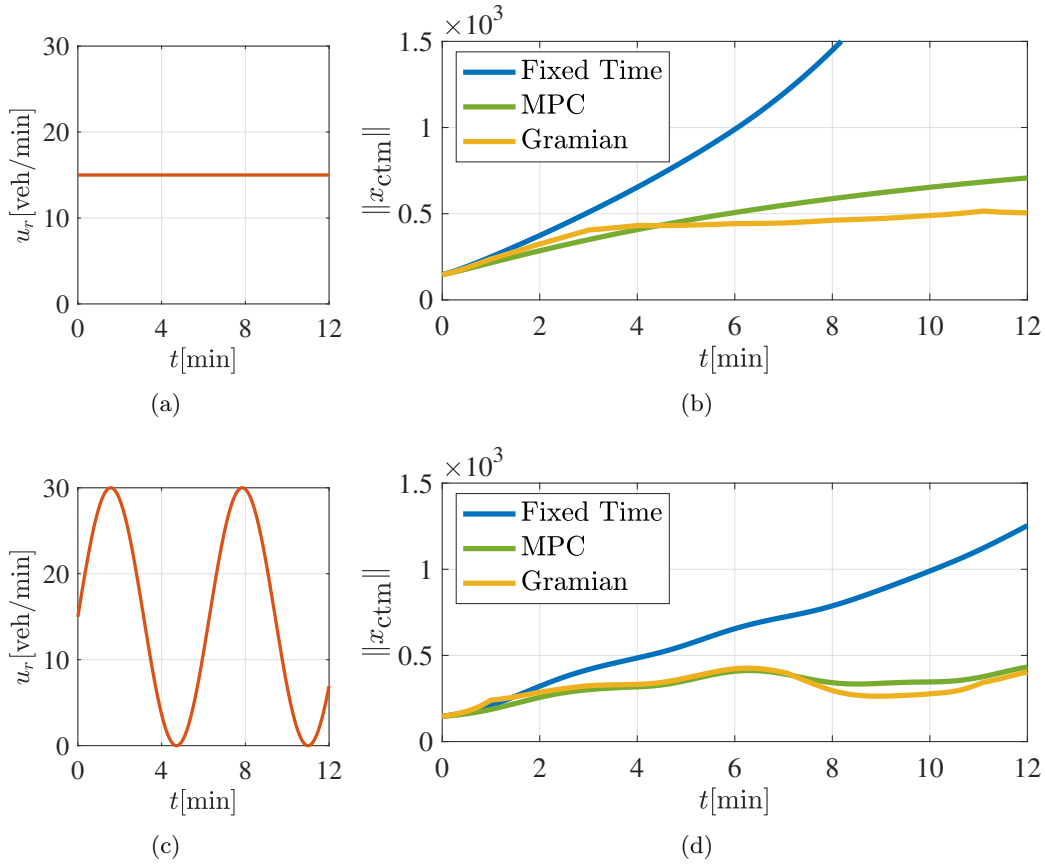

Figure 4.6: Performance of the method evaluated on the Cell Transmission Model. (a)-(b) constant network inflows. (c)-(d) time-varying network inflows.

ciating a state (cell) to each section of road interconnecting two signalized intersections. For all cells, we let the free-flow speed be $v_{\text{ff}} = 30\text{mi/h}$, the speed of backward propagation be $v_{\text{bp}} = -30\text{mi/h}$, the jam density be $x^{\max} = 20\text{veh}$, and use maximum flows ${f_s}^{\max} = {f_d}^{\max} = 30\text{veh/min}$. Turning ratios at each intersections are chosen so that vehicles are split equally among all outgoing links, and the cycle time is $T = 100\text{sec}$.

In order to generate comparable results between the CTM and our model, we construct (4.4) by letting $\sigma_i = \ell_i$ for all $r_i \in \mathcal{R}$ (i.e. we model each road by means of a single state variable). In all simulations, source roads $\mathcal{S}$ and destination roads $\mathcal{D}$ are the

roads at the boundaries of the network, network inflows are identical $u_{r_i} = u_r$ for all $r_i \in \mathcal{S}$, and $x_0 = 10$veh in all roads.

We evaluate the benefits of our intersection-control method by comparing its performance with: (i) a fixed-time control policy, and (ii) the control technique proposed in [62], that we briefly illustrate in the following. The fixed-time control policy consists in assigning constant split times at all the intersections, where green times are divided uniformly among all links connected at downstream to that intersection. The method discussed in [62] consists in performing network-wide design of the green split times by implementing a Model Predictive Control (MPC) optimization technique that relies on the averaged Cell Transmission Model for state prediction. We remark that the latter technique is adopted here for comparison because of its similarity with our framework in the adoption of a time-averaging method. In particular, MPC is performed by discretizing the averaged Cell Transmission Model and by considering a one-step ahead prediction horizon (representing a full cycle of the intersections, with $T = 100$sec), where the instantaneous values of the network state (density) are sensed from the network at each time step. In particular, we discretized the system using the Euler discretization with sample time $T_s = 10$sec, which satisfies the stability assumption $v_{\text{ff}} T_s / \ell < 1$ that guarantees convergence of the model [34].

We report in Fig. 4.6 a comparison between the time-evolution of the cost of congestion obtained by simulating the averaged Cell Transmission Model for the three controllers under consideration. In particular, we consider two scenarios. First, we let the inflows be constant $u_r = 15$ veh/min for all source roads (Fig. 4.6(a)-(b)). Second, we let the inflows be time-varying $u_r = 15(1+\sin(t))$veh/min (Fig. 4.6(c)-(d)). We observe that in

both cases our controller outperforms the two control policies considered in the comparison. In particular, for constant network inflows our controller achieves an improvement of over 80% with respect to fixed-time control, and of about 40% with respect to the MPC-based control technique. We interpret these results by observing that, although our approach is based on a simplified model description of the system, it allows us to take into account larger control horizons with respect to (tractable) MPC control policies, thus resulting in increased network performance in the long term. This observation is further supported by the transient phase of the cost function in Fig. 4.6(b). In fact, we can observe that during the time interval $0 - 3$min the MPC-based control method reacts more effectively to changes in inflows thanks to (i) the availability of a more precise model that can capture quickly-varying regimes, and (ii) the shorter update interval. However, the benefits of a faster response degrade over time (see time interval $3 - 12$min) due to the lack in adequate prediction horizons that can capture all the relevant system dynamics. We conclude by observing that in the presence of quickly-varying inflow rates, both methods suffer from the lack of appropriate knowledge in the unknown network inflow rates and, in this case, the performance of the two techniques is comparable.

4.5.3 Microscopic Simulations

We consider a test case scenario inspired by the area of Manhattan, NY (Fig. 4.7), which features $n_{\mathrm{r}} = 958$ roads and $n_{\mathcal{I}} = 332$ signalized intersections. We replicate a daily-commute scenario, where sources of traffic $\mathcal{S}$ are uniformly distributed in the central area of the island (Area 1), and routing is chosen so that traffic flows are departing from the city,

(a) (b)

Figure 4.7: Urban interconnection of Manhattan, NY. (a) Red dots denote the set of signalized intersections considered in the study. (b) Commute zones.

that is, destinations $\mathcal{D}$ are uniformly distributed within Area 2. Inflow rates used in the simulations are illustrated in Table 4.2. To estimate the network turning rates, we set the simulator so that each vehicle follows the shortest path between its source and destination, and derive the turning rates $\varphi(r_i, r_k)$ for every pair of roads by computing the fraction of traffic flow on every route. Although in our simulations we make the assumption that the traffic patterns are known, in many practical scenarios the turning preferences are typically inferred from measured or historical traffic data [61].

We consider three control policies, described next.

Gramian-Optimization Settings: We model the network by means of the technique discussed in Section 4.2, where we let $h = 0.1$mi and associate $\sigma_i = \lceil \ell_i/h \rceil \geq 1$ states to each section of road interconnecting two signalized intersections. We observe that, for

Table 4.2: Manhattan Network Inflow Rates

Time [sec] (From - To)	Area 1 Inflow [veh/h]	Area 2 Inflow [veh/h]
$0 - 2500$	4000	0
$2500 - 4000$	0	0

the Manhattan interconnection shown in Fig. 4.7, we obtain $n = \sum_{i=1}^{n_r} \sigma_i = 3091$, which corresponds to an average of approximately 3 states associated with each link. We solve the optimization (4.11) with cycle time $T = 100$sec (corresponding to $\text{Error}_{\%} \approx 3\%$, see Fig. 4.5). Moreover, the solution to (4.10) is re-computed with updated network conditions A_{av} and x_0 every $T_{\text{update}} = 500$sec by sensing these parameters from the microscopic simulation. The implementation of the gradient-descent algorithm was performed in Python, and the computation of the descent direction (Lemma 4.9) was performed using tools from the NumPy library. Finally, in order to emphasize the benefits of our optimization method and to make the results independent on the offset optimization algorithm adopted, we performed no offset optimization to decide the specific sequence of phases at the intersections. Thus, our simulation results represent a lower bound on the performance that can be achieved when offset optimization is applied to the output of our optimization.

Max-Pressure Settings: The Max-Pressure [57] is a controller that can be distributively implemented at the single-intersection level, and that requires only local information concerning the instantaneous traffic densities in the roads that are adjacent to that intersection. In particular, at each intersection and at each time step, the controller computes the difference between the number of vehicles waiting (on each road) and the number of vehicles at their downstream road, and activates the phase associated to the road with the largest

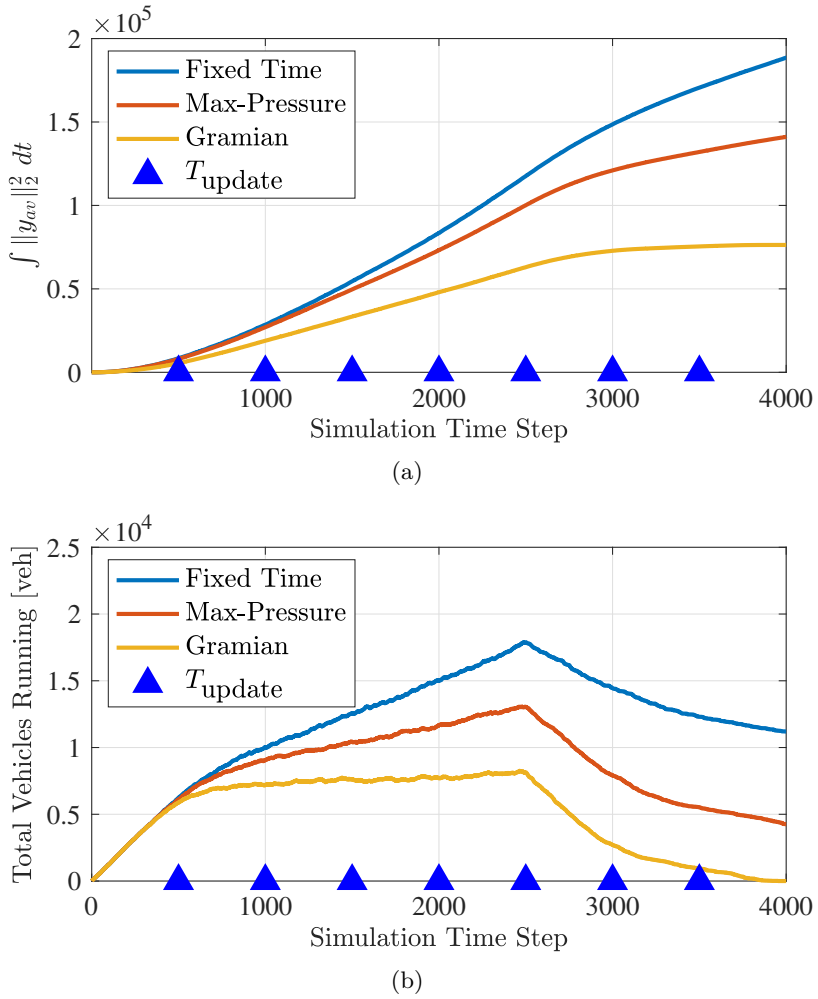

Figure 4.8: Network performance of the Manhattan interconnection assessed via a microscopic simulator for three control policies. Blue triangles denote the instants when the optimal solution is recomputed with updated A_{av} and x_0.

difference value ("pressure") for a fixed time interval. In the simulation, the Max-Pressure is implemented through the Sumo TraCI tool, by associating a set of four phases to each intersection, where the activation time of each phase is set to $T/4 = 25$sec (thus, similarly to the Gramian-based optimization settings, the cycle time is $T = 100$sec).

Fixed-Time Settings: Fixed-time control is widely-adopted policy in practice thanks to its simplicity [58]. In this policy, the activation time of each phase is constant and

proportional to the average traffic flow in the upstream roads, which are inferred from historical data. To implement this policy we estimated the average traffic flows by combining the network demand with the vehicles routing policy, and used $T = 100$sec.

Fig. 4.8(a) shows a comparison between the cost functions resulting from the three policies considered, while Fig. 4.8(b) shows the time evolution of the total number of vehicles in the network (network occupancy). The plots demonstrate the benefits of using the optimization (4.7): the improvement in cost function is of almost 60% with respect to fixed-time control, and of about 46% with respect to Max-Pressure. Moreover, Fig. 4.8(b) demonstrate the effectiveness of the cost function in (4.7) to capture the network congestion. In fact, control policies that minimize the cost (4.7) result in networks with reduced overall congestion (i.e. total number of vehicles in the network), and thus in increased network throughput.

The benefits of more efficient control policies on the network overall congestion can be further visualized by means of the illustration in Fig. 4.9. The figure illustrates the time evolution of the network congestion (measured as [veh/mi]) in the simulation for two control policies: Gramian-Based and Max-Pressure. The graphic shows that in the absence of external inflows, the network is evacuated faster when the former control technique is adopted, supporting our claim that a global model description results in increased network performance as compared to distributed techniques that rely on local knowledge of the traffic dynamics.

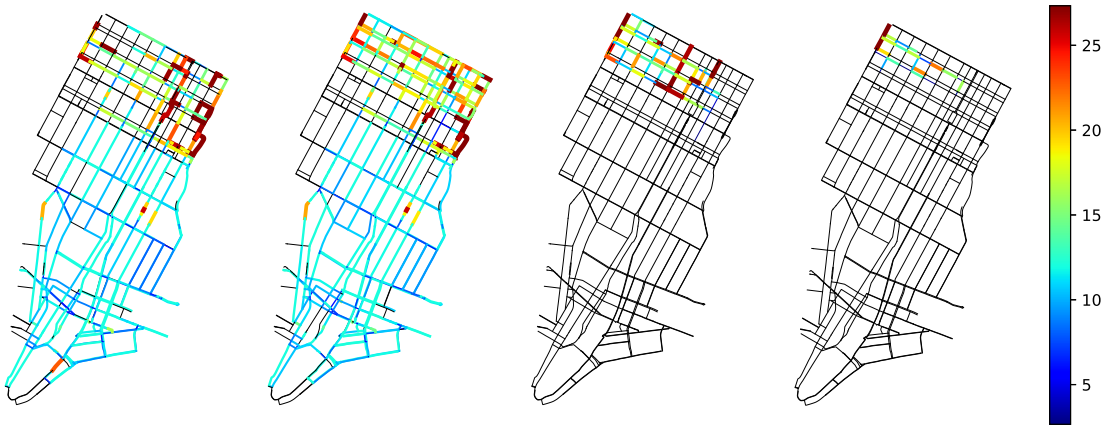

(a)

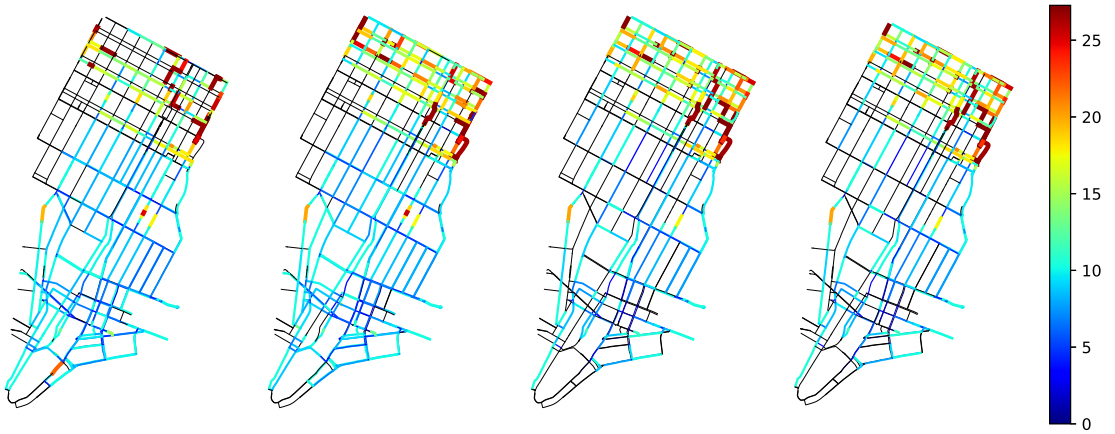

(b)

Figure 4.9: Time evolution of the network state [×10veh/mi] for two control policies. (a) solution to (4.7). (b) Max-Pressure policies. Simulation time from left to right is 1000sec, 2000sec, 3000sec, 4000sec.

Chapter 5

Optimization-Based Techniques to Quantify Resilience

In this chapter we investigate the resilience of traffic networks against changes in the user behavior, namely, we quantify the magnitude of the smallest perturbation in the routing decisions of the travelers that causes one of the highways to reach its jam density. We refer to [7] for a comprehensive discussion of the results contained in this chapter.

5.1 Introduction

Recent advances in vehicle technologies, such as Infrastructure-To-Vehicle (I2V) communication and Vehicle-To-Vehicle (V2V) communication, set out an enormous potential to overcome the inefficiencies of traditional transportation systems. Notwithstanding, the development efficient control algorithms capable of effectively engaging these capabilities is an extremely-challenging task due to the tremendous complexity of the interconnections

[65], that often results in suboptimal performance [17], and that can potentially generate novel fragilities [18, 13].

In this chapter, we propose the use of Infrastructure to Vehicle (I2V) communication to influence the routing decisions of certain travelers in the network with the goal of optimizing the system overall congestion. We define highway-specific levels of trust to tolerate the non-cooperative behavior of a certain fraction of the drivers, and we develop an optimization-based control mechanism to provide the cooperative drivers real-time routing suggestions. Differently from traditional approaches for network routing design, our methods allow us to take into account quickly-varying traffic volumes, and do not require the knowledge of the traffic demands associated with every origin-destination pair. Moreover, we study the impact of changes in routing that result in roads reaching their maximum capacity, thus leading to traffic jams or cascading failure effects. We develop a technique to classify the links based on their resilience, and we study the fragility of the network against changes in routing. Surprisingly, our findings demonstrate that networks where the routing is partially controlled by a system planner can be more fragile to traffic jam phenomena as compared to networks where drivers perform traditional selfish routing choices.

Routing decisions of traditional human drivers are *non-cooperative*, namely, drivers act as a group of distinct agents that make selfish routing decisions with the goal of minimizing their individual travel delay [21]. The inefficiencies of such noncooperative behavior are often quantified through the *price of anarchy* [73, 74, 75], a measure that captures the cost of suboptimality with respect to the societal optimal efficiency. The availability of V2V and I2V has recently demonstrated the potential to influence the traditional behavior of

drivers in a transportation system [17, 76]. In particular, the control of the routing choices was proposed as a promising solution to improve the efficiency of the network [76] and to enhance its resilience [41]. Differently from this line of previous work, this chapter focuses on systems operating at non-equilibrium points, on tolerating the presence of non-cooperative driver behaviors, and on characterizing the impact of controlled routing on the resilience of the system.

The contribution of this chapter is fourfold. First, we formulate and solve an optimization problem to design optimal routing suggestions with the goal of minimizing the travel time experienced by all network users. The optimization problem incorporates link-wise trust parameters that describe the extent to which drivers on that link are willing to follow the suggested routing policy. Second, we develop an online update scheme that takes into account instantaneous changes in the levels of trust on the provided routing suggestions. Discrepancies between the modeled and actual trust parameters can be the result of quickly varying traffic demands, or can be the effect of selfish routing decisions. Third, we study the resilience of the network, measured as the smallest change in the trust parameters that results in roads reaching their maximum capacity. We present an efficient technique to approximate the resilience of the network links, and we discuss how these quantities can be computed from the output of the optimization problem. Fourth, we demonstrate through simulations that, although partially controlling the routing may improve the travel time for all network users, it also results in increased network fragility due to possible fluctuations in the trust parameters.

The rest of this chapter is organized as follows. Section 5.2 describes the dynamical network framework, and formulates the problem of optimal network routing with varying levels of trust. Section 5.3 presents a method to numerically solve the optimization, and illustrates our real-time update mechanism. Section 5.4 is devoted to the study and characterization of the network resilience, while Section 5.5 presents simulations results to validate our methods.

5.2 Design of Optimal Routing Suggestions

We model a traffic network with a directed graph $\mathcal{G} = (\mathcal{V}, \mathcal{E})$, where $\mathcal{V} = \{1, \dots, m\}$ denotes the set of nodes, and $\mathcal{E} = \{1, \dots, n\} \subseteq \mathcal{V} \times \mathcal{V}$ denotes the set of edges. Nodes of the graph identify traffic junctions, while edges identify sections of roads (links) that interconnect two junctions. An element $(i, j) \in \mathcal{E}$ denotes a directed link from node j to node i. We associate to every link $i \in \mathcal{E}$ a dynamical equation of the form

$$\dot{x}_i = f_i^{\text{in}}(x, t) - f_i^{\text{out}}(x, t),$$

where $t \in \mathbb{R}_{\geq 0}$, $x_i : \mathbb{R}_{\geq 0} \to \mathbb{R}_{\geq 0}$ denotes the traffic density of link i, and $f_i^{\text{in}}(x, t)$ and $f_i^{\text{out}}(x, t)$ denote the inflow and outflow of the link, respectively. We assume that vehicle inflows enter the network at on-ramp links $\mathcal{E}^{\text{on}}$, while vehicle outflows exit the network at off-ramp links $\mathcal{E}^{\text{off}}$. We denote by $\mathcal{E}^{\text{in}}$ the set of internal links that are connected through junctions, and assume that $\mathcal{E}^{\text{on}}$, $\mathcal{E}^{\text{off}}$, and $\mathcal{E}^{\text{in}}$ are disjoint sets, with $\mathcal{E} = \mathcal{E}^{\text{on}} \cup \mathcal{E}^{\text{off}} \cup \mathcal{E}^{\text{in}}$ (see Fig. 5.1 for an illustration). The network topology described by $\mathcal{G}$ imposes natural constraints on the dynamics of the links, where flow is possible only between links that are

interconnected by a node. We associate to every pair of links a turning ratio $r_{ij} \in [0,1]$, describing the fraction of vehicles entering link $i \in \mathcal{E}$ after exiting $j \in \mathcal{E}$. We combine the drivers turning preferences into a matrix $R = [r_{ij}] \in \mathbb{R}^{n \times n}$, where

$$r_{ij} \in [0,1], \qquad r_{ij} \neq 0 \text{ only if } (i,j) \in \mathcal{E}. \tag{5.1}$$

The conservation of flows at the junctions imposes the following constraints on the entries of R:

$$\begin{aligned} &\sum_i r_{ij} = 1, \text{ for all } j \in \mathcal{E} \setminus \mathcal{E}^{\text{off}}, \\ &\sum_i r_{ij} = 0, \text{ for all } j \in \mathcal{E}^{\text{off}}. \end{aligned} \tag{5.2}$$

We let $\mathcal{R}_{\mathcal{G}}$ be the set of matrices

$$\mathcal{R}_{\mathcal{G}} = \{R = [r_{ij}] \in \mathbb{R}^{n \times n} \ : \ r_{ij} \text{ satisfy (5.1) and (5.2)}\},$$

and let $n_r = \|R\|_0$ denote the number of nonzero entries in matrix R. We assume that the vehicles routing is partially controllable, and denote by $\sigma_i : \mathbb{R}_{\geq 0} \to [0,1]$ the ratio of controllable vehicles that instantaneously occupy link i. For every $i \in \mathcal{E}$, we assume that a fraction $(1 - \sigma_i)$ of vehicles leaving i will follow a selfish route choice r^{s}_{ij}, for all $j \in \mathcal{E}$, while the remaining vehicles can be routed according to the routing decisions made by a system planner, namely r^{c}_{ij}. The parameter σ_i can be interpreted as the (average) extent to which drivers follow the routing suggestion r^{c}_{ij}. We combine the selfish and controllable

routing parameters into matrices $R^{\mathrm{S}} \in \mathbb{R}^{n\times n}$ and $R^{\mathrm{C}} \in \mathbb{R}^{n\times n}$, respectively, and decompose the matrix of turning preferences as

$$R = \Sigma R^{\mathrm{C}} + (I - \Sigma)R^{\mathrm{S}},$$

where Σ is a diagonal matrix $\Sigma = \mathrm{Diag}(\sigma_1, \ldots, \sigma_n)$. Note that the graph topology and sparsity pattern of R impose the following constraints on R^{S} and R^{C}:

$$R^{\mathrm{S}} \in \mathcal{R}_{\mathcal{G}}, \qquad\qquad R^{\mathrm{C}} \in \mathcal{R}_{\mathcal{G}}.$$

We stress that in this work R^{C} is a design parameter containing the set of routing suggestions provided by the system planner to influence the drivers routing choices.

Remark 5.1. ***(Selfish Route Choices)*** *Typically, the selfish behavior of drivers is captured by a Wardrop equilibrium [21], that is, a configuration in which the travel time associated to any source-destination path chosen by a nonzero fraction of the drivers does not exceed the travel time associated to any other path. We remark that, in our settings, such equilibrium configuration is captured by the selfish routing matrix R^{S}.* □

We adopt Daganzo's Cell Transmission Model [34], and model the physical characteristic of each link by a demand function $d_i(x_i)$ and a supply function $s_i(x_i)$, that represent upper bounds on the outflow and inflow of each link, respectively:

$$f_i^{\mathrm{in}}(x,t) \leq s_i(x_i), \qquad\qquad f_i^{\mathrm{out}}(x,t) \leq d_i(x_i). \tag{5.3}$$

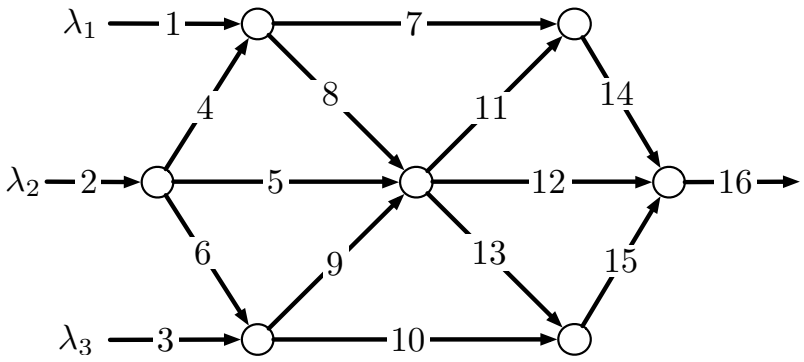

Figure 5.1: Example of traffic network interconnection. For this network, $\mathcal{E}^{\text{on}} = \{1, 2, 3\}$, $\mathcal{E}^{\text{in}} = \{4, \ldots, 15\}$, and $\mathcal{E}^{\text{off}} = \{16\}$.

For every link $i \in \mathcal{E}$ we let $B_i := \sup\{x : s_i(x) > 0\}$ denote its saturation density, which corresponds to the jam density of the road. We model on-ramps $i \in \mathcal{E}^{\text{on}}$ as links with infinite supply functions $s_i(x_i) = +\infty$, and denote by $\lambda_i(t)$ the corresponding inflow rate. Then, road inflows and outflows are related by means of the following equations

$$f_i^{\text{in}}(x,t) = \begin{cases} \lambda_i(t), & i \in \mathcal{E}^{\text{on}}, \\ \sum_j r_{ij} f_j^{\text{out}}(x,t), & i \in \mathcal{E} \setminus \mathcal{E}^{\text{on}}, \end{cases} \tag{5.4}$$

which capture the conservation of flows at the junctions. We model the outflows from the links as

$$f_i^{\text{out}}(x,t) = \kappa_i(x) d_i(x_i), \tag{5.5}$$

where $\kappa_i(x) \in [0,1]$ is a parameter that enforces the bounds (5.3) or, in other words, guarantees that every outgoing link has adequate supply to accommodate the demand of its incoming links. Different models for $\kappa_i(x)$ have been proposed in the literature, and

prevalent roles have been played by FIFO policies [35] and proportional allocation rules [36]. We combine the link dynamical equations with (5.4) and (5.5) to derive the overall network dynamics

$$\dot{x} = (R - I)f(x,t) + \lambda, \tag{5.6}$$

where $I \in \mathbb{R}^{n\times n}$ is the identity matrix, $x = [x_1 \ \dots \ x_n]^{\mathsf{T}}$ is the vector of link densities, $f = [f_1^{\text{out}} \ \dots \ f_n^{\text{out}}]^{\mathsf{T}}$ is the vector of link outflows, and $\lambda = [\lambda_1 \ \dots \ \lambda_n]^{\mathsf{T}}$ denotes the vector of exogenous inflows, where we let $\lambda_i = 0$ if $i \notin \mathcal{E}^{\text{on}}$.

We consider the network performance measured by the *Total Travel Time* (TTT),

$$\text{TTT} := \int_0^{\mathcal{H}} x_1(t) + \cdots + x_n(t) \ dt,$$

which is a measure of the delay experienced by all users [50], and we focus on the problem of designing the matrix of turning preferences in a way that

$$\begin{aligned}
\min_{R^{\text{C}}} \quad & \text{TTT} \\
\text{subject to} \quad & \dot{x} = (R - I)f(x,t) + \lambda, && \text{(5.7a)} \\
& R = \Sigma R^{\text{C}} + (I - \Sigma)R^{\text{S}}, && \text{(5.7b)} \\
& R^{\text{C}} \in \mathcal{R}_{\mathcal{G}}, && \text{(5.7c)} \\
& x \leq B, && \text{(5.7d)}
\end{aligned}$$

where $\mathcal{H}$ is the control horizon, $x(0) = x_0$ is the (given) network initial configuration, and $B = [B_1 \dots B_n]^\mathsf{T}$ denotes the vector of jam densities. From a real-time control and implementation perspective, solving (5.7) sets out a number of challenges. First, the length of the optimization horizon $\mathcal{H}$ is a fundamental parameter that should be accurately chosen. One should chose $\mathcal{H}$ adequately large to include all relevant system dynamics, but unnecessarily large values of $\mathcal{H}$ can drastically increase the computational burden. Second, rapid changes in traffic volumes and driver preferences require the development of control mechanisms that are capable to adapt in real-time to sudden variations of σ. In fact, the performance of the optimization strongly depends on σ, and fluctuations in this parameter can lead to considerable variability in network performance and efficiency.

To study the effects of fluctuations in σ, in the second part of this chapter we consider the problem of quantifying the fragility of the network against changes in the trust levels that result in links reaching their jam density. We assume that a link irreversibly fails if it reaches its jam density, and argue that such failure may propagate in the network and potentially cause a cascading failure effect. We measure the network resilience $\rho(\mathcal{G}, x_0)$ as the L^1-norm of the smallest variation in σ that results in such failure phenomena, that is,

$$\begin{aligned} \rho(\mathcal{G}, x_0) := \quad & \min_{\tilde{\sigma}} \quad \|\tilde{\sigma} - \sigma\|_1 \\ & \text{such that} \quad \dot{x} = (R - I) f(x, t) + \lambda, \\ & \qquad\qquad\quad R = \Sigma R^{\mathrm{C}} + (I - \Sigma) R^{\mathrm{S}}, \\ & \qquad\qquad\quad x_i \geq B_i, \end{aligned}$$

where $x(0) = x_0$, $t \in [0, \mathcal{H}]$, and $i \in \{1, \dots, n\}$.

5.3 Design of the Turning Preferences

In this section we present a method to numerically solve the optimization problem (5.7), and illustrate an online-update technique to address the control challenges outlined above.

5.3.1 Computing Optimal Routing Suggestions

We begin by recasting the optimization problem (5.7) in a way that allows us to numerically compute its solutions. We perform three simplifying steps, described next.

First, in order to generate a tractable prediction of the time evolution of the network state, we discretize (5.6) by means of the Euler discretization technique. We use a sampling time $T_s \in \mathbb{R}_{>0}$ that is chosen to guarantee the Courant-Friedrichs-Lewy assumption $\max_i \frac{v_i T_s}{L_i} \leq 1$ for all links [34], where $v_i \in \mathbb{R}_{\geq 0}$ and $L_i \in \mathbb{R}_{>0}$ denote the maximum speed and the length of the section of road, respectively. Let $\text{vec}\,(R) = [r_{11} \dots r_{n1}\ r_{12} \dots r_{nn}]$ denote the vectorization of matrix $R = [r_{ij}]$, and let $t_k = kT_s$, $k \in \mathbb{N}$. Then, the time-evolution of (5.6) from t_k to $t_{k+1} = t_k + T_s$ can be discretized as

$$x_{k+1} = x_k + T_s((R_k - I)f(x_k) + \lambda_k) := \mathcal{F}(x_k, r_k, \lambda_k), \tag{5.8}$$

where $r_k = \text{vec}\,(R_k)$. We remark that the dependency on time of the routing matrix is the result of time-varying σ.

Second, we vectorize equation (5.7b) and let

$$r_k = (\Sigma_k^{\mathsf{T}} \otimes I) r^{\mathrm{c}} + ((I - \Sigma_k)^{\mathsf{T}} \otimes I) r^{\mathrm{s}} := \Psi(\sigma_k, r^{\mathrm{s}}, r^{\mathrm{c}}),$$

where $r^{\mathrm{c}} = \operatorname{vec}\left(R^{\mathrm{C}}\right)$, $r^{\mathrm{s}} = \operatorname{vec}\left(R^{\mathrm{S}}\right)$, the symbol $\otimes$ denotes the Kronecker product, and where we used the identity $\operatorname{vec}(AXB) = (B^{\mathsf{T}} \otimes A) \operatorname{vec}(X)$ for matrices A, X, and B of appropriate dimensions.

Third, we observe that the Euler discretization technique employed in (5.8) preserves the sparsity pattern of R^{C}, and we rewrite the sparsity constraints (5.7c) as

$$\sum_i r_{ij}^{\mathrm{c}} = b_j, \qquad\qquad 0 \le r_{ij}^{\mathrm{c}} \le 1, \quad (i,j) \in \mathcal{E},$$

where $b_j = 1$ if $j \in \mathcal{E} \setminus \mathcal{E}^{\mathrm{off}}$, and $b_j = 0$ if $j \in \mathcal{E}^{\mathrm{off}}$.

Finally, we recast the optimization problem (5.7) by using the discretized dynamics as

$$\begin{aligned}
\min_{r^{\mathrm{c}}} \quad & \sum_{k=1}^{h} \mathbb{1}^{\mathsf{T}} x_k \\
\text{subject to} \quad & x_{k+1} = \mathcal{F}(x_k, r_k, \lambda_k), && k = 1, \ldots, h, && \text{(5.9a)} \\
& r_k = \Psi(\sigma_k, r^{\mathrm{s}}, r^{\mathrm{c}}), && k = 1, \ldots, h, && \text{(5.9b)} \\
& \sum_i r_{ij} = b_j, && j = 1, \ldots, n, && \text{(5.9c)} \\
& 0 \le r_{ij}^{\mathrm{c}} \le 1, && (i,j) \in \mathcal{E}, && \text{(5.9d)} \\
& x_k \le B, && k = 1, \ldots, h, && \text{(5.9e)}
\end{aligned}$$

where $\mathbb{1} \in \mathbb{R}^n$ denotes the vector of all ones, and h and T_s are chosen so that $hT_s = \mathcal{H}$. As discussed in e.g. [77], the constraints (5.9a) are often nonconvex in the decision variables. Thus, the optimization problem (5.9) is of the form of a nonconvex nonlinear programming optimization problem, over $n_r = \|R\|_0$ decision variables, and can be solved numerically through common nonlinear optimization solvers, such as interior-point methods [78].

5.3.2 Online Update Mechanism

In order to take into account for the quick variability of the parameter σ and to deal with the considerable computational effort required to determine the solution to (5.9), we propose an adaptive control scheme that generates real-time updates based on the instantaneous changes in σ. The proposed adaptive mechanism is outlined in Fig. 5.2, and is structured as follows. We assume that a central processing unit is in charge of computing $R^{\mathrm{C}*}(\sigma_0)$, that is, the solution to the optimization problem (5.9) with a given (fixed) set of trust parameters σ_0. The underlying choice for σ_0 can reflect the current network conditions, or can be dictated by the availability of historical data. Moreover, we assume that the solution $R^{\mathrm{C}*}(\sigma_0)$ is intermittently made available at time instants $t = kT_c$, where $T_c \in \mathbb{R}_{>0}$ is the time required to solve the optimization. We are interested in constructing an efficient mechanism to determine $R^{\mathrm{C}*}(\sigma)$, the optimal solution to (5.9) with the instantaneous value of σ, by updating $R^{\mathrm{C}*}(\sigma_0)$. Our online update method is motivated by the fact that σ is subject to small variations from the nominal value σ_0. In fact, the following inequality

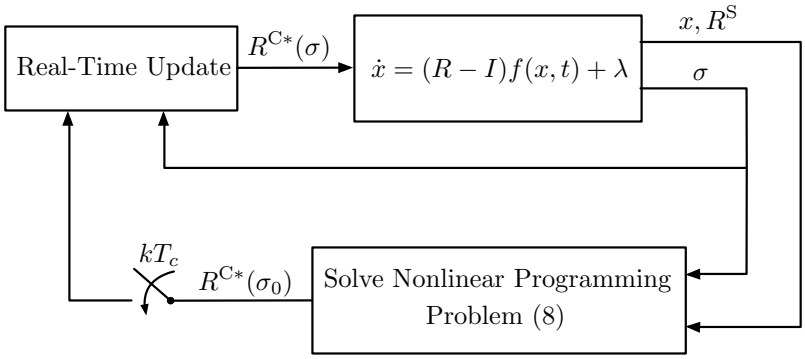

Figure 5.2: Real-time update scheme.

follows from (5.1)

$$\|\sigma - \sigma_0\| \leq \|[1 \cdots 1]^{\mathsf{T}}\| = \sqrt{n_r}.$$

Next, we derive our online update mechanism. We denote in compact form by

$$f_0(r^{\mathrm{c}}, \hat{x}, \sigma) = \sum_{k=1}^{h} \mathbb{1}^{\mathsf{T}} x_k, \quad g(r^{\mathrm{c}}, \hat{x}, \sigma) = \begin{bmatrix} r_{ij}^{\mathrm{c}} - 1 \\ -r_{ij}^{\mathrm{c}} \\ x_k - B \end{bmatrix},$$

$$h(r^{\mathrm{c}}, \hat{x}, \sigma) = \begin{bmatrix} x_{k+1} - \mathcal{F}(x_k, r_k, \lambda_k) \\ r_k - \Psi(\sigma, r^{\mathrm{s}}, r^{\mathrm{c}}) \\ \sum_i r_{ij} - b_j \end{bmatrix},$$

where $\hat{x} = [x_1^\mathsf{T} \dots x_h^\mathsf{T}]^\mathsf{T} \in \mathbb{R}^{nh}$ denotes the joint vector of model-prediction variables, and rewrite (5.9) as

$$\begin{aligned} \min_{r^{\mathrm{c}}} \quad & f_0(r^{\mathrm{c}}, \hat{x}, \sigma) \\ \text{subject to} \quad & g_i(r^{\mathrm{c}}, \hat{x}, \sigma) \leq 0, \qquad && i \in \{1, \dots, q\}, \\ & h_j(r^{\mathrm{c}}, \hat{x}, \sigma) = 0, && j \in \{1, \dots, p\}, \end{aligned} \tag{5.10}$$

where we have made explicit the dependency of the optimization problem on the decision variables r^{c}, on the prediction variables $\hat{x}$, and on the parameter σ. To characterize the solutions to (5.10), we compose the Lagrangian

$$\begin{aligned} \mathcal{L}(r^{\mathrm{c}}, \hat{x}, \sigma, w, u) = f_0(r^{\mathrm{c}}, \hat{x}, \sigma) + \\ u^\mathsf{T} g(r^{\mathrm{c}}, \hat{x}, \sigma) + w^\mathsf{T} h(r^{\mathrm{c}}, \hat{x}, \sigma), \end{aligned}$$

where $u = [u_1 \dots u_q]^\mathsf{T}$ and $w = [w_1 \dots w_p]^\mathsf{T}$ are the vectors of Lagrange Multipliers, and we write the first order Karush-Kuhn-Tucker (KKT) conditions:

$$\begin{aligned} \nabla \mathcal{L}(r^{\mathrm{c}*}, \hat{x}^*, \sigma_0, w^*, u^*) = 0, \\ u_i g_i(r^{\mathrm{c}*}, \hat{x}^*, \sigma_0) = 0, \\ h_j(r^{\mathrm{c}*}, \hat{x}^*, \sigma_0) = 0, \end{aligned}$$

with the additional inequalities $u_i^* \geq 0$, and $g_i(r^{\mathrm{c}*}, \hat{x}^*, \sigma_0) \leq 0$, where $\nabla = [\partial/\partial r_1^{\mathrm{c}} \dots \partial/\partial r_{n_r}^{\mathrm{c}}]^\mathsf{T}$ denotes the gradient operator with respect to the decision variables

r^{c}. We denote the set of KKT equality conditions in compact form as

$$F(r^{\mathrm{c}*}, \hat{x}^*, \sigma_0, u^*, w^*) = 0, \tag{5.11}$$

and note that (5.11) is an implicit equation that characterizes the optimal solutions to (5.10). Finally, by letting $y = [r^{\mathrm{c}}(\sigma)\ u(\sigma)\ w(\sigma)]$ and by assuming that (5.11) holds for σ near σ_0, we compute the total derivative of the implicit function (5.11) with respect to σ to obtain the following relationship that holds at optimality:

$$M(\sigma)\frac{dy}{d\sigma} + N(\sigma) = 0,$$

where the matrices $M(\sigma) = [\partial F_i/\partial y_j]$, $dy/d\sigma = [dy_i/d\sigma_j]$, and $N(\sigma) = [\partial F_i/\partial \sigma_j]$. Finally, to formalize our online update rule we make the following classical assumption (see e.g. [79]), which guarantees: (i) that $r^{\mathrm{c}*}$ is a local isolated minimizing point, (ii) the uniqueness of the Lagrange Multipliers, and (iii) the invertibility of matrix $M(\sigma_0)$.

Assumption 5.2. ***(Second Order Minimizer Point)***

(Second-order KKT conditions) The inequality $v^{\mathsf{T}}\nabla^2\mathcal{L}(r^{c*}, \hat{x}^*, \sigma, w^*, u^*)v > 0$ *holds for every vector* $v \in \mathbb{R}^{n+m+p}$, $v \neq 0$, *that satisfies*

$$v^{\mathsf{T}}\nabla g_i(r^{c*}, \hat{x}^*, \sigma_0) \leq 0, \ \textit{for all } i \textit{ where } u_i^* = 0,$$

$$v^{\mathsf{T}}\nabla g_i(r^{c*}, \hat{x}^*, \sigma_0) = 0, \ \textit{for all } i \textit{ where } u_i^* > 0,$$

$$v^{\mathsf{T}}\nabla h(r^{c*}, \hat{x}^*, \sigma_0) = 0.$$

(Constraints independence) The vectors $\nabla g(r^{c*}, \hat{x}^*, \sigma_0)$ *and* $\nabla h(r^{c*}, \hat{x}^*, \sigma_0)$ *are linearly independent.*

(Strict complementary slackness) If $g_i(r^{c*}, \hat{x}^*, \sigma_0) = 0$*, then* $u_i^* > 0$. □

Lemma 5.3. ***(Linear Update Rule)*** *Let Assumption 5.2 hold, let* $r^{c*}(\sigma_0)$ *denote a solution to* (5.9) *with* $\sigma = \sigma_0$*, and let* $\eta := M^{-1}(\sigma_0)N(\sigma_0)$ *be partitioned as*

$$\eta = \begin{bmatrix} \eta_1 \\ \eta_2 \\ \eta_3 \end{bmatrix},$$

where $\eta_1 \in \mathbb{R}^{n_r \times n}$*,* $\eta_2 \in \mathbb{R}^{q \times n}$*, and* $\eta_3 \in \mathbb{R}^{p \times n}$*. Then,*

$$r^{c*}(\sigma) = r^{c*}(\sigma_0) + \eta_1(\sigma - \sigma_0) + o(\|\sigma - \sigma_0\|^2). \tag{5.12}$$

We argue that the update (5.12) can be computed through simple vector multiplications, and thus is significantly more efficient than solving (5.9). The accuracy of the linear approximation rule is numerically validated in Fig. 5.3, which demonstrates the quadratic decay of the approximation error as σ approaches σ_0 (see Section 5.5 for a thorough discussion).

5.4 Network Resilience

In this section, we study the resilience of the network against changes in the degrees of trust of the drivers, and we illustrate a technique that allows us to classify the links in

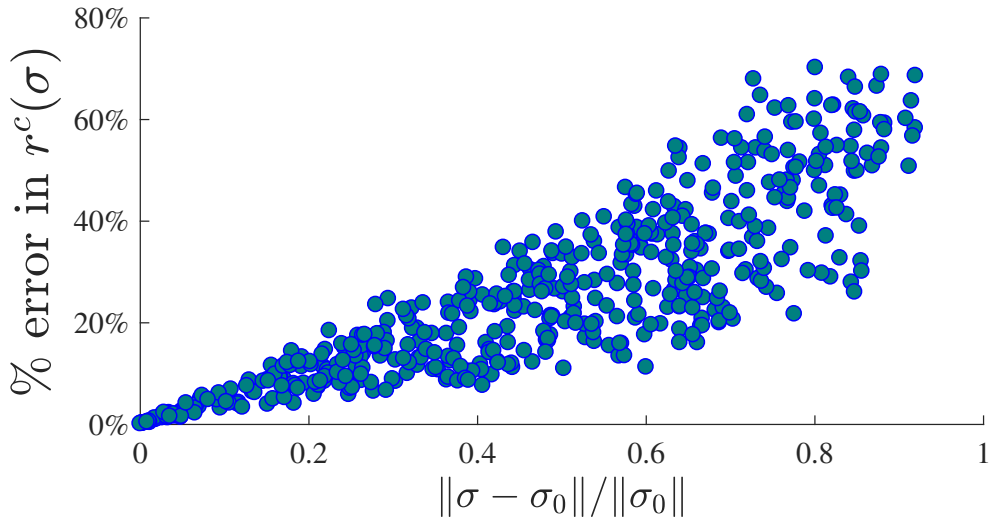

Figure 5.3: Numerical validation of the update rule (5.12).

relation to their resilience properties. We start with the following definition of margin of resilience of a network link.

Definition 5.4. ***(Links Margin of Resilience)*** *Let $i \in \mathcal{E}$, and let B_i be its jam density. The margin of resilience of link i is*

$$\begin{aligned} \rho_i(x_0) := \quad & \min_{\sigma} \quad && \|\sigma - \sigma_0\|_1 \\ & \textit{such that} && \dot{x} = (R - I) f(x, t) + \lambda, \\ & && R = \Sigma R^{\mathrm{C}} + (I - \Sigma) R^{\mathrm{S}}, \\ & && x_i \geq B_i, \ \textit{for some } t \in [0, \mathcal{H}]. \end{aligned}$$

□

In other words, the resilience of a certain link is defined as the smallest change in σ that generates its jam failure. Next, we present a lower bound on the margin of resilience

of the links. Our approach is based on the real-time control rule (5.12), and on first-order approximations of the constraints.

Theorem 5.5. ***(Lower Bound on Margin of Resilience)*** *Let $i \in \mathcal{E}$, let $\mathcal{F}(x_k, r_k, \lambda_k) = [\mathcal{F}_1(x_k, r_k, \lambda_k) \dots \mathcal{F}_n(x_k, r_k, \lambda_k)]^\mathsf{T}$, and let*

$$\Psi_i(r_k, x_k, \lambda_k, \sigma) := \frac{\partial \mathcal{F}_i(x_k, r_k, \lambda_k)}{\partial \sigma} + \frac{\partial \mathcal{F}_i(x_k, r_k, \lambda_k)}{\partial r^{\mathrm{c}}}\ \eta_1,$$

where η_1 is defined in (5.12)*. Then,*

$$\rho_i(x_0) \geq \min_k \frac{B_i - \mathcal{F}_i(x_k, r_k, \lambda_k)}{\|\Psi_i(k, \lambda, \sigma_0)\|_\infty}.$$

Proof. We first recast the notion of margin of resilience in terms of the discretized system (5.9). The margin of resilience of link i is the smallest change $\|\sigma - \sigma_0\|_1$ such that

$$\mathcal{F}_i(x_k, r_k(\sigma), \lambda_k) \geq B_i, \tag{5.13}$$

for some $k \in \{1, \dots, h\}$. We then rewrite $\mathcal{F}_i(x_k, r_k(\sigma), \lambda_k)$ by taking its Taylor expansion for around σ_0

$$\begin{aligned}\mathcal{F}_i(x_k, r_k(\sigma), \lambda_k) = \mathcal{F}_i(x_k, r_k(\sigma_0), \lambda_k) + \\ \underbrace{\frac{d\mathcal{F}_i}{d\sigma}(x_k, r_k(\sigma), \lambda_k)\bigg|_{\sigma=\sigma_0}}_{\Psi_i(r_k, x_k, \lambda_k, \sigma)} \delta_\sigma + o(\|\delta_\sigma\|^2),\end{aligned}$$

where $\delta_\sigma = \sigma - \sigma_0$, and where we used the implicit differentiation rule to compute $\Psi_i(r_k, x_k, \lambda_k, \sigma) = \frac{\partial \mathcal{F}_i}{\partial \sigma} + \frac{d\mathcal{F}_i}{dr^{\mathrm{c}}} \frac{dr^{\mathrm{c}}}{d\sigma}$, with $dr^{\mathrm{c}}/d\sigma = \eta_1$. By substituting into (5.13) and by rearranging the terms we obtain

$$B_i - \mathcal{F}_i(x_k, r_k(\sigma_0), \lambda_k) + o(\|\delta_\sigma\|^2) \leq \Psi_i(r_k, x_k, \lambda_k, \sigma)\delta_\sigma.$$

Finally, we take the L^1-norm on both sides of the above inequality, which yields

$$\begin{aligned} &|B_i - \mathcal{F}_i(x_k, r_k(\sigma_0), \lambda_k) + o(\|\delta_\sigma\|^2)| \\ &\quad \leq |\Psi_i(r^{\mathrm{c}}, x_k, \lambda_k, \sigma)\delta_\sigma| \leq \|\Psi_i(r^{\mathrm{c}}, x_k, \lambda_k, \sigma)\|_\infty \|(\delta_\sigma)\|_1 \end{aligned}$$

where we used Holder's inequality [80]. To conclude, we iterate the above reasoning for all times $k \in \{1, \ldots, h\}$, which yields the given bound for the margin of resilience and concludes the proof. ■

We conclude this section by observing that the quantity $\Psi_i(r_k, x_k, \lambda_k, \sigma)$ is also a constraint of (5.9), and thus can be directly computed from the output of the optimization. The tightness of the bound and the implications of the theorem are discussed in the next section.

5.5 Simulation Results

This section provides numerical simulations in support to the assumptions made in this chapter, and includes discussions and demonstrations of the benefits of the proposed

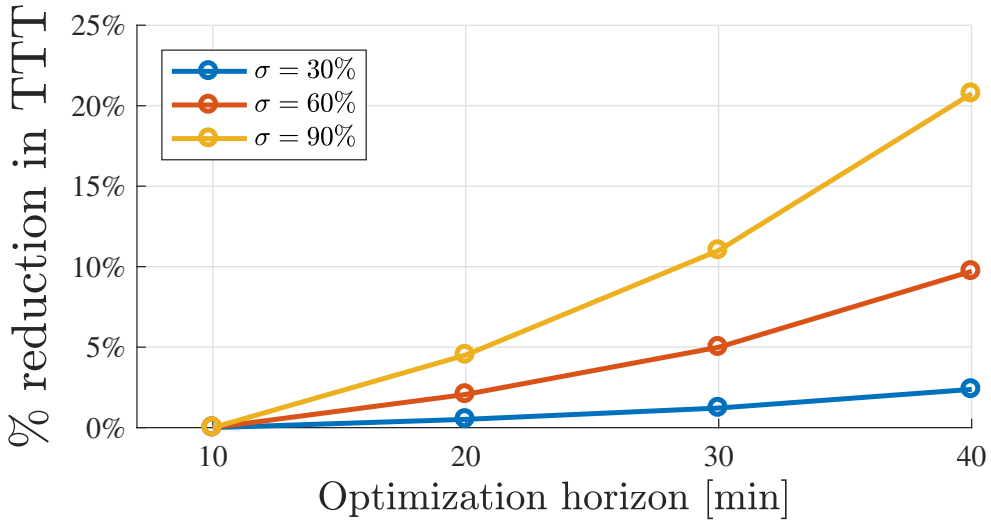

Figure 5.4: Travel time reduction for different degrees of trust and optimization horizons.

methods. We consider the network shown in Fig. 5.1, which comprises $n = 16$ links and $m = 7$ nodes. Each link has capacity $B_i = B = 200$veh, length $L_i = L = 5.25$mi, and velocity $v_i = v = 35$mi/h. For all i, we let $d_i(x_i) = v(1 - \exp(-ax_i))$, $a = 0.01$, and $s_i(x_i) = \frac{v}{L}(B - x_i)$ be the link demand and supply functions, respectively, and choose $\kappa_i(x)$ according to a proportional allocation rule [36]. We let $T_s = 0.15$h, and observe that $\max_i \frac{vT_s}{L} = 1$ satisfies the Courant-Friedrichs-Lewy assumption [34]. We let the network inflows be $\lambda_i = 10$veh/min for all $i \in \mathcal{E}^{\text{on}}$, and assume that the density of the each link at time $t = 0$ is 100veh/mi, for all $i \in \mathcal{E}$. The selfish turning preferences are chosen so that r^{s}_{ij} is split uniformly between the outgoing links at every node. Moreover, we assume $\sigma_i = \sigma$ for all i.

We begin by evaluating the benefits of partially controlling the network routing. Fig. 5.4 illustrates the reduction in Total Travel Time in relation to different trust levels. The figure highlights that a consistent reduction in Total Travel Time is the combined result of significant levels of trust in the provided routing suggestions and of considerably-large

control horizons. Next, we investigate the network resilience in relation to changes in σ (Fig. 5.5 (a) and (b)). To this aim, we show in Fig. 5.5(a) the distance from jam density of every link in the network when drivers follow non-cooperative routing (i.e. $\sigma = 0$). Formally, this quantity is captured by the link residual capacity

$$\mathrm{RC}_i := \min_k \frac{B_i - \mathcal{F}_i(x_k, r_k, \lambda_k)}{B_i},$$

which is a measure of the distance between the link density over time and its jam density B_i. Note that, for the considered case study, all links operate with less than 30% of their residual capacity. The lower bound on the links margin of resilience (Theorem 5.5) is show in Fig. 5.5(b). Two important implications follow from the simulation results illustrated in Fig. 5.5(b). First, the trends observed in the figure support our observation that partially controlling the routing can result in increased fragility. In fact, $\rho_i(x_0)$ for $\sigma_0 = 0$ is strictly larger that $\rho_i(x_0)$ for $\sigma_0 = 30\%$ for all $i \in \{4, \dots 16\} \setminus \{5, 12\}$. Second, values of $\rho_i(x_0)$ greater than 100% (observed, for instance, on link $i = 16$) imply that no feasible change in σ can lead to a jam failure of that link, while values of $\rho_i(x_0) < 100\%$ imply that there exists a feasible perturbation in σ that results in jam-failures of that link. We note that the values reported in Fig. 5.5(b) are consistent with the considered network topology. In fact, the dynamics of link $i = 16$ are independent of the routing choices performed by the drivers in the rest of the network.

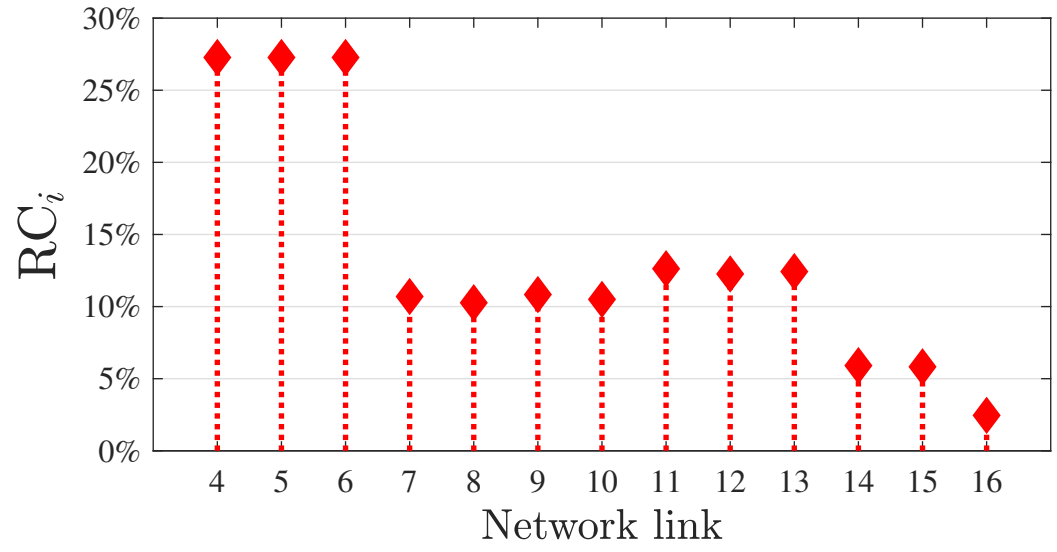

(a)

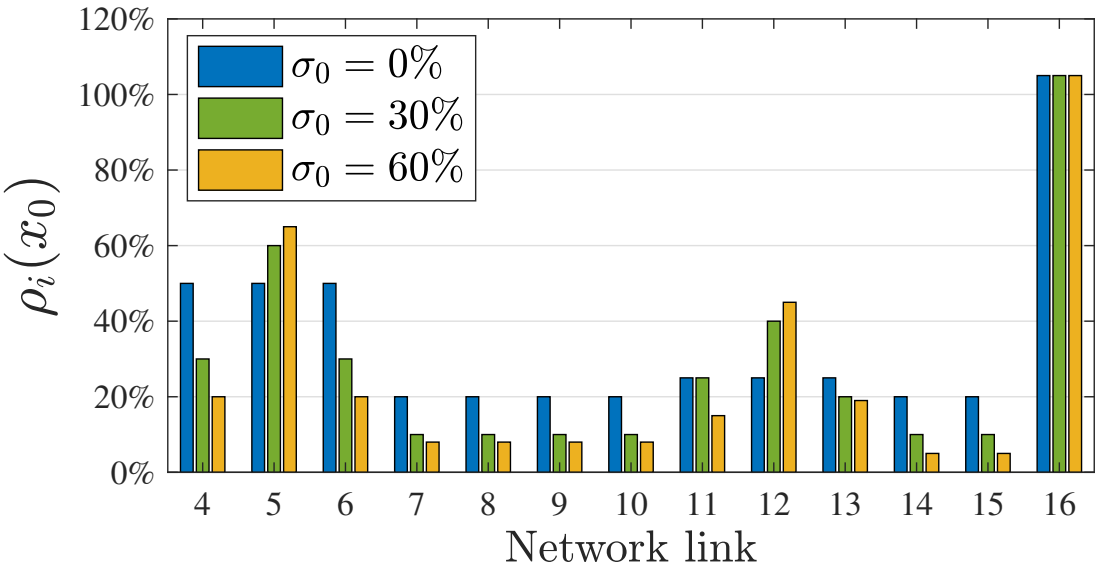

(b)

Figure 5.5: (a) Distance from constraint violation (non-cooperative routing). (b) Lower bound on links margin of resilience.

Part II

Application to Security in Complex Networks and Robotics

Chapter 6

Robustness Against Perturbations of the Network Edges

In this chapter we study the observability radius of network systems, which measures how robust is the property of system observability against perturbations of the communication edges. The goal of this chapter is to relate robustness of a network to the topological properties of the underlying communication structure. To this aim, we will specifically focus on networks with common communication structures, such as lines and stars. We refer to the published works [5, 10] for a comprehensive discussion of the results.

6.1 Introduction

Observability of a network guarantees the ability to reconstruct the system overall state from sparse measurements. While observability is a binary notion [23], the degree of observability, akin to the degree of controllability, can be quantified in different ways,

including the energy associated with the measurements [24, 25], the novelty of the output signal [26], the number of necessary sensor nodes [27, 28], and the robustness to removal of interconnection edges [29]. A quantitative notion of observability is preferable over a binary one, as it allows to compare different observable networks, select optimal sensor nodes, and identify topological features favoring observability.

Our notion of robustness is motivated by the fact that observability is a generic property [81] and network weights are rarely known without uncertainty. For these reasons numerical tests to assess observability may be unreliable and in fact fail to recognize unobservable systems: instead, our measure of observability robustness can be more reliably evaluated [82]. Among our contributions, we highlight connections between the robustness of a network and its structure, and we propose an algorithmic procedure to construct optimal perturbations. Our work finds applicability in network control problems where the network weights are subject to perturbations, in security applications where an attacker gains control of some network edges, and in network science for the classification of edges and the design of robust topologies.

Our study is inspired by classic works on the observability radius of dynamical systems [83, 84, 85], defined as the norm of the smallest perturbation yielding unobservability or, equivalently, the distance to the nearest unobservable realization. For a linear system

described by the pair (A, C), the radius of observability has been classically defined as

$$\mu(A,C) = \min_{\Delta_A, \Delta_C} \left\| \begin{bmatrix} \Delta_A \\ \Delta_C \end{bmatrix} \right\|_2 ,$$

$$\text{s.t. } (A + \Delta_A, C + \Delta_C) \text{ is unobservable.}$$

As a known result [84], the observability radius satisfies

$$\mu(A,C) = \min_s \sigma_n \left(\begin{bmatrix} sI - A \\ C \end{bmatrix} \right),$$

where σ_n denotes the smallest singular value, and $s \in \mathbb{R}$ ($s \in \mathbb{C}$ if complex perturbations are allowed). The optimal perturbations Δ_A and Δ_C are typically full matrices and, to the best of our knowledge, all existing results and procedures are not applicable to the case where the perturbations must satisfy a desired sparsity constraint (e.g., see [86]). This scenario is in fact the relevant one for network systems, where the nonzero entries of the network matrices A and C correspond to existing network edges, and it would be undesirable or unrealistic for a perturbation to modify the interaction of disconnected nodes. An exception is the recent paper [29], where structured perturbations are considered in a controllability problem, yet the discussion is limited to the removal of edges.

We depart from the literature by requiring the perturbation to be real, with a desired sparsity pattern, and confined to the network matrix ($\Delta_C = 0$). Our approach builds on the theory of *total least squares* [87]. With respect to existing results on this topic,

our work proposes procedures tailored to networks, fundamental bounds, and insights into the robustness of different network topologies.

The contribution of this chapter is fourfold. First, we define a metric of network robustness that captures the resilience of a network system to structural, possibly malicious, perturbations. Our metric evaluates the distance of a network from the set of unobservable networks with the same interconnection structure, and it extends existing works on the observability radius of linear systems.

Second, we formulate a problem to determine optimal perturbations (with smallest Frobenius norm) preventing observability. We show that the problem is not convex, derive optimality conditions, and prove that any optimal solution solves a nonlinear generalized eigenvalue problem. Additionally, we propose a numerical procedure based on the power iteration method to determine (sub)optimal solutions.

Third, we derive a fundamental bound on the expected observability radius for networks with random weights. In particular, we present a class of networks for which the expected observability radius decays to zero as the network cardinality increases. Furthermore, we characterize the robustness of line and star networks. In accordance with recent findings on the role of symmetries for the observability and controllability of networks [88, 89], we demonstrate that line networks are inherently more robust than star networks to perturbations of the edge weights. This analysis shows that our measure of robustness can in fact be used to compare different network topologies and guide the design of robust complex systems.

Because the networks we consider are in fact systems with linear dynamics, our results are generally applicable to linear dynamical systems. Yet, our setup allows for perturbations with a fixed sparsity pattern, which may arise from the organization of a network system.

Fourth, we discuss several generalizations of our basic framework, including its extension to continuous-time descriptor dynamics. This extension allows us to study a novel class of attacks in power systems, where an attacker tampers with generators and network parameters. Finally, although our presentation focuses on perturbations preventing observability only, the extension to controllability is straightforward.

The rest of the chapter is organized as follows. Section 6.2 contains our network model, the definition of the network observability radius, and some preliminary considerations. Section 6.3 describes our method to compute network perturbations with smallest Frobenius norm, our optimization algorithm, and an illustrative example. Our bounds on the observability radius of random networks are in Section 6.4.

6.2 The Observability Radius of Network Systems

Consider a directed graph $\mathcal{G} := (\mathcal{V}, \mathcal{E})$, where $\mathcal{V} := \{1, \ldots, n\}$ and $\mathcal{E} \subseteq \mathcal{V} \times \mathcal{V}$ are the vertex and edge sets, respectively. Let $A = [a_{ij}]$ be the *weighted adjacency matrix* of $\mathcal{G}$, where $a_{ij} \in \mathbb{R}$ denotes the weight associated with the edge $(i, j) \in \mathcal{E}$ (representing flow of information from node j to node i), and $a_{ij} = 0$ whenever $(i, j) \notin \mathcal{E}$. Let e_i denote the i-th canonical vector of dimension n. Let $\mathcal{O} = \{o_1, \ldots, o_p\} \subseteq \mathcal{V}$ be the set of *sensor nodes*, and define the network output matrix as $C_{\mathcal{O}} = \begin{bmatrix} e_{o_1} & \ldots & e_{o_p} \end{bmatrix}^{\mathsf{T}}$. Let $x_i(t) \in \mathbb{R}$ denote the *state*

of node i at time t, and let $x : \mathbb{N}_{\geq 0} \to \mathbb{R}^n$ be the map describing the evolution over time of the network state. The network dynamics are described by the linear discrete-time system

$$x(t+1) = A\,x(t), \text{ and } y(t) = C_{\mathcal{O}}\,x(t), \tag{6.1}$$

where $y : \mathbb{N}_{\geq 0} \to \mathbb{R}^p$ is the output of the sensor nodes $\mathcal{O}$.

In this work we characterize structured network perturbations that prevent observability from the sensor nodes. To this aim, let $\mathcal{H} = (\mathcal{V}_{\mathcal{H}}, \mathcal{E}_{\mathcal{H}})$ be the *constraint graph*, and define the set of matrices compatible with $\mathcal{H}$ as

$$\mathcal{A}_{\mathcal{H}} = \{M \ : \ M \in \mathbb{R}^{|\mathcal{V}|\times|\mathcal{V}|}, M_{ij} = 0 \text{ if } (i,j) \notin \mathcal{E}_{\mathcal{H}}\}.$$

Recall from the eigenvector observability test that the network (6.1) is observable if and only if there is no right eigenvector of A that lies in the kernel of $C_{\mathcal{O}}$, that is, $C_{\mathcal{O}}x \neq 0$ whenever $x \neq 0$, $Ax = \lambda x$, and $\lambda \in \mathbb{C}$ [30]. In this work we consider and study the following optimization problem:

$$\begin{aligned}
\min \quad & \|\Delta\|_{\mathrm{F}}^2, \\
\text{s.t.} \quad & (A+\Delta)x = \lambda x, && \text{(eigenvalue constraint)}, \\
& \|x\|_2 = 1, && \text{(eigenvector constraint)}, \\
& C_{\mathcal{O}}x = 0, && \text{(unobservability)}, \\
& \Delta \in \mathcal{A}_{\mathcal{H}}, && \text{(structural constraint)},
\end{aligned} \tag{6.2}$$

where the minimization is carried out over the eigenvector $x \in \mathbb{C}^n$, the unobservable eigenvalue $\lambda \in \mathbb{C}$, and the network perturbation $\Delta \in \mathbb{R}^{n \times n}$. The function $\|\cdot\|_{\mathrm{F}} : \mathbb{R}^{n \times n} \to \mathbb{R}_{\geq 0}$ is the Frobenius norm, and $\mathcal{A}_{\mathcal{H}}$ expresses the desired sparsity pattern of the perturbation. It should be observed that (i) the minimization problem (6.2) is not convex because the variables Δ and x are multiplied each other in the eigenvector constraint $(A + \Delta)x = \lambda x$, (ii) if $A \in \mathcal{A}_{\mathcal{H}}$, then the minimization problem is feasible if and only if there exists a network matrix $A + \Delta = \tilde{A} \in \mathcal{A}_{\mathcal{H}}$ satisfying the eigenvalue and eigenvector constraint, and (iii) if $\mathcal{H} = \mathcal{G}$, then the perturbation modifies the weights of the existing edges only. We make the following assumption:

(A1) The pair $(A, C_{\mathcal{O}})$ is observable.

Assumption (A1) implies that the perturbation Δ must be nonzero to satisfy the constraints in (6.2).

For the pair $(A, C_{\mathcal{O}})$, the *network observability radius* is the solution to the optimization problem (6.2), which quantifies the total edge perturbation to achieve unobservability. Different cost functions may be of interest and are left as the subject of future research.

The minimization problem (6.2) can be solved by two subsequent steps. First, we fix the eigenvalue λ, and compute an optimal perturbation that solves the minimization problem for that λ. This computation is the topic of the next section. Second, we search the complex plane for the optimal λ yielding the perturbation with minimum cost. We observe that (i) the exhaustive search of the optimal λ is an inherent feature of this class of problems, as also highlighted in prior work [85]; (ii) in some cases and for certain network

topologies the optimal λ can be found analytically, as we do in Section 6.4 for line and star networks; and (iii) in certain applications the choice of λ is guided by the objective of the network perturbation, such as inducing unobservability of unstable modes.

6.3 Optimality Conditions and Algorithms to Compute the Observability Radius

In this section we consider problem (6.2) with *fixed* λ. Specifically, we address the following minimization problem: given a constraint graph $\mathcal{H}$, the network matrix $A \in \mathcal{A}_{\mathcal{G}}$, an output matrix $C_{\mathcal{O}}$, and a desired unobservable eigenvalue $\lambda \in \mathbb{C}$, determine a perturbation $\Delta^* \in \mathbb{R}^{n\times n}$ satisfying

$$\begin{aligned} \|\Delta^*\|_{\mathrm{F}}^2 = \min_{x\in\mathbb{C}^n, \Delta\in\mathbb{R}^{n\times n}} \quad & \|\Delta\|_{\mathrm{F}}^2, \\ \text{s.t.} \quad & (A+\Delta)x = \lambda x, \\ & \|x\|_2 = 1, \\ & C_{\mathcal{O}} x = 0, \\ & \Delta \in \mathcal{A}_{\mathcal{H}}. \end{aligned} \tag{6.3}$$

From (6.3), the value $\|\Delta^*\|_{\mathrm{F}}^2$ equals the observability radius of the network A with sensor nodes $\mathcal{O}$, constraint graph $\mathcal{H}$, and fixed unobservable eigenvalue λ.

6.3.1 Optimal network perturbation

We now shape minimization problem (6.3) to facilitate its solution. Without affecting generality, relabel the network nodes such that the sensor nodes set satisfy

$$\mathcal{O} = \{1, \ldots, p\}, \text{ so that } C_{\mathcal{O}} = \begin{bmatrix} I_p & 0 \end{bmatrix}. \tag{6.4}$$

Accordingly,

$$A = \begin{bmatrix} A_{11} & A_{12} \\ A_{21} & A_{22} \end{bmatrix}, \text{ and } \Delta = \begin{bmatrix} \Delta_{11} & \Delta_{12} \\ \Delta_{21} & \Delta_{22} \end{bmatrix}, \tag{6.5}$$

where $A_{11} \in \mathbb{R}^{p \times p}$, $A_{12} \in \mathbb{R}^{p \times n-p}$, $A_{21} \in \mathbb{R}^{n-p \times p}$, and $A_{22} \in \mathbb{R}^{n-p \times n-p}$. Let $V = [v_{ij}]$ be the unweighted adjacency matrix of $\mathcal{H}$, where $v_{ij} = 1$ if $(i, j) \in \mathcal{E}_{\mathcal{H}}$, and $v_{ij} = 0$ otherwise. Following the partitioning of A in (6.5), let

$$V = \begin{bmatrix} V_{11} & V_{12} \\ V_{21} & V_{22} \end{bmatrix}.$$

We perform the following three simplifying steps.

(1–Rewriting the structural constraints) Let $B = A + \Delta$, and notice that $\|\Delta\|_{\mathrm{F}}^2 = \sum_{i=1}^{n} \sum_{j=1}^{n} (b_{ij} - a_{ij})^2$. Then, the minimization problem (6.3) can equivalently be rewritten restating the constraint $\Delta \in \mathcal{A}_{\mathcal{H}}$, as in the following:

$$\|\Delta\|_{\mathrm{F}}^2 = \|B - A\|_{\mathrm{F}}^2 = \sum_{i=1}^{n} \sum_{j=1}^{n} (b_{ij} - a_{ij})^2 v_{ij}^{-1}.$$

Notice that $\|\Delta\|_{\mathrm{F}}^2 = \infty$ whenever Δ does not satisfy the structural constraint, that is, when $v_{ij} = 0$ and $b_{ij} \neq a_{ij}$.

(2–Minimization with real variables) Let $\lambda = \lambda_{\Re} + \mathrm{i}\lambda_{\Im}$, where i denotes the imaginary unit. Let

$$x_{\Re} = \begin{bmatrix} x_{\Re}^1 \\ \\ x_{\Re}^2 \end{bmatrix}, \text{ and } x_{\Im} = \begin{bmatrix} x_{\Im}^1 \\ \\ x_{\Im}^2 \end{bmatrix},$$

denote the real and imaginary parts of the eigenvector x, with $x_{\Re}^1 \in \mathbb{R}^p$, $x_{\Im}^1 \in \mathbb{R}^p$, $x_{\Re}^2 \in \mathbb{R}^{n-p}$, and $x_{\Im}^2 \in \mathbb{R}^{n-p}$.

Lemma 6.1. ***(Minimization with real eigenvector constraint)*** *The constraint* $(A + \Delta)x = \lambda x$ *can equivalently be written as*

$$\begin{aligned} (A + \Delta - \lambda_{\Re} I)x_{\Re} &= -\lambda_{\Im} x_{\Im}, \\ (A + \Delta - \lambda_{\Re} I)x_{\Im} &= \lambda_{\Im} x_{\Re}. \end{aligned} \tag{6.6}$$

Proof. By considering separately the real and imaginary part of the eigenvalue constraint, we have $(A+\Delta)x = \lambda_{\Re} x + \mathrm{i}\lambda_{\Im} x$ and $(A+\Delta)\bar{x} = \lambda_{\Re}\bar{x} - \mathrm{i}\lambda_{\Im}\bar{x}$, where $\bar{x}$ denotes the complex conjugate of x. Notice that

$$\underbrace{(A + \Delta)(x + \bar{x})}_{(A+\Delta)2x_{\Re}} = \underbrace{(\lambda_{\Re} + \mathrm{i}\lambda_{\Im})x + (\lambda_{\Re} - \mathrm{i}\lambda_{\Im})\bar{x}}_{2\lambda_{\Re}x_{\Re} - 2\lambda_{\Im}x_{\Im}},$$

and, analogously,

$$\underbrace{(A+\Delta)(x-\bar{x})}_{(A+\Delta)2\mathrm{i}x_{\Im}} = \underbrace{(\lambda_{\Re}+\mathrm{i}\lambda_{\Im})x-(\lambda_{\Re}-\mathrm{i}\lambda_{\Im})\bar{x}}_{2\mathrm{i}\lambda_{\Re}x_{\Im}+2\mathrm{i}\lambda_{\Im}x_{\Re}},$$

which concludes the proof. ■

Thus, the problem (6.3) can be solved over real variables only.

(3–Reduction of dimensionality) The constraint $C_{\mathcal{O}}x = 0$ and equation (6.4) imply that $x^1_{\Re} = x^1_{\Im} = 0$. Thus, in the minimization problem (6.5) we set $\Delta_{11} = 0$, $\Delta_{21} = 0$, and consider the minimization variables $x^2_{\Re}$, $x^2_{\Im}$, Δ_{12}, and Δ_{22}.

These simplifications lead to the following result.

Lemma 6.2. ***(Equivalent minimization problem)*** *Let*

$$\begin{aligned} \bar{A} &= \begin{bmatrix} A_{12} \\ A_{22} \end{bmatrix}, \bar{\Delta} = \begin{bmatrix} \Delta_{12} \\ \Delta_{22} \end{bmatrix}, \bar{M} = \begin{bmatrix} 0_{p\times n-p} \\ \lambda_{\Im} I_{n-p} \end{bmatrix}, \\ \bar{N} &= \begin{bmatrix} 0_{p\times n-p} \\ \lambda_{\Re} I_{n-p} \end{bmatrix}, \bar{V} = \begin{bmatrix} V_{12} \\ V_{22} \end{bmatrix}, \text{ and } \bar{B} = \bar{A} + \bar{\Delta}. \end{aligned} \tag{6.7}$$

The following minimization problem is equivalent to (6.3)*:*

$$
\begin{aligned}
\|\bar{\Delta}^*\|_F^2 \;=\; \min_{\bar{B},x_{\Re}^2,x_{\Im}^2} \quad & \sum_{i=1}^{n}\sum_{j=1}^{n-p}(\bar{b}_{ij}-\bar{a}_{ij})^2 v_{ij}^{-1}, \\
s.t. \quad & \begin{bmatrix} \bar{B}-\bar{N} & \bar{M} \\ -\bar{M} & \bar{B}-\bar{N} \end{bmatrix} \begin{bmatrix} x_{\Re}^2 \\ x_{\Im}^2 \end{bmatrix} = 0, \\
& \left\| \begin{bmatrix} x_{\Re}^2 \\ x_{\Im}^2 \end{bmatrix} \right\|_2 = 1.
\end{aligned}
\tag{6.8}
$$

The minimization problem (6.8) belongs to the class of *(structured) total least squares* problems, which arise in several estimation and identification problems in control theory and signal processing. Our approach is inspired by [87], with the difference that we focus on real perturbations Δ and complex eigenvalue λ: this constraint leads to different optimality conditions and algorithms. Let $A \otimes B$ denote the Kronecker product between the matrices A and B, and $\mathrm{diag}(d_1, \ldots, d_n)$ the diagonal matrix with scalar entries $d_1, \ldots, d_n$. We now derive the optimality conditions for the problem (6.8).

Theorem 6.3. ***(Optimality conditions)*** *Let $x_{\Re}^*$, and $x_{\Im}^*$ be a solution to the minimization problem* (6.8)*. Then,*

$$
\begin{aligned}
\underbrace{\begin{bmatrix} \bar{A}-\bar{N} & \bar{M} \\ -\bar{M} & \bar{A}-\bar{N} \end{bmatrix}}_{\tilde{A}} \underbrace{\begin{bmatrix} x_{\Re}^* \\ x_{\Im}^* \end{bmatrix}}_{x^*} &= \sigma \underbrace{\begin{bmatrix} S_x & T_x \\ T_x & Q_x \end{bmatrix}}_{D_x} \underbrace{\begin{bmatrix} y_1 \\ y_2 \end{bmatrix}}_{y^*}, \\
\underbrace{\begin{bmatrix} \bar{A}-\bar{N} & \bar{M} \\ -\bar{M} & \bar{A}-\bar{N} \end{bmatrix}^{\mathsf{T}}}_{\tilde{A}^{\mathsf{T}}} \underbrace{\begin{bmatrix} y_1 \\ y_2 \end{bmatrix}}_{y^*} &= \sigma \underbrace{\begin{bmatrix} S_y & T_y \\ T_y & Q_y \end{bmatrix}}_{D_y} \underbrace{\begin{bmatrix} x_{\Re}^* \\ x_{\Im}^* \end{bmatrix}}_{x^*},
\end{aligned}
\tag{6.9}
$$

for some $\sigma > 0$ *and* $y^* \in \mathbb{R}^{2n}$ *with* $\|y^*\| = 1$, *and where*

$$
\begin{aligned}
D_1 &= diag(v_{11}, \ldots, v_{1n}, v_{21}, \ldots, v_{2n}, \ldots, v_{n1}, \ldots, v_{nn}), \\
D_2 &= diag(v_{11}, \ldots, v_{n1}, v_{12}, \ldots, v_{n2}, \ldots, v_{1n}, \ldots, v_{nn}), \\
S_x &= (I \otimes x^*_{\Re})^{\mathsf{T}} D_1 (I \otimes x^*_{\Re}),\ T_x = (I \otimes x^*_{\Re})^{\mathsf{T}} D_1 (I \otimes x^*_{\Im}), \\
Q_x &= (I \otimes x^*_{\Im})^{\mathsf{T}} D_1 (I \otimes x^*_{\Im}),\ S_y = (I \otimes y_1)^{\mathsf{T}} D_2 (I \otimes y_1), \\
T_y &= (I \otimes y_1)^{\mathsf{T}} D_2 (I \otimes y_2),\ Q_y = (I \otimes y_2)^{\mathsf{T}} D_2 (I \otimes y_2).
\end{aligned}
\tag{6.10}
$$

Proof. We adopt the method of Lagrange multipliers to derive optimality conditions for the problem (6.8). The Lagrangian is

$$
\begin{aligned}
\mathcal{L}(\bar{B}, x^2_{\Re}, x^2_{\Im}, \ell_1, \ell_2, \rho) &= \sum_i \sum_j (\bar{b}_{ij} - \bar{a}_{ij})^2 v_{ij}^{-1} \\
&+ \ell_1^{\mathsf{T}} ((\bar{B} - \bar{N}) x^2_{\Re} + \bar{M} x^2_{\Im}) + \ell_2^{\mathsf{T}} ((\bar{B} - \bar{N}) x^2_{\Im} - \bar{M} x^2_{\Re}) \\
&+ \rho (1 - x^{2\mathsf{T}}_{\Re} x^2_{\Re} - x^{2\mathsf{T}}_{\Im} x^2_{\Im}),
\end{aligned}
\tag{6.11}
$$

where $\ell_1 \in \mathbb{R}^n$, $\ell_2 \in \mathbb{R}^n$, and $\rho \in \mathbb{R}$ are Lagrange multipliers. By equating the partial derivatives of $\mathcal{L}$ to zero we obtain

$$\frac{\partial \mathcal{L}}{\partial b_{ij}} = 0 \Rightarrow -2(\bar{a}_{ij} - \bar{b}_{ij})v_{ij}^{-1} + \ell_{1i}x_{\Re j}^2 + \ell_{2i}x_{\Im j}^2 = 0, \tag{6.12}$$

$$\frac{\partial \mathcal{L}}{\partial x_{\Re}^2} = 0 \Rightarrow \ell_1^{\mathsf{T}}(\bar{B} - \bar{N}) - \ell_2^{\mathsf{T}}\bar{M} - 2\rho x_{\Re}^{2\mathsf{T}} = 0, \tag{6.13}$$

$$\frac{\partial \mathcal{L}}{\partial x_{\Im}^2} = 0 \Rightarrow \ell_1^{\mathsf{T}}\bar{M} + \ell_2^{\mathsf{T}}(\bar{B} - \bar{N}) - 2\rho x_{\Im}^{2\mathsf{T}} = 0, \tag{6.14}$$

$$\frac{\partial \mathcal{L}}{\partial \ell_1} = 0 \Rightarrow (\bar{B} - \bar{N})x_{\Re}^2 + \bar{M}x_{\Im}^2 = 0, \tag{6.15}$$

$$\frac{\partial \mathcal{L}}{\partial \ell_2} = 0 \Rightarrow (\bar{B} - \bar{N})x_{\Im}^2 - \bar{M}x_{\Re}^2 = 0, \tag{6.16}$$

$$\frac{\partial \mathcal{L}}{\partial \rho} = 0 \Rightarrow x_{\Re}^{2\mathsf{T}}x_{\Re}^2 + x_{\Im}^{2\mathsf{T}}x_{\Im}^2 = 1. \tag{6.17}$$

Let $L_1 = \operatorname{diag}(\ell_1)$, $L_2 = \operatorname{diag}(\ell_2)$, $X_{\Re} = \operatorname{diag}(x_{\Re}^2)$, $X_{\Im} = \operatorname{diag}(x_{\Im}^2)$. After including the factor 2 into the multipliers, equation (6.12) can be written in matrix form as

$$\bar{A} - \bar{B} = L_1\bar{V}X_{\Re} + L_2\bar{V}X_{\Im}. \tag{6.18}$$

Analogously, equations (6.13) and (6.14) can be written as

$$\begin{bmatrix} \ell_1^{\mathsf{T}} & \ell_2^{\mathsf{T}} \end{bmatrix} \begin{bmatrix} \bar{B} - \bar{N} & \bar{M} \\ -\bar{M} & \bar{B} - \bar{N} \end{bmatrix} - 2\rho \begin{bmatrix} x_{\Re}^{2\mathsf{T}} & x_{\Im}^{2\mathsf{T}} \end{bmatrix} = 0, \tag{6.19}$$

From equation (6.19) we have

$$\begin{bmatrix} \ell_1^\mathsf{T} & \ell_2^\mathsf{T} \end{bmatrix} \underbrace{\begin{bmatrix} \bar{B}-\bar{N} & \bar{M} \\ -\bar{M} & \bar{B}-\bar{N} \end{bmatrix} \begin{bmatrix} x_\Re^2 \\ x_\Im^2 \end{bmatrix}}_{=0 \text{ due to (6.15) and (6.16)}} - 2\rho = 0,$$

from which we conclude $\rho = 0$. By combining (6.15) and (6.18) (respectively, (6.16) and (6.18)) we obtain

$$(\bar{A}-\bar{N})x_\Re^2 + \bar{M}x_\Im^2 = \left(L_1\bar{V}X_\Re + L_2\bar{V}X_\Im\right)x_\Re^2,$$
$$(\bar{A}-\bar{N})x_\Im^2 - \bar{M}x_\Re^2 = \left(L_1\bar{V}X_\Re + L_2\bar{V}X_\Im\right)x_\Im^2.$$

Analogously, by combining (6.13) and (6.18), (6.14) and (6.18), we obtain

$$\ell_1^\mathsf{T}(\bar{A}-\bar{N}) - \ell_2^\mathsf{T}\bar{M} = \ell_1^\mathsf{T}\left(L_1\bar{V}X_\Re + L_2\bar{V}X_\Im\right),$$
$$\ell_2^\mathsf{T}(\bar{A}-\bar{N}) + \ell_1^\mathsf{T}\bar{M} = \ell_2^\mathsf{T}\left(L_1\bar{V}X_\Re + L_2\bar{V}X_\Im\right).$$

Let $\sigma = \sqrt{\ell_1^\mathsf{T}\ell_1 + \ell_2^\mathsf{T}\ell_2}$ and observe that σ cannot be zero. Indeed, due to Assumption (A1), the optimal perturbation can not be zero; thus, the first constraint in (6.8) must be active and the corresponding multiplier must be nonzero. Then, we can define $y_1 = \ell_1/\sigma$ and $y_2 = \ell_2/\sigma$ and we can verify that

$$\left(L_1\bar{V}X_\Re + L_2\bar{V}X_\Im\right)x_\Re^2 = \sigma\left(S_x y_1 + T_x y_2\right),$$
$$\left(L_1\bar{V}X_\Re + L_2\bar{V}X_\Im\right)x_\Im^2 = \sigma\left(T_x y_1 + Q_x y_2\right),$$

and

$$\begin{aligned}\sigma\left(y_1^{\mathsf{T}}(\bar{A}-\bar{N})-y_2^{\mathsf{T}}\bar{M}\right) &= \ell_1^{\mathsf{T}}\left(L_1\bar{V}X_{\Re}+L_2\bar{V}X_{\Im}\right)\\ &= \sigma^2\left(S_y x_{\Re}^2+T_y x_{\Im}^2\right)^{\mathsf{T}},\\ \sigma\left(y_2^{\mathsf{T}}(\bar{A}-\bar{N})+y_1^{\mathsf{T}}\bar{M}\right) &= \ell_2^{\mathsf{T}}\left(L_1\bar{V}X_{\Re}+L_2\bar{V}X_{\Im}\right)\\ &= \sigma^2\left(T_y x_{\Re}^2+Q_y x_{\Im}^2\right)^{\mathsf{T}},\end{aligned}$$

which conclude the proof. ■

Note that equations (6.9) may admit multiple solutions, and that every solution to (6.9) yields a network perturbation that satisfies the constraints in the minimization problem (6.8). We now present the following result to compute perturbations.

Corollary 6.4. ***(Minimum norm perturbation)*** *Let* Δ^* *be a solution to* (6.3)*. Then,* $\Delta^* = [0^{n\times p}\ \bar{\Delta}^*]$*, where*

$$\bar{\Delta}^* = -\sigma\left(diag(y_1)\bar{V}\,diag(x_{\Re}^*) - diag(y_2)\bar{V}\,diag(x_{\Im}^*)\right),$$

and $x_{\Re}^*$*,* $x_{\Im}^*$*,* y_1*,* y_2*,* σ *satisfy the equations* (6.9)*. Moreover,*

$$\|\Delta\|_F^2 = \sigma^2 x^{*\mathsf{T}} D_y x^* = \sigma x^{*\mathsf{T}}\tilde{A}^{\mathsf{T}} y^* \le \sigma\|\tilde{A}\|_F.$$

Proof. The expression for the perturbation Δ^* comes from Lemma 6.2 and (6.18), and the fact that $L_1 = \sigma \operatorname{diag}(y_1)$, $L_2 = \sigma \operatorname{diag}(y_2)$. To show the second part notice that

$$\begin{aligned}\|\Delta\|_{\mathrm{F}}^2 = \|A - B\|_{\mathrm{F}}^2 &= \|L_1 \bar{V} X_{\Re} + L_2 \bar{V} X_{\Im}\|_{\mathrm{F}}^2 \\ &= \sigma^2 \sum_i \sum_j \left(y_{1i}^2 x_{\Re j}^2 + y_{2i}^2 x_{\Im j}^2\right) v_{ij} \\ &= \sigma^2 x^{*\mathsf{T}} D_y x^* = \sigma x^{*\mathsf{T}} \tilde{A}^{\mathsf{T}} y^*,\end{aligned}$$

where the last equalities follow from (6.9). Finally, the inequality follows from $\|x^*\|_2 = \|x^*\|_{\mathrm{F}} = \|y^*\|_2 = \|y^*\|_{\mathrm{F}} = 1$. ■

To compute a triple (σ, x^*, y^*) satisfying the condition in Theorem 6.3, observe that (6.9) can be written in matrix form as

$$\underbrace{\begin{bmatrix} 0 & \tilde{A}^{\mathsf{T}} \\ \tilde{A} & 0 \end{bmatrix}}_{H} \underbrace{\begin{bmatrix} x \\ y \end{bmatrix}}_{z} = \bar{\sigma} \underbrace{\begin{bmatrix} D_y & 0 \\ 0 & D_x \end{bmatrix}}_{D} \underbrace{\begin{bmatrix} x \\ y \end{bmatrix}}_{z}. \tag{6.20}$$

Lemma 6.5. ***(Equivalence between Theorem 6.3 and*** (6.20)***)*** *Let (σ, x, y), with $x \neq 0$, solve* (6.20)*. Then, $\sigma \neq 0$ and $y \neq 0$, and the triple $((\alpha\beta)^{-1}\sigma, \alpha x, \beta y)$, with $\alpha = sgn(\sigma)\|x\|^{-1}$ and $\beta = \|y\|^{-1}$, satisfies the conditions in Theorem 6.3.*

Proof. Because $x \neq 0$ and $\tilde{A}$ has full column rank due to Assumption (A1), it follows $\sigma \neq 0$ and $y \neq 0$. Let D_x and D_y be as in (6.9). Notice that $D_{\alpha x} = \alpha^2 D_x$ and $D_{\beta y} = \beta^2 D_y$.

Notice that $(\alpha\beta)^{-1}\sigma > 0$. We have

$$\tilde{A}\alpha x = \frac{\sigma}{\alpha\beta}\alpha^2 D_x \beta y = \alpha\sigma D_x y,$$
$$\tilde{A}^{\mathsf{T}}\beta y = \frac{\sigma}{\alpha\beta}\beta^2 D_y \alpha x = \beta\sigma D_y x,$$

which concludes the proof. ■

Lemma 6.5 shows that a (sub)optimal network perturbation can in fact be constructed by solving equations (6.20). It should be observed that, if the matrices S_x, T_x, Q_x, S_y, T_y, and Q_y were constant, then (6.20) would describe a generalized eigenvalue problem, thus a solution $(\bar{\sigma}, z)$ would be a pair of generalized eigenvalue and eigenvector. These facts will be exploited in the next section to develop a heuristic algorithm to compute a (sub)optimal network perturbation.

Remark 6.6. ***(Smallest network perturbation with respect to the unobservable eigenvalue)*** *In the minimization problem* (6.3) *the size of the perturbation* Δ^* *depends on the desired eigenvalue* λ*, and it may be of interest to characterize the unobservable eigenvalue* $\lambda^* = \lambda^*_{\Re} + \mathrm{i}\lambda^*_{\Im}$ *yielding the smallest network perturbation that prevents observability. To this aim, we equate to zero the derivatives of the Lagrangian* (6.11) *with respect to* $\lambda_{\Re}$ *and* $\lambda_{\Im}$

to obtain

$$\frac{\partial \mathcal{L}}{\partial \lambda_{\Re}} = 0 \Rightarrow \ell_1^{\mathsf{T}} \begin{bmatrix} 0_p \\ x_{\Re}^2 \end{bmatrix} + \ell_2^{\mathsf{T}} \begin{bmatrix} 0_p \\ x_{\Im}^2 \end{bmatrix} = 0,$$

$$\frac{\partial \mathcal{L}}{\partial \lambda_{\Im}} = 0 \Rightarrow \ell_1^{\mathsf{T}} \begin{bmatrix} 0_p \\ x_{\Im}^2 \end{bmatrix} - \ell_2^{\mathsf{T}} \begin{bmatrix} 0_p \\ x_{\Re}^2 \end{bmatrix} = 0.$$

The above conditions clarify that, for the perturbation Δ to be of the smallest size with respect to λ, the Lagrange multipliers ℓ_1 and ℓ_2, and the vectors $x_{\Re}^2$ and $x_{\Im}^2$ must verify an orthogonality condition. □

Remark 6.7. ***(Real unobservable eigenvalue)*** *When the unobservable eigenvalue λ in* (6.3) *is real, the optimality conditions in Theorem 6.3 can be simplified to*

$$(\bar{A} - \bar{N})x_{\Re} = \sigma S_x y_1, \text{ and } (\bar{A} - \bar{N})y_1 = \sigma S_y x_{\Re}.$$

The generalized eigenvalue equation (6.20) *becomes*

$$\begin{bmatrix} 0 & \bar{A}^{\mathsf{T}} - \bar{N}^{\mathsf{T}} \\ \bar{A} - \bar{N} & 0 \end{bmatrix} \begin{bmatrix} y_1 \\ x_{\Re} \end{bmatrix} = \sigma \begin{bmatrix} S_x & 0 \\ 0 & S_y \end{bmatrix} \begin{bmatrix} y_1 \\ x_{\Re} \end{bmatrix},$$

and the optimality conditions with respect to the unobservable eigenvalue λ (see Remark 6.6) simplify to $\ell_1^{\mathsf{T}} \begin{bmatrix} 0_p \\ x_{\Re}^2 \end{bmatrix} = 0.$ □

6.3.2 A heuristic procedure to compute structural perturbations

In this section we propose an algorithm to find a solution to the set of nonlinear equations (6.20), and thus to find a (sub)optimal solution to the minimization problem (6.3). Our procedure is motivated by (6.20) and Corollary 6.4, and it consists of fixing a vector z, computing the matrix D, and approximating an eigenvector associated with the smallest generalized eigenvalue of the pair (H, D). Because the size of the perturbation is bounded by the generalized eigenvalue σ as in Corollary 6.4, we adopt an iterative procedure based on the *inverse iteration* method for the computation of the smallest eigenvalue of a matrix [90]. We remark that our procedure is heuristic, because (6.20) is in fact a nonlinear generalized eigenvalue problem due to the dependency of the matrix D on the eigenvector z. To the best of our knowledge, no complete algorithm is known for the solution of (6.20). We start by characterizing certain properties of the matrices H and D, which will be used to derive our algorithm. Let

$$\text{spec}(H, D) = \{\lambda \in \mathbb{C} \ : \ \det(H - \lambda D) = 0\},$$

and recall that the pencil (H, D) is regular if the determinant $\det(H - \lambda D)$ does not vanish for some value of λ, see [91]. Notice that, if (H, D) is not regular, then $\text{spec}(H, D) = \mathbb{C}$.

Lemma 6.8. ***(Generalized eigenvalues of*** (H, D)***)*** *Given a vector $z \in \mathbb{R}^{4n-2p}$, define the matrices H and D as in* (6.20)*. Then,*

1. $0 \in$ *spec*(H, D)*;*

2. *if* $\lambda \in$ *spec*(H, D)*, then* $-\lambda \in$ *spec*(H, D)*; and*

3. if (H, D) is regular, then spec$(H, D) \subset \mathbb{R}$.

Proof. Statement (i) is equivalent to $\tilde{A}x = 0$ and $\tilde{A}^{\mathsf{T}}y = 0$, for some vectors x and y. Because $\tilde{A}^{\mathsf{T}} \in \mathbb{R}^{(2n-2p)\times 2n}$ with $p \geq 1$, the matrix $\tilde{A}^{\mathsf{T}}$ features a nontrivial null space. Thus, the two equations are satisfied with $x = 0$ and $y \in \mathrm{Ker}(\tilde{A}^{\mathsf{T}})$, and the statement follows.

To prove statement (ii) notice that, due to the block structure of H and D, if the triple $(\lambda, \bar{x}, \bar{y})$ satisfies the generalized eigenvalue equations $\tilde{A}^{\mathsf{T}}\bar{y} = \lambda D_y \bar{x}$ and $\tilde{A}\bar{x} = \lambda D_x \bar{y}$, so does $(-\lambda, \bar{x}, -\bar{y})$.

To show statement (iii), let $\mathrm{Rank}(D) = k \leq n$, and notice that the regularity of the pencil (H, D) implies $H\bar{z} \neq 0$ whenever $D\bar{z} = 0$ and $\bar{z} \neq 0$. Notice that (H, D) has $n-k$ infinite eigenvalues [91] because $H\bar{z} = \lambda D\bar{z} = \lambda \cdot 0$ for every nontrivial $\bar{z} \in \mathrm{Ker}(D)$. Because D is symmetric, it admits an orthonormal basis of eigenvectors. Let $V_1 \in \mathbb{R}^{n\times k}$ contain the orthonormal eigenvectors of D associated with its nonzero eigenvalues, let Λ_D be the corresponding diagonal matrix of the eigenvalues, and let $T_1 = V_1 \Lambda_D^{-1/2}$. Then, $T_1^{\mathsf{T}} D T_1 = I$. Let $\tilde{H} = T_1^{\mathsf{T}} H T_1$, and notice that $\tilde{H}$ is symmetric. Let $T_2 \in \mathbb{R}^{k\times k}$ be an orthonormal matrix of the eigenvectors of $\tilde{H}$. Let $T = T_1 T_2$ and note that $T^{\mathsf{T}} H T = \Lambda$ and $T^{\mathsf{T}} D T = I$, where Λ is a diagonal matrix. To conclude, consider the generalized eigenvalue problem $H\bar{z} = \lambda D\bar{z}$. Let $\bar{z} = T\tilde{z}$. Because T has full column rank k, we have $T^{\mathsf{T}} H T \tilde{z} = \Lambda \tilde{z} = \lambda T^{\mathsf{T}} D T \tilde{z} = \lambda \tilde{z}$, from which we conclude that (H, D) has k real eigenvalues. ■

Lemma 6.8 implies that the inverse iteration method is not directly applicable to (6.20). In fact, the zero eigenvalue of (H, D) leads the inverse iteration to instability, while the presence of eigenvalues of (H, D) with equal magnitude may induce non-decaying

oscillations in the solution vector. To overcome these issues, we employ a shifting mechanism as detailed in Algorithm 2, where the eigenvector z is iteratively updated by solving the equation $(H - \mu D)z_{k+1} = Dz_k$ until a convergence criteria is met. Notice that (i) the eigenvalues of $(H - \mu D, D)$ are shifted with respect to the eigenvalues of (H, D), that is, if $\sigma \in \text{spec}(H, D)$, then $\sigma - \mu \in \text{spec}(H - \mu D, D)$,[1] (ii) the pairs $(H - \mu D, D)$ and (H, D) share the same eigenvectors, and (iii) by selecting $\mu = \psi \cdot \min\{\sigma \in \text{spec}(H, D) \ : \ \sigma > 0\}$, the pair $(H - \mu D, D)$ has nonzero eigenvalues with distinct magnitude. Thus, Algorithm 2 estimates the eigenvector z associated with the smallest nonzero eigenvalue σ of (H, D), and converges when z and σ also satisfy equations (6.20). The parameter ψ determines a compromise between numerical stability and convergence speed; larger values of ψ improve the convergence speed.[2]

Algorithm 2: Heuristic solution to (6.20)

Input: Matrix H; max iterations $\max_{\text{iter}}$; $\psi \in (0.5, 1)$.
Output: (σ, z) satisfying (6.20), or fail.

repeat
  $z \leftarrow (H - \mu D)^{-1} D z$;
  $\phi \leftarrow \|z\|$;
  $z \leftarrow z/\phi$;
  $\mu = \psi \cdot \min\{\phi \in \text{spec}(H, D) \ : \ \phi > 0\}$;
  update D according to (6.10);
  $i \leftarrow i + 1$
until *convergence or* $i > \max_{\text{iter}}$;
return $(\phi + \mu, z)$ *or fail if* $i = \max_{\text{iter}}$;

When convergent, Algorithm 2 finds a solution to (6.20) and, consequently, the algorithm could stop at a local minimum and return a (sub)optimal network perturbation

[1] To see this, let σ be an eigenvalue of (H, D), that is, $Hx = \sigma Dx$. Then, $(H - \mu D)x = Hx - \mu Dx = \sigma Dx - \mu Dx = (\sigma - \mu)Dx$. That is $(H - \mu D)x = (\sigma - \mu)Dx$ thus $\sigma - \mu$ is an eigenvalue of $(H - \mu D, D)$.

[2] In Algorithm 2 the range for ψ has been empirically determined during our numerical studies.

preventing observability of a desired eigenvalue. All information about the network matrix, the sensor nodes, the constraint graph, and the unobservable eigenvalue is encoded in the matrix H as in (6.7), (6.9) and (6.20). Although convergence of Algorithm 2 is not guaranteed, numerical studies show that it performs well in practice; see Sections 6.3.3 and 6.4.

6.3.3 Optimal perturbations and algorithm validation

In this section we validate Algorithm 2 on a small network. We start with the following result.

Theorem 6.9. ***(Optimal perturbations of 3-dimensional line networks with fixed*** $\lambda \in \mathbb{C}$***)*** *Consider a network with graph* $\mathcal{G} = (\mathcal{V}, \mathcal{E})$*, where* $|\mathcal{V}| = 3$*, weighted adjacency matrix*

$$A = \begin{bmatrix} a_{11} & a_{12} & 0 \\ a_{21} & a_{22} & a_{23} \\ 0 & a_{32} & a_{33} \end{bmatrix},$$

and sensor node $\mathcal{O} = \{1\}$*. Let* $B = [b_{ij}] = A + \Delta^*$*, where* Δ^* *solves the minimization problem* (6.3) *with constraint graph* $\mathcal{H} = \mathcal{G}$ *and unobservable eigenvalue* $\lambda = \lambda_{\Re} + \mathrm{i}\lambda_{\Im} \in \mathbb{C}$*,* $\lambda_{\Im} \neq 0$*. Then:*

$$b_{11} = a_{11}, \quad b_{21} = a_{21}, \quad b_{12} = 0,$$

and b_{22}*,* b_{23}*,* b_{32}*, and* b_{33} *satisfy:*

$$\begin{aligned}(b_{22}-a_{22})-(b_{33}-a_{33})+\frac{b_{33}-b_{22}}{b_{32}}(b_{23}-a_{23})&=0,\\ (b_{32}-a_{32})-\frac{b_{23}}{b_{32}}(b_{23}-a_{23})&=0,\\ b_{22}+b_{33}-2\lambda_{\Re}&=0,\\ b_{22}b_{33}-b_{23}b_{32}-\lambda_{\Re}^2-\lambda_{\Im}^2&=0.\end{aligned}\tag{6.21}$$

Proof. Let $Bx=\lambda x$ and notice that, because λ is unobservable, $C_{\mathcal{O}}x=[1\ 0\ 0]x=0$. Then, $x=[x_1\ x_2\ x_3]^{\mathsf{T}}$, $x_1=0$, $b_{11}=a_{11}$, and $b_{21}=a_{21}$. By contradiction, let $x_2=0$. Notice that $Bx=\lambda x$ implies $b_{33}=\lambda$, which contradicts the assumption that $\lambda_{\Im}\neq 0$ and $b_{33}\in\mathbb{R}$. Thus, $x_2\neq 0$. Because $x_2\neq 0$, the relation $Bx=\lambda x$ and $x_1=0$ imply $b_{12}=0$. Additionally, λ is an eigenvalue of

$$B_2=\begin{bmatrix}b_{22} & b_{23}\\ b_{32} & b_{33}\end{bmatrix}.$$

The characteristic polynomial of B_2 is

$$P_{B_2}(s)=s^2-(b_{22}+b_{33})s+b_{22}b_{33}-b_{23}b_{32}.$$

For $\lambda\in\operatorname{spec}(B_2)$, we must have $P_{B_2}(s)=(s-\lambda)(s-\bar{\lambda})$, where $\bar{\lambda}$ is the complex conjugate of λ. Thus,

$$P_{B_2}(s)=(s-\lambda_{\Re}-\mathrm{i}\lambda_{\Im})(s-\lambda_{\Re}+\mathrm{i}\lambda_{\Im})=s^2-2\lambda_{\Re}s+\lambda_{\Re}^2+\lambda_{\Im}^2,$$

which leads to

$$b_{22} + b_{33} - 2\lambda_{\Re} = 0, \text{ and } b_{22}b_{33} - b_{23}b_{32} - \lambda_{\Re}^2 - \lambda_{\Im}^2 = 0. \tag{6.22}$$

The Lagrange function of the minimization problem with cost function $\|\Delta^*\|_{\mathrm{F}}^2 = \sum_{i=2}^{3}\sum_{j=2}^{3}(b_{ij} - a_{ij})^2$ and constraints (6.22) is

$$\begin{aligned}\mathcal{L}(b_{22}, b_{23}, b_{32}, b_{33}, p_1, p_2) &= d_{22}^2 + d_{23}^2 + d_{32}^2 + d_{33}^2 \\ &+ p_1(2\lambda_{\Re} + b_{22} + b_{33}) + p_2(b_{22}b_{33} - b_{23}b_{32} - (\lambda_{\Re}^2 + \lambda_{\Im}^2)),\end{aligned}$$

where $p_1, p_2 \in \mathbb{R}$ are Lagrange multipliers, and $d_{ij} = b_{ij} - a_{ij}$. By equating the partial derivatives of $\mathcal{L}$ to zero we obtain

$$\frac{\partial \mathcal{L}}{\partial b_{22}} = 0 \Rightarrow 2d_{22} + p_1 + p_2 b_{33} = 0, \tag{6.23}$$

$$\frac{\partial \mathcal{L}}{\partial b_{33}} = 0 \Rightarrow 2d_{33} + p_1 + p_2 b_{22} = 0, \tag{6.24}$$

$$\frac{\partial \mathcal{L}}{\partial b_{23}} = 0 \Rightarrow 2d_{23} - p_2 b_{32} = 0, \tag{6.25}$$

$$\frac{\partial \mathcal{L}}{\partial b_{32}} = 0 \Rightarrow 2d_{32} - p_2 b_{23} = 0, \tag{6.26}$$

together with (6.22). The statement follows by substituting the Lagrange multipliers p_1 and p_2 into (6.23) and (6.26). ■

To validate Algorithm 2, in Fig. 6.1 we compute optimal perturbations for 3-dimensional line networks based on Theorem 6.9, and compare them with the perturbation obtained at with Algorithm 2.

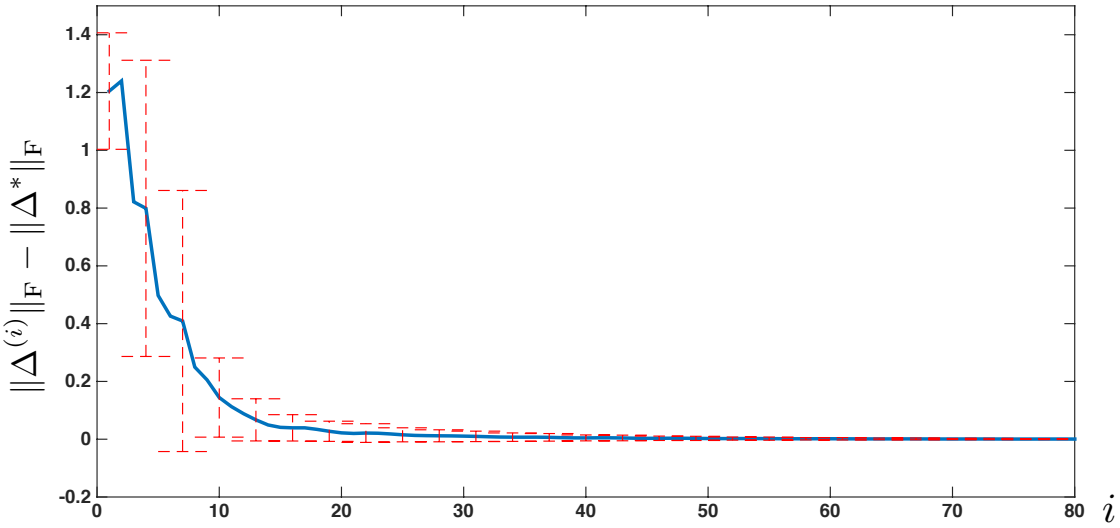

Figure 6.1: This figure validates the effectiveness of Algorithm 2 to compute optimal perturbations for the line network in Section 6.3.3. The plot shows the mean and standard deviation over 100 networks of the difference between Δ^*, obtained via the optimality conditions (6.21), and $\Delta^{(i)}$, computed at the i-th iteration of Algorithm 2. The unobservable eigenvalue is $\lambda = \mathrm{i}$ and the values a_{ij} are chosen independently and uniformly distributed in $[0, 1]$.

6.4 Observability Radius of Random Networks: Line and Star Topologies

In this section we study the observability radius of networks with fixed structure and random weights, when the desired unobservable eigenvalue is an optimization parameter as in (6.2). First, we give a general upper bound on the size of an optimal perturbation. Next, we explicitly compute optimal perturbations for line and star networks, showing that their robustness is essentially different.

We start with some necessary definitions. Given a directed graph $\mathcal{G} = (\mathcal{V}, \mathcal{E})$, a cut is a subset of edges $\bar{\mathcal{E}} \subseteq \mathcal{E}$. Given two disjoint sets of vertices $\mathcal{S}_1, \mathcal{S}_2 \subset \mathcal{V}$, we say that a cut $\bar{\mathcal{E}}$ disconnects $\mathcal{S}_2$ from $\mathcal{S}_1$ if there exists no path from any vertex in $\mathcal{S}_2$ to any vertex in $\mathcal{S}_1$

in the subgraph $(\mathcal{V}, \mathcal{E} \setminus \bar{\mathcal{E}})$. Two cuts $\mathcal{E}_1$ and $\mathcal{E}_2$ are disjoint if they have no edge in common, that is, if $\mathcal{E}_1 \cap \mathcal{E}_2 = \emptyset$. Finally, the Gamma function is defined as $\Gamma(z) = \int_0^\infty x^{z-1} e^{-x}\, \mathrm{d}x$. With this notation in place, we are in the position to prove a general upper bound on the (expected) norm of the smallest perturbation that prevents observability. The proof is based on the following intuition: a perturbation that disconnects the graph prevents observability.

Theorem 6.10. ***(Bound on expected network observability radius)*** *Consider a network with graph $\mathcal{G} = (\mathcal{V}, \mathcal{E})$, weighted adjacency matrix $A = [a_{ij}]$, and sensor nodes $\mathcal{O} \subseteq \mathcal{V}$. Let the weights a_{ij} be independent random variables uniformly distributed in the interval $[0, 1]$. Define the minimal observability-preventing perturbation as*

$$\begin{aligned} \delta = \min_{\lambda \in \mathbb{C}, x \in \mathbb{C}^n, \Delta \in \mathbb{R}^{n \times n}} & \|\Delta\|_F, \\ s.t. \quad & (A + \Delta)x = \lambda x, \\ & \|x\|_2 = 1, \\ & C_{\mathcal{O}} x = 0, \\ & \Delta \in \mathcal{A}_{\mathcal{G}}. \end{aligned} \tag{6.27}$$

Let $\Omega_k(\mathcal{O})$ be a collection of disjoint cuts of cardinality k, where each cut disconnects a non-empty subset of nodes from $\mathcal{O}$. Let $\omega = |\Omega_k(\mathcal{O})|$ be the cardinality of $\Omega_k(\mathcal{O})$. Then,

$$\mathbb{E}[\delta] \leq \frac{\Gamma(1/k)\, \Gamma(\omega + 1)}{\sqrt{k}\, \Gamma(\omega + 1 + 1/k)}.$$

Proof. Let $\bar{\mathcal{E}} \in \Omega_k(\mathcal{O})$. Notice that, after removing the edges $\bar{\mathcal{E}}$, the nodes are partitioned as $\mathcal{V} = \mathcal{V}_1 \cup \mathcal{V}_2$, where $\mathcal{V}_1 \cap \mathcal{V}_2 = \emptyset$, $\mathcal{O} \subseteq \mathcal{V}_1$, and $\mathcal{V}_2$ is disconnected from $\mathcal{V}_1$. Reorder the network nodes so that $\mathcal{V}_1 = \{1, \ldots, |\mathcal{V}_1|\}$ and $\mathcal{V}_2 = \{|\mathcal{V}_1| + 1, \ldots, |\mathcal{V}|\}$. Accordingly, the modified network matrix is reducible and reads as

$$\bar{A} = \begin{bmatrix} A_{11} & 0 \\ A_{21} & A_{22} \end{bmatrix}.$$

Let x_2 be an eigenvector of A_{22} with corresponding eigenvalue λ. Notice that λ is an eigenvalue of $\bar{A}$ with eigenvector $x = [0 \ x_2^{\mathsf{T}}]^{\mathsf{T}}$. Since $\mathcal{O} \subseteq \mathcal{V}_1$, $C_{\mathcal{O}} x = 0$, so that the eigenvalue λ is unobservable.

From the above discussion we conclude that, for each $\bar{\mathcal{E}} \in \Omega_k(\mathcal{O})$, there exists a perturbation $\Delta = [\delta_{ij}]$ that is compatible with $\mathcal{G}$ and ensures that one eigenvalue is unobservable. Moreover, the perturbation Δ is defined as $\delta_{ij} = -a_{ij}$ if $(i,j) \in \bar{\mathcal{E}}$, and $\delta_{ij} = 0$ otherwise. We thus have

$$\mathbb{E}[\delta] \leq \mathbb{E}\left[\min_{\bar{\mathcal{E}} \in \Omega_k(\mathcal{O})} \sqrt{\sum_{(i,j) \in \bar{\mathcal{E}}} a_{ij}^2}\right].$$

Because any two elements of $\Omega_k(\mathcal{O})$ have empty intersection and all edge weights are independent, we have

$$\begin{aligned} &\Pr\left(\min_{\bar{\mathcal{E}} \in \Omega_k(\mathcal{O})} \sqrt{\sum_{(i,j) \in \bar{\mathcal{E}}} a_{ij}^2} \geq x\right) = \Pr\left(\sqrt{\sum_{(i,j) \in \bar{\mathcal{E}}} a_{ij}^2} \geq x\right)^{\omega} \\ &= \Pr\left(\sum_{(i,j) \in \bar{\mathcal{E}}} a_{ij}^2 \geq x^2\right)^{\omega} = \left(1 - \Pr\left(\sum_{(i,j) \in \bar{\mathcal{E}}} a_{ij}^2 \leq x^2\right)\right)^{\omega}. \end{aligned}$$

In order to obtain a more explicit expression for this probability, we resort to using a lower bound. Let a denote the vector of a_{ij} with $(i,j) \in \bar{\mathcal{E}}$. The condition $\sum_{(i,j)\in\bar{\mathcal{E}}} a_{ij}^2 \leq x^2$ implies that a belongs to the k-dimensional sphere of radius x (centered at the origin). In fact, since a is sampled in $[0,1]^k$, it belongs to the intersection between the sphere and the first orthant. By computing the volume of the k-dimensional cube inscribed in the sphere, we obtain

$$\Pr\left(\sum_{(i,j)\in\bar{\mathcal{E}}} a_{ij}^2 \leq x^2\right) \geq \begin{cases} \frac{\left(2x/\sqrt{k}\right)^k}{2^k} = \left(\frac{x}{\sqrt{k}}\right)^k, & x \leq \sqrt{k}, \\ 1, & \text{otherwise.} \end{cases}$$

Since δ takes on nonnegative values only, its expectation can be computed by integrating the survival function

$$\mathbb{E}[\delta] = \int_0^\infty \Pr\left(\delta \geq t\right) \mathrm{d}t,$$

which leads us to obtain, by suitable changes of variables,

$$\begin{aligned} \mathbb{E}[\delta] &\leq \int_0^{\sqrt{k}} \left(1 - \left(\frac{x}{\sqrt{k}}\right)^k\right)^\omega \mathrm{d}x = \sqrt{k} \int_0^1 \left(1 - t^k\right)^\omega \mathrm{d}t \\ &= \frac{1}{\sqrt{k}} \int_0^1 (1-z)^\omega \, z^{\frac{1}{k}-1} \mathrm{d}z = \frac{1}{\sqrt{k}} \frac{\Gamma(1/k)\Gamma(\omega+1)}{\Gamma(\omega+1/k+1)}, \end{aligned}$$

where the last equality follows from the definition of the Beta function, $B(x,y) = \int_0^1 t^{x-1}(1-t)^{y-1}\mathrm{d}t$ for $\mathrm{Real}(x) > 0$, $\mathrm{Real}(y) > 0$, and its relation with the Gamma function, $B(x,y) = \frac{\Gamma(x)\,\Gamma(y)}{\Gamma(x+y)}$. ■

We now use Theorem 6.10 to investigate the asymptotic behavior of the expected observability radius on sequences of networks of increasing cardinality n. In order to emphasize the dependence on n, we shall write $\mathbb{E}[\delta(n)]$ from now on. As a first step, we can apply Wendel's inequalities [92] to find

$$\frac{1}{(\omega+1)^{1/k}} \leq \frac{\Gamma(\omega+1)}{\Gamma(\omega+1+1/k)} \leq \frac{(\omega+1+1/k)^{1-1/k}}{(\omega+1)}.$$

If in a sequence of networks ω grows to infinity and k remains constant, then the ratio between the lower and the upper bounds goes to one, yielding the asymptotic equivalence

$$\mathbb{E}[\delta(n)] \leq \frac{\Gamma(1/k)\,\Gamma(\omega+1)}{\sqrt{k}\,\Gamma(\omega+1+1/k)} \sim \frac{\Gamma(1/k)}{\sqrt{k}} \frac{1}{(\omega+1)^{1/k}}.$$

This relation implies that a network becomes less robust to perturbations as the size of the network increases, with a rate determined by k. In the rest of this section we study two network topologies with different robustness properties. In particular, we show that line networks achieve the bound in Theorem 6.10, proving its tightness, whereas star networks have on average a smaller observability radius.

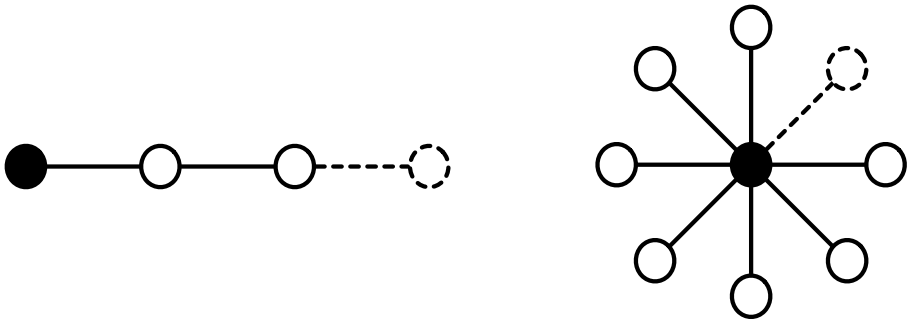

(a) Line network (b) Star network

Figure 6.2: Line and star networks. Sensor nodes are marked in black.

(Line network) Let $\mathcal{G}$ be a line network with n nodes and one sensor node as in Fig. 6.2. The adjacency and output matrices read as

$$A = \begin{bmatrix} a_{11} & a_{12} & 0 & \cdots & 0 \\ a_{21} & a_{22} & a_{23} & \cdots & 0 \\ \vdots & \ddots & \ddots & \ddots & \vdots \\ 0 & \cdots & a_{n-1,n-2} & a_{n-1,n-1} & a_{n-1,n} \\ 0 & \cdots & 0 & a_{n,n-1} & a_{nn} \end{bmatrix}, \tag{6.28}$$

$$C_{\mathcal{O}} = \begin{bmatrix} 1 & 0 & 0 & \cdots & 0 \end{bmatrix}.$$

We obtain the following result.

Theorem 6.11. ***(Structured perturbation of line networks)*** *Consider a line network with matrices as in* (6.28)*, where the weights a_{ij} are independent random variables uniformly*

distributed in the interval $[0, 1]$. *Let* $\delta(n)$ *be the minimal cost defined as in* (6.27). *Then,*

$$\delta(n) = \min\{a_{12}, \ldots, a_{n-1,n}\}, \text{ and } \mathbb{E}[\delta(n)] = \frac{1}{n}.$$

Proof. It is known that line networks, when observed from one of their extremes, are strongly structurally observable, that is, they are observable for every nonzero choice of the edge weights [93]. Consequently, for the perturbed system to feature an unobservable eigenvalue, the perturbation Δ must be such that $\delta_{i,i+1} = -a_{i,i+1}$ for some $i \in \{2, \ldots, n-1\}$. Thus, a minimum norm perturbation is obtained by selecting the smallest entry $a_{i,i+1}$. Since the $a_{i,i+1}$ are independent and identically distributed, $\delta(n) = \min a_{i,i+1}$ is a random variable with survival function $\Pr(\delta(n) \geq x) = (1-x)^{n-1}$ for $0 \leq x \leq 1$, and $\Pr(\delta(n) \geq x) = 0$ otherwise. Thus,

$$\mathbb{E}[\delta(n)] = \int_0^1 \Pr(\delta(n) \geq x) \mathrm{d}x = \frac{1}{n}.$$

■

Theorem 6.11 characterizes the resilience of line networks to structured perturbations. We remark that, because line networks are strongly structurally observable, structured perturbations preventing observability necessarily disconnect the network by zeroing some network weights. Consistently with this remark, line networks achieve the upper bound in Theorem 6.10, being therefore maximally robust to structured perturbations. In fact, for $\mathcal{O} = \{1\}$ and a cut size $k = 1$ we have $\Omega_1(\mathcal{O}) = \{a_{12}, \ldots, a_{n-1,n}\}$ and $\omega = n - 1$.

Thus,

$$\mathbb{E}[\delta(n)] \leq \frac{\Gamma(1)\Gamma(n)}{\sqrt{1}\Gamma(n+1)} = \frac{(n-1)!}{n!} = \frac{1}{n},$$

which equals the behavior identified in Theorem 6.11. Further, Theorem 6.11 also identifies an unobservable eigenvalue yielding a perturbation with minimum norm. In fact, if $a_{i^*-1,i^*} = \min\{a_{12}, \ldots, a_{n-1,n}\}$, then all eigenvalues of the submatrix of A with rows/columns in the set $\{i^*, \ldots, n\}$ are unobservable, and thus minimizers in (6.27).

Both Theorems 6.10 and 6.11 are based on constructing perturbations by disconnecting the graph. This strategy, however, suffers from performance limitations and may not be optimal in general. The next example shows that different kinds of perturbations, when applicable, may yield a lower cost.

(Star network) Let $\mathcal{G}$ be a star network with n nodes and one sensor node as in Fig. 6.2. The adjacency and output matrices read as

$$\begin{aligned} A &= \begin{bmatrix} a_{11} & a_{12} & a_{13} & \cdots & a_{1n} \\ a_{21} & a_{22} & 0 & \cdots & 0 \\ a_{31} & 0 & \ddots & \ddots & \vdots \\ \vdots & \vdots & 0 & a_{n-1,n-1} & 0 \\ a_{n1} & 0 & 0 & 0 & a_{nn} \end{bmatrix}, \\ C_{\mathcal{O}} &= \begin{bmatrix} 1 & 0 & 0 & \cdots & 0 \end{bmatrix}. \end{aligned} \tag{6.29}$$

Differently from the case of line networks, star networks are not strongly structurally observable, so that different perturbations may result in unobservability of some modes.

Theorem 6.12. ***(Structured perturbation of star networks)*** *Consider a star network with matrices as in* (6.29)*, where the weights* a_{ij} *are independent random variables uniformly distributed in the interval* $[0, 1]$*. Let* $\delta(n)$ *be the minimal cost defined as in* (6.27)*. Let*

$$\gamma = \min_{i,j\in\{2,\ldots,n\},i\neq j} \frac{|a_{ii} - a_{jj}|}{\sqrt{2}}.$$

Then,

$$\delta(n) = \min\{a_{12}, a_{13}, \ldots, a_{1n}, \gamma\}, \text{ and}$$

$$\frac{1}{\sqrt{2}\, n(n-1)} \leq \mathbb{E}[\delta(n)] \leq \frac{1}{\sqrt{2}\, n(n-2)}.$$

Proof. Partition the network matrix A in (6.29) as

$$A = \begin{bmatrix} a_{11} & A_{12} \\ A_{21} & A_{22} \end{bmatrix},$$

where $A_{12} \in \mathbb{R}^{1,n-1}$, $A_{21} \in \mathbb{R}^{n-1,1}$, $A_{22} \in \mathbb{R}^{n-1,n-1}$. Accordingly, let $x = [x_1\ x_2^{\mathsf{T}}]^{\mathsf{T}}$. The condition $C_{\mathcal{O}}x = 0$ implies $x_1 = 0$. Consequently, for the condition $(A + \Delta)x = \lambda x$ to be satisfied, we must have $(A_{12} + \Delta_{12})x_2 = 0$ and $(A_{22} + \Delta_{22})x_2 = \lambda x_2$. Notice that, because A_{22} is diagonal and $\Delta \in \mathcal{A}_{\mathcal{G}}$, the condition $(A_{22} + \Delta_{22})x_2 = \lambda x_2$ implies that $\lambda = a_{ii} + \delta_{ii}$

for all indices i such that $i \in \mathrm{Supp}(x_2)$, where $\mathrm{Supp}(x_2)$ denotes the set of nonzero entries of x_2. Because $\|x\| = 1$, $|\mathrm{Supp}(x_2)| > 0$. We have two cases:

Case $|Supp(x_2)| = 1$: Let $\mathrm{Supp}(x) = \{i\}$, with $i \in \{2, \ldots, n\}$. Then, the condition $(A_{12} + \Delta_{12})x_2 = 0$ implies $\delta_{1,i} = -a_{1,i}$, and the condition $(A_{22} + \Delta_{22})x_2 = \lambda x_2$ is satisfied with $\Delta_{22} = 0$, $\lambda = a_{ii}$, and $x = e_i$, where e_i is the i-th canonical vector of dimension n. Thus, if $|\mathrm{Supp}(x_2)| = 1$, then $\delta(n) = \min_{i \in \{2,\ldots,n\}} a_{1,i}$.

Case $|Supp(x_2)| > 1$: Let $S = \mathrm{Supp}(x_2)$. Then, $\delta_{ii} = \lambda - a_{ii}$. Notice that the condition $(A_{22} + \Delta_{22})x_2 = \lambda x_2$ is satisfied for every x_2 with support S and, particularly, for $x_2 \in \mathrm{Ker}(A_{12})$. Thus, we let $\Delta_{12} = 0$. Notice that

$$\delta(n) = \min_{\lambda, S} \sqrt{\sum_{i \in S} (\lambda - a_{ii})^2},$$

and that $\delta(n)$ is obtained when $S = \{i, j\}$, for some $i, j \in \{2, \ldots, n\}$, and $\lambda = (a_{ii} + a_{jj})/2$. Specifically, for the indexes $\{i, j\}$, we have $\|\Delta\|_{\mathrm{F}} = |a_{ii} - a_{jj}|/\sqrt{2}$. Thus, if $|\mathrm{Supp}(x_2)| > 1$, then $\delta(n) = \gamma$, which concludes the proof of the first statement.

In order to estimate $\mathbb{E}[\delta(n)]$, notice that $\delta(n) = \min\{\alpha, \gamma\}$, where $\alpha = \min\{a_{12}, a_{13}, \ldots, a_{1n}\}$, and that α and γ are independent random variables. Then, from [94, Chapter 6.4] we have

$$\begin{aligned} \Pr(\delta(n) \geq x) &= \Pr(\alpha \geq x)\Pr(\gamma \geq x) \\ &= (1 - x)^{n-1}(1 - (n-2)\sqrt{2}x)^{n-1}, \end{aligned}$$

for $x \leq (\sqrt{2}(n-2))^{-1}$, and $\Pr(\delta(n) \geq x) = 0$ otherwise. Thus,

$$\mathbb{E}[\delta(n)] = \int_0^{\frac{1}{\sqrt{2}(n-2)}} (1-x)^{n-1}(1-(n-2)\sqrt{2}x)^{n-1}\mathrm{d}x.$$

Next, for the upper bound observe that

$$\begin{aligned}
&\int_0^{\frac{1}{\sqrt{2}(n-2)}} (1-x)^{n-1}(1-(n-2)\sqrt{2}x)^{n-1}\mathrm{d}x \\
&\leq \int_0^{\frac{1}{\sqrt{2}(n-2)}} (1-(n-2)\sqrt{2}x)^{n-1}\mathrm{d}x = \frac{1}{\sqrt{2}n(n-2)},
\end{aligned}$$

and for the lower bound observe that

$$\begin{aligned}
&\int_0^{\frac{1}{\sqrt{2}(n-2)}} (1-x)^{n-1}(1-(n-2)\sqrt{2}x)^{n-1}\mathrm{d}x \\
&= \int_0^{\frac{1}{\sqrt{2}(n-2)}} (1-((n-2)\sqrt{2}+1)x+((n-2)\sqrt{2})x^2)^{n-1}\mathrm{d}x \\
&\geq \int_0^{\frac{1}{\sqrt{2}(n-1)}} (1-(n-1)\sqrt{2}x)^{n-1}\mathrm{d}x = \frac{1}{\sqrt{2}n(n-1)}.
\end{aligned}$$

■

Theorem 6.12 quantifies the resilience of star networks, and the unobservable eigenvalues requiring minimum norm perturbations; see the proof for a characterization of this eigenvalues.

The bounds in Theorem 6.12 are asymptotically tight and imply

$$\mathbb{E}[\delta(n)] \sim \frac{1}{\sqrt{2}\,n^2}, \quad \text{as } n \to \infty.$$

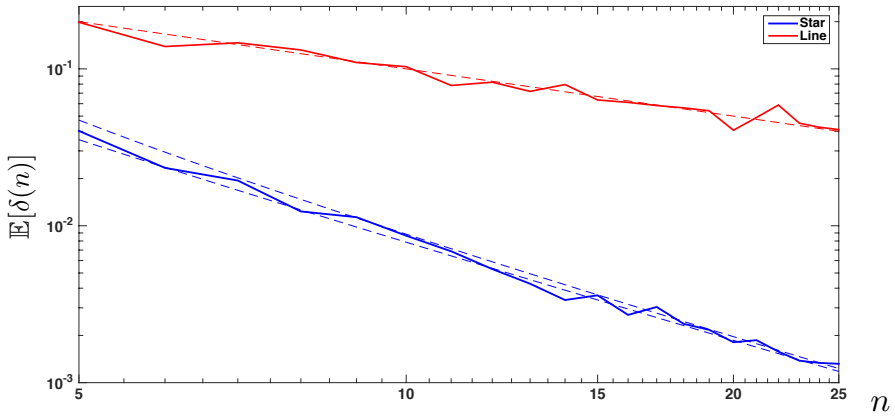

Figure 6.3: Expected values $\mathbb{E}[\delta(n)]$ for the two network topologies in Fig. 6.2 as functions of the network cardinality n. Dotted lines represent upper and lower bounds in Theorems 6.11 and 6.12. Solid lines show the mean over 100 networks of the Frobenius norm of the perturbations obtained by Algorithm 2.

See Fig. 6.3 for a numerical validation of this result. This rate of decrease implies that star networks are *structurally* less robust to perturbations than line networks. Crucially, unobservability in star networks may be caused by two different phenomena: the deletion of an edge disconnecting a node from the sensor node (deletion of the smallest among the edges $\{a_{12}, a_{13}, \ldots, a_{1n}\}$), and the creation of a dynamical symmetry with respect to the sensor node by perturbing two diagonal elements to make them equal in weight. It turns out that, on average, creating symmetries is "cheaper" than disconnecting the network. The role of network symmetries in preventing observability and controllability has been observed in several independent works; see for instance [88, 89]. Finally, the comparison of line and star networks shows that Algorithm 2 is a useful tool to systematically investigate the robustness of different topologies.

6.5 Robustness of Power Systems Against Topology Attacks

In this section, we employ our methods to quantify the resilience of power networks against attacks to the power lines. We begin by formalizing attacks against the topology of the power networks, and then we extend the applicability of our analysis to linear, continuous-time, descriptor systems.

We adopt the small-signal version of the classic structure-preserving power model to describe the dynamics of a power network. The interested reader is referred to [95, 96] for a detailed derivation from the full nonlinear structure-preserving power network model. Consider a connected power network with n generators $\{g_1, \ldots, g_n\}$ and m load buses $\{b_{n+1}, \ldots, b_{n+m}\}$. The interconnection structure of the power network is encoded by a connected susceptance-weighted graph $\mathcal{G}$. The vertices of $\mathcal{G}$ are the generators g_i and the buses b_i. The edges of $\mathcal{G}$ are the transmission lines $\{b_i, b_j\}$ and the connections $\{g_i, b_i\}$, weighted by their susceptance values. The Laplacian associated with the susceptance-weighted graph is the symmetric susceptance matrix $\mathcal{S} \in \mathbb{R}^{(n+m)\times(n+m)}$ defined by

$$\mathcal{S} = \begin{bmatrix} \mathcal{S}_{\text{gg}} & \mathcal{S}_{\text{gl}} \\ \mathcal{S}_{\text{lg}} & \mathcal{S}_{\text{ll}} \end{bmatrix}, \tag{6.30}$$

where generators and load buses have been labeled so that the first n rows of $\mathcal{S}$ are associated with the generators and the last m rows of $\mathcal{S}$ correspond to the load buses. The dynamic

model of the power network is

$$\underbrace{\begin{bmatrix} I & 0 & 0 \\ 0 & M_{\mathrm{g}} & 0 \\ 0 & 0 & 0 \end{bmatrix}}_{E} \begin{bmatrix} \dot{\delta} \\ \dot{\omega} \\ \dot{\theta} \end{bmatrix} = - \underbrace{\begin{bmatrix} 0 & -I & 0 \\ \mathcal{S}_{\mathrm{gg}} & D_{\mathrm{g}} & \mathcal{S}_{\mathrm{gl}} \\ \mathcal{S}_{\mathrm{lg}} & 0 & \mathcal{S}_{\mathrm{ll}} \end{bmatrix}}_{A} \begin{bmatrix} \delta \\ \omega \\ \theta \end{bmatrix} + \begin{bmatrix} 0 \\ P_{\omega} \\ P_{\theta} \end{bmatrix}, \tag{6.31}$$

where $\delta : \mathbb{R} \to \mathbb{R}^n$ and $\omega : \mathbb{R} \to \mathbb{R}^n$ denote the generator rotor angles and frequencies, and $\theta : \mathbb{R} \to \mathbb{R}^m$ are the voltage angles at the buses. The matrices M_{g} and D_{g} are the diagonal matrices of the generator inertial and damping coefficients, and the inputs $P_{\omega} : \mathbb{R} \to \mathbb{R}^n$ and $P_{\theta} : \mathbb{R} \to \mathbb{R}^m$ are due to *known* changes in the mechanical input power to the generators or real power demand at the loads.

Let $\mathcal{O}$ be the set of p sensors, and $C_{\mathcal{O}}$ the measurement matrix. We consider topology attacks yielding unobservability of the slow dynamics of the descriptor system (6.31). We refer the interested reader to [97] for a detailed discussion of the observability of descriptor systems. In particular, we look for a perturbation Δ that is compatible with the structure of the network matrix A, and satisfies $(A + \Delta)x = \lambda E x$ and $C_{\mathcal{O}} x = 0$, for some $\lambda \in \mathbb{C}$ with $\Re(\lambda) > 0$ and $x \neq 0$. It should be observed that the matrix A features structural zeros due to the power network topology encoded in $\mathcal{S}$, as well as zeros due to the second order dynamical model of generators.

Following (6.5), let the matrix E of the descriptor system (6.31) be partitioned as

$$E = \begin{bmatrix} E_{11} & E_{12} \\ E_{21} & E_{22} \end{bmatrix}, \tag{6.32}$$

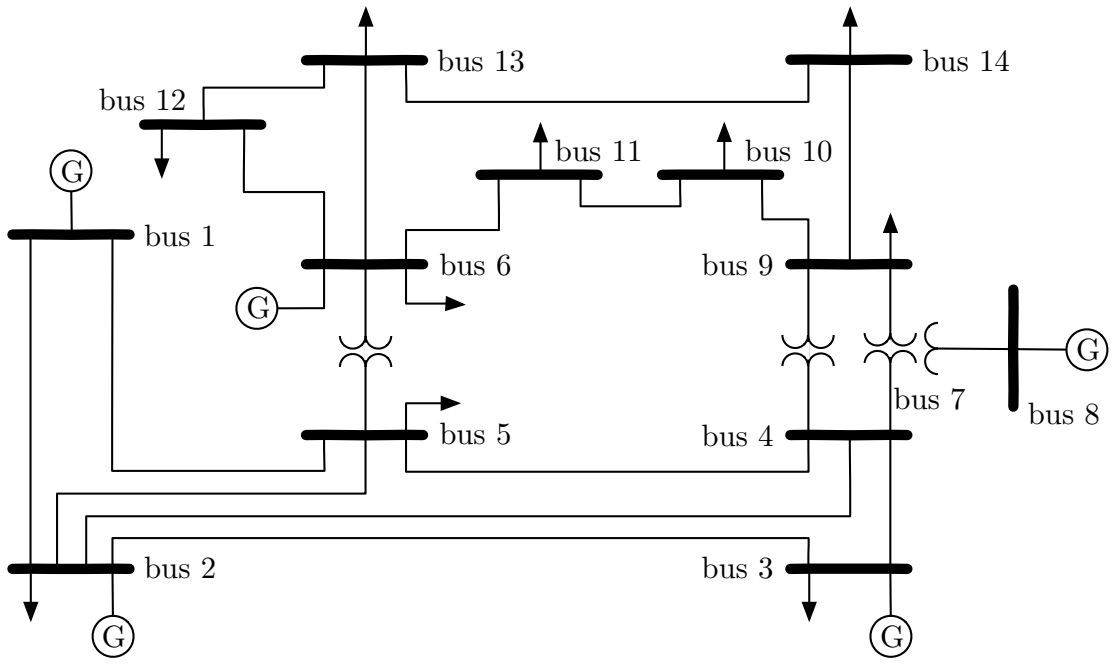

Figure 6.4: IEEE 14 power grid, with 5 generators and 14 load buses.

where $E_{11} \in \mathbb{R}^{p\times p}$, $E_{12} \in \mathbb{R}^{p\times n-p}$, $E_{21} \in \mathbb{R}^{n-p\times p}$, and $E_{22} \in \mathbb{R}^{n-p\times n-p}$. In order to apply Theorem 6.3 and Algorithm 2 to (6.31), it is sufficient to let

$$\bar{M} = \begin{bmatrix} 0_p \\ \lambda_{\Im} E_{22} \end{bmatrix} \text{ and } \bar{N} = \begin{bmatrix} 0_p \\ \lambda_{\Re} E_{22} \end{bmatrix} \tag{6.33}$$

replace the corresponding expressions in (6.7).

We employ Algorithm 2 to study vulnerabilities of the IEEE 14 bus system shown in Fig. 6.4 to structural perturbations. We model the IEEE 14 bus system as a descriptor model of the form (6.31) and we let $C_{\mathcal{O}} = \begin{bmatrix} 1 & 0 & 0 & \cdots & 0 \end{bmatrix}$, that is, the generator rotor angle connected to bus 1 is directly measured. For given generators inertia and damping

Table 6.1: Network perturbations inducing unobservable modes.

Perturbation	$\|\Delta\|_F$	Unobservable mode
Disconnect load 1 ($[\mathcal{S}_{\mathrm{ll}}]_{1,2} = 0$)	$4,60$	10.92
Stop generator 1 ($\dot{\delta}_1 = 0$)	2.59	$10.92 \pm 20.95j$
Modify impedance (53 lines modified)	2.34	$10.92 \pm 10^4 j$

coefficients, the finite eigenvalues of the system are $\lambda_{1,2} = -10.9234 \pm 20.9469j$, $\lambda_{3,4} = -1.6568 \pm 18.2687i$, $\lambda_{5,6} = -1.4761 \pm 15.2247i$, $\lambda_{7,8} = -0.2275 \pm 8.3227i$, $\lambda_9 = 0$, and $\lambda_{10} = -2.1867$. In Table 6.1 we report the results of our numerical study. In particular, we compute three different network perturbations yielding (unstable) unobservable eigenvalues. Table 6.1 shows that an attacker may induce unstable and unobservable modes by tampering with different phenomena including (i) disconnecting load buses, (ii) stopping a generator, and (iii) altering the impedance of certain lines. Consistently with the observations made in Section 6.4, creating artificial dynamical symmetries seems to require smaller perturbations than disconnecting certain lines.

Chapter 7

Robustness Against Attacks: Secure Navigation of Robots

In this chapter, we consider robustness in a mobile-robotic application, where the objective is to navigate a robot despite unknown and arbitrary attack actions against the localization signals utilized by the onboard navigation algorithms. We refer to the previously-published works [2, 3] for a comprehensive discussion of the technical results.

7.1 Introduction

Autonomous robots rely on sensors to measure their states and use this information to make decisions and to generate control commands to send to their actuators. Despite the tremendous advances in the development of more reliable sensing and communication devices, sensory data and communication channels can be accidentally and maliciously compromised, thus undermining the effectiveness of autonomous operations in critical and

adversarial applications. To the best of our knowledge, tools to study the effects of attacks on the trajectories and to design controls that securely steer the robot to a desired final configurations are still critically lacking.

This work focuses on robots with integrator dynamics,

$$\dot{x}_{\mathrm{n}} = u_{\mathrm{n}}, \tag{7.1}$$

where $x_{\mathrm{n}} : \mathbb{R}_{\geq 0} \to \mathbb{R}^2$ denotes the robot position in a two-dimensional space, and $u_{\mathrm{n}} : \mathbb{R}_{\geq 0} \to \mathbb{R}^2$ denotes the nominal control input that actuates the robot velocity. The input u_{n} is a design parameter that is used to plan the robot trajectory between two desired positions. We assume that u_{n} is piecewise continuous and $\|u_{\mathrm{n}}\| \leq u_{\max}$ at all times, with $u_{\max} \in \mathbb{R}_{>0}$.

We consider robots equipped with two noiseless sensors: a GNSS receiver that provides an absolute measure of the position, and a RSSI sensor that provides a measure of the relative distance between the robot and n_{b} radio stations. Let $b_i \in \mathbb{R}^2$ and $r_i \in \mathbb{R}_{>0}$ denote the position of the i-th station with respect to an absolute reference frame and its coverage range, respectively, with $b_i \neq b_j$ if $i \neq j$. We assume that the robot can measure its distance from the i-th station only when its position is within the communication range defined by r_i. The sensor readings are

$$y_{\mathrm{n}}^{\mathrm{GNSS}} = x_{\mathrm{n}}, \text{ and } y_{\mathrm{n},i}^{\mathrm{RSSI}} = \|x_{\mathrm{n}} - b_i\|^2, \tag{7.2}$$

where $i \in \Omega$ and

$$\Omega(x_{\mathrm{n}}) = \{i \ : \ i \in \{1, \ldots, n_{\mathrm{b}}\} \text{ and } \|x_{\mathrm{n}} - b_i\| \leq r_i\}.$$

Although our results can be extended to include different classes of sensors, we focus on GNSS and RSSI sensors because they are available in many practical applications [98].

We assume that the robot operates in an adversarial environment, where adversaries can simultaneously spoof the GNSS readings and override the nominal input u_{n} with a compromised attack input. To distinguish between the nominal measurements and those obtained in the presence of attacks, we denote the dynamics of the robot under attack as

$$\dot{x} = u, \tag{7.3}$$

where $x : \mathbb{R}_{\geq 0} \to \mathbb{R}^2$ represents the attacked robot position and $u : \mathbb{R}_{\geq 0} \to \mathbb{R}^2$ denotes the attacked control input, which also obeys the bound on maximum velocity $\|u\| \leq u_{\max}$. The sensor readings in the presence of attacks are

$$y^{\mathrm{GNSS}} = x + u^{\mathrm{GNSS}}, \quad \text{and} \quad y_i^{\mathrm{RSSI}} = \|x - b_i\|^2, \tag{7.4}$$

where $u^{\mathrm{GNSS}} : \mathbb{R}_{\geq 0} \to \mathbb{R}^2$ denotes the GNSS spoofing signal, and $i \in \Omega(x)$. We assume that the RSSI readings are not compromised by the attacker, and that the nominal and attacked initial positions satisfy $x_{\mathrm{n}}(0) = x(0)$.

In this work, we study the competing objectives of the attacker and of the trajectory planner, summarized as follows:

(i) The attacker aims to design the attack inputs (u, u^{GNSS}) so that the deviation between the robot nominal trajectory and the actual (attacked) trajectory is maximized, while maintaining undetectability (as defined below).

(ii) The trajectory planner seeks for a nominal control input u_{n} to guarantee that, in the absence of attacks, u_{n} allows the robot to reach a desired final state, and, in the presence of attacks, the measurements y^{GNSS} and y_i^{RSSI} allow the robot to detect the attack.

The actions of the attacker and of the trajectory planner can be interpreted in terms of two sequential phases. In the first phase, the trajectory planner designs the nominal control input u_{n} and the control horizon T to satisfy objective (ii). In the second phase, the attacker designs the attacks (u, u^{GNSS}) given the nominal input u_{n} and the nominal model (7.1)-(7.2) to satisfy objective (i). We stress that in our settings the nominal control input u_{n} is replaced with the input u by the attacker in the second phase, and thus the choice of the trajectory planner is irreversible and cannot be changed in the second phase.

Despite their popularity, GNSS-based localization techniques are subject to a number of well-known vulnerabilities that are typically associated with the lack of appropriate encryption [99]. Existing methods to detect and identify GNSS spoofing attacks are based on filtering techniques to reveal compromised streams of sensory data [100, 101]. Differently, in this work we focus on characterizing the detectability of attacks modifying both the measurements and the inputs to the system, and on the problem of designing nominal control inputs to restrict or prevent undetectable attacks against this class of cyber-physical systems. Although the security of cyber-physical systems is an extensively-studied topic

(see e.g. [102]), most of the available methods are applicable to static systems or systems with linear dynamics [103, 104]. Few exceptions are [105, 106, 107, 108], which are however restricted to particular classes of nonlinear dynamics, and to attacks modifying the system measurements only. A secure trajectory planning problem has been studied also in our early work [109]. Differently from [109], in this work we focus on single integrator dynamics that allow us to derive more stringent conditions and explicit controls, and on the possibility of having multiple radio stations.

The contribution of this chapter is threefold. First, we characterize the class of undetectable attacks against robots with single integrator dynamics operating on a plane. We show how to design undetectable attacks, and demonstrate that attacks can exist only when the robot is located in certain regions of the plane. Second, we formulate and solve an optimization problem that captures the attacker's goal of maximally deviating the robot trajectory from the nominal path. We characterize the form of optimal undetectable attacks, we provide algorithms for their design, and we study the set of positions that are reachable by the attacker. Third, we formalize the trajectory planner's goal of designing secure control inputs, that is, inputs that allow the detection of any attack action. We show that secure control inputs exist only between certain subsets of states, and we illustrate through an example how the trajectory planner can leverage the layout of the radio stations to plan trajectories that are secure.

The remainder of this chapter is organized as follows. In Section 7.2 we tackle the problem from the perspective of a potential attacker. To this aim, we formalize the notion of undetectable attack, we give necessary conditions for their existence, and we solve

the attacker trajectory planning problem. On the other hand, in Section 7.3 we tackle the problem from the point of view of the system planner (or trajectory planner). To this aim, we characterize the class of secure control inputs, we study the set of configurations that are reachable under secure control policies, and we illustrate how a system planner can leverage the existence of multiple radio stations to plan waypoints that yield secure trajectories.

7.2 Undetectable attacks

We start by formalizing the notion of undetectable attacks.

Definition 7.1. *(**Undetectable attack**) The attack (u, u^{GNSS}), with $u \neq u_{\mathrm{n}}$, is undetectable if $\Omega(x) = \Omega(x_{\mathrm{n}})$ at all times and*

$$y^{\mathrm{GNSS}} = y_n^{\mathrm{GNSS}}, \quad \textit{and} \quad y_i^{\mathrm{RSSI}} = y_{n,i}^{\mathrm{RSSI}},$$

for all $i \in \Omega(x_{\mathrm{n}})$. Otherwise, the attack is detectable. □

Loosely speaking, an attack is undetectable if the measurements generated by the attacked trajectory are compatible with their nominal counterparts and with the nominal dynamics at all times. On the other hand, when Definition 7.1 is not satisfied, then the attack is readily detected by comparison between the actual and nominal measurements. In particular, an attack is detectable if the stations visited by the nominal and attacked trajectories differ, that is, $\Omega(x(t)) \neq \Omega(x_{\mathrm{n}}(t))$ for some t.

Remark 7.2. (*Undetectability with GNSS sensor only*) *In scenarios where GNSS is the only sensor for detection, an adversary can deliberately alter the control input and*

remain undetected (under the constraint $\Omega(x) = \Omega(x_{\rm n})$). To see this, we note that the effect of any attack u can be canceled from the GNSS readings by selecting $u^{\rm GNSS} = p_{\rm n} - p$. Thus, secure trajectories can exist only if the robot has redundant measurement in addition to the GNSS readings. □

7.2.1 Characterization of undetectable attacks

Let $\rho_{{\rm n},i} = x_{\rm n} - b_i$ and $\rho_i = x - b_i$ denote the robot nominal and attacked positions relative to the i-th station, and

$$\mathcal{R}(x_{\rm n}) = \begin{bmatrix} \rho_{{\rm n},i_1} & \cdots & \rho_{{\rm n},i_s} \end{bmatrix},$$

where $\Omega(x_{\rm n}) = \{i_1, \ldots, i_s\}$. Let $\mathrm{Rank}(M)$ denote the rank of the matrix M. In the following result we characterize the existence and general expression of undetectable attacks.

Theorem 7.3. ***(Undetectable attacks)*** *There exist undetectable attacks $(u, u^{\rm GNSS})$ with $u \neq u_{\rm n}$ only if*

$$\mathrm{Rank}(\mathcal{R}(x_{\rm n}(t))) < 2, \tag{7.5}$$

for some time t. Moreover, when $\mathrm{Rank}(\mathcal{R}(x_{\rm n}(t))) \neq 0$ at all times, every undetectable attack satisfies

$$u^{\rm GNSS} = x_{\rm n} - x, \ \textit{and}\ u = v_{{\rm r},i}\rho_i + w, \tag{7.6}$$

for all $i \in \Omega(x_{\rm n}(t))$, where $v_{{\rm r},i} = u_n^{\mathsf{T}}\rho_{{\rm n},i}/\|\rho_i\|^2$, $w^{\mathsf{T}}\rho_i = 0$.

Proof. We prove (7.5) by contrapositive, that is, we show that if $\mathrm{Rank}(\mathcal{R}(x_{\mathrm{n}}(t))) \geq 2$ for all t then every undetectable attack satisfies $u = u_{\mathrm{n}}$ at all times. Let u denote an undetectable attack, and consider the time instant $\tau = 0$. From the assumption $x_{\mathrm{n}}(0) = x(0)$ we obtain $\rho_i(0) = \rho_{\mathrm{n},i}(0)$ and $\rho_j(0) = \rho_{\mathrm{n},j}(0)$ for all $i, j \in \Omega(x_{\mathrm{n}}(\tau))$. Moreover, from undetectability of u, we have $y_i^{\mathrm{RSSI}} - y_{\mathrm{n},i}^{\mathrm{RSSI}} = 0$ and therefore

$$\dot{y}_i^{\mathrm{RSSI}} - \dot{y}_{\mathrm{n},i}^{\mathrm{RSSI}} = u^{\mathsf{T}}\rho_i - u_{\mathrm{n}}^{\mathsf{T}}\rho_{\mathrm{n},i} = 0,$$

for all $i \in \Omega(x_{\mathrm{n}})$ or, equivalently,

$$(u(\tau) - u_{\mathrm{n}}(\tau))^{\mathsf{T}} \begin{bmatrix} \rho_i(\tau) & \rho_j(\tau) \end{bmatrix} = 0,$$

Since $\mathrm{Rank}(\mathcal{R}(x_{\mathrm{n}}(\tau))) \geq 2$, $\rho_i(\tau)$ and $\rho_j(\tau)$ are linearly independent, and thus $u(\tau) = u_{\mathrm{n}}(\tau)$ and $x(\tau^+) = x_{\mathrm{n}}(\tau^+)$. To conclude, we iterate the above reasoning for all $\tau \geq 0$, which yields $u = u_{\mathrm{n}}$, and shows the implication.

(Expression of undetectable attacks) By substituting (7.2) and (7.4) into Definition 7.1 we obtain $x + u^{\mathrm{GNSS}} = x_{\mathrm{n}}$, from which $u^{\mathrm{GNSS}} = x_{\mathrm{n}} - x$ follows. Next, we take the time derivative of $y_i^{\mathrm{RSSI}} - y_{\mathrm{n},i}^{\mathrm{RSSI}} = 0$ and substitute (7.1) and (7.3) to obtain

$$\dot{y}_i^{\mathrm{RSSI}} - \dot{y}_{\mathrm{n},i}^{\mathrm{RSSI}} = u^{\mathsf{T}}\rho_i - u_{\mathrm{n}}^{\mathsf{T}}\rho_{\mathrm{n},i} = 0, \tag{7.7}$$

which implies that u can be decomposed as $u = v_{\mathrm{r},i}\rho_i + w$, with $w^{\mathsf{T}}\rho_i = 0$ and $v_{\mathrm{r},i} = u_{\mathrm{n}}^{\mathsf{T}}\rho_{\mathrm{n},i}/\|\rho_i\|^2$, which shows the claimed result and concludes the proof. ■

Theorem 7.3 suggests that the existence of undetectable attacks depends on $\Omega(x_{\mathrm{n}})$, and thus on the set of radio stations visited by the nominal trajectory. In particular, the theorem implies that undetectable attacks can exist only under three circumstances. First, $|\Omega(x_{\mathrm{n}}(t))| = 0$ for some $t \in \mathbb{R}_{\geq 0}$ (in this case, any attack is undetectable as also discussed in Remark 7.2). Second, $|\Omega(x_{\mathrm{n}}(t))| = 1$ for some $t \in \mathbb{R}_{\geq 0}$ (i.e. there exists a time t such that the nominal trajectory visits a single radio station). Third, $|\Omega(x_{\mathrm{n}}(t)| > 1$ and the robot position $x_{\mathrm{n}}(t)$ is collinear with the coordinates of all available radio stations for some $t \in \mathbb{R}_{\geq 0}$ (i.e., there exists a time t such that $x_{\mathrm{n}}(t)$ and b_i for all $i \in \Omega(x_{\mathrm{n}}(t))$ are collinear). Further, the theorem provides a systematic way to design undetectable attacks when the attacker knows the nominal input. In particular, the signal w in equation (7.6) can be arbitrarily selected by an attacker and it does not affect detectability. Finally, we emphasize that the theorem characterizes the existence of undetectable attacks in relation to the nominal path followed by the robot. As we will later demonstrate in this work (see Section 7.3), the existence of undetectable attacks can be further refined by appropriately designing the nominal control inputs. Fig. 7.1 illustrates the regions of the plane where undetectable attacks can exist.

Remark 7.4. ***(Condition*** $\mathrm{Rank}(\mathcal{R}(x_{\mathbf{n}}(t))) = 0$***)*** *In the particular situation where* $\mathrm{Rank}(\mathcal{R}(x_{\mathrm{n}}(t))) = 0$ *for some* t*, we necessarily have* $|\Omega(x_{\mathrm{n}}(t))| = 1$ *and* $x_{\mathrm{n}}(t) = b_i$*, that is, the nominal position of the robot overlaps with the position of the (unique) radio station. In fact, these circumstances and under the assumption of non-overlapping radio stations* ($b_i \neq b_j$*, if* $i \neq j$*) we either have* $\rho_{\mathrm{n},i}(t) = 0$ *or* $\rho_{\mathrm{n},j}(t) = 0$*. In this case, undetectability*

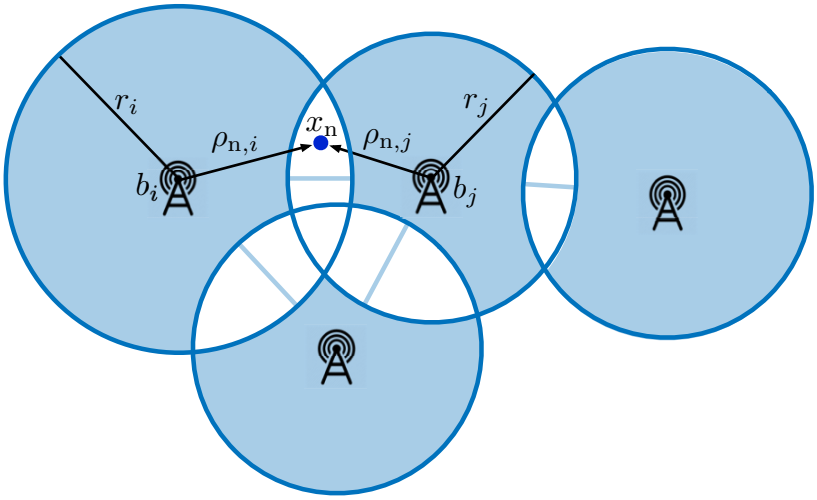

Figure 7.1: Areas shaded in blue denote the regions where $\mathrm{Rank}(\mathcal{R}(x_{\mathrm{n}})) < 2$, that is, the regions of the plane that admit the existence of undetectable attacks.

imposes no constraints on the attack input. In fact, whenever $x_{\mathrm{n}}(t) - b_i = 0$*, any bounded* $u(t)$ *satisfies the notion of undetectability in Definition 7.1.* □

7.2.2 Design of optimal undetectable attacks

We now illustrate how an attacker can design optimal undetectable attacks, that is, attacks that maximize the deviation between the nominal and attacked trajectories while maintaining undetectability. We focus on the case $|\Omega(x_{\mathrm{n}})| = 1$, and formalize the problem

as follows:

$$\begin{aligned} \delta^* = \max_{w} \quad & \|x(T) - x_{\mathrm{n}}(T)\|, \\ \text{subject to} \quad & \dot{x} = u, && \text{(7.8a)} \\ & u = v_{\mathrm{r}}\ \rho + w, && \text{(7.8b)} \\ & \|u\| \leq u_{\max}, && \text{(7.8c)} \end{aligned}$$

where $T \in \mathbb{R}_{\geq 0}$ denotes the control horizon of u_{n}, constraint (7.8b) ensures undetectability of the attack, and the expression for v_{r} and w are listed[1] in Theorem 7.3. Let e_i denote the i-th canonical vector of appropriate dimension. The following result characterizes the general expression of optimal attacks.

Theorem 7.5. ***(Optimal undetectable attacks)*** *Let w^* be an optimal solution to the maximization problem* (7.8)*. Then,*

$$w^* = \gamma \sqrt{u_{\max}^2 - v_{\mathrm{r}}^2 \|\rho\|^2}\, \frac{\tilde{w}}{\|\tilde{w}\|}, \tag{7.9}$$

where $\gamma : [0, T] \to \{-1, 0, 1\}$, and $\tilde{w}$ is any vector that satisfies $\tilde{w}^{\mathsf{T}} \rho = 0$. Moreover, let the nominal input be decomposed as $u_{\mathrm{n}} = \alpha \rho_{\mathrm{n}} + z$, with $\rho_{\mathrm{n}}^{\mathsf{T}} z = 0$ and $\alpha \in \mathbb{R}$. Then, the optimal deviation δ^* satisfies

$$\delta^* = 2\|x_{\mathrm{n}}(T)\| \sin(\theta_T/2),$$

[1] In the remainder, we omit the subscript i when $|\Omega(x_{\mathrm{n}})| = 1$.

where

$$\theta_T = \int_0^T \frac{\|w^*\| - \|z\|}{\|r\|} dt.$$

Proof. To show (7.9), we use the Pontryagin's Maximum Principle [110] to derive optimality conditions for the optimization problem (7.8). In particular, we rewrite $w = \sigma \frac{\tilde{w}}{\|\tilde{w}\|}$, where $\sigma \in \mathbb{R}$ and $\tilde{w}^\mathsf{T}\rho = 0$, and consider the Hamiltonian

$$\mathcal{H}(t, x, w, \lambda) = \lambda^\mathsf{T}(v_\mathrm{r}\ \rho + \sigma \frac{\tilde{w}}{\|\tilde{w}\|}),$$

where $\lambda : [0, T] \to \mathbb{R}^2$, with the additional constraint $\|u\|^2 \leq u_{\max}^2$ or, equivalently, $v_\mathrm{r}^2\|\rho\|^2 + \sigma^2 \leq u_{\max}^2$. Notice that the Hamiltonian is a function of time because of the dependence on v_r. By application of the Maximum Principle [111], the optimal control input at all times minimizes the Hamiltonian over the set of bounded attack inputs $U(t) = \{\sigma : v_\mathrm{r}^2\|\rho\|^2 + \sigma^2 \leq u_{\max}^2\}$, that is, the optimal σ^* satisfies

$$\begin{aligned}\sigma^* &= \arg\min_{\sigma \in U(t)} \mathcal{H}(t, x, w, \lambda) = \arg\min_{\sigma \in U(t)} \left(\frac{\sigma}{\|\tilde{w}\|}\lambda^\mathsf{T}\tilde{w}\right) \\ &= -\sqrt{u_{\max}^2 - v_\mathrm{r}^2\|\rho\|^2}\,\mathrm{sign}(\lambda^\mathsf{T}\tilde{w}),\end{aligned}$$

where sign denotes the sign function, which proves (7.9).

To show the given expression for δ^*, we observe that the ratio $\|w\|/|\rho\|$ is the tangential velocity of the attacked trajectory; similarly, $\|z\|/\|r\|$ is the tangential velocity in the nominal trajectory. Thus, the angle between the vectors $x_\mathrm{n}(T)$ and $x(T)$ can be

obtained by integrating the instantaneous difference between the two tangential velocities as

$$\theta_T = \int_0^T \frac{\|w^*\|}{\|\rho\|} - \frac{\|z\|}{\|r\|} dt = \int_0^T \frac{\|w^*\| - \|z\|}{\|r\|} dt, \tag{7.10}$$

where we used $\|r\| = \|\rho\|$ since the attack is undetectable. To conclude, we note that when $\|x_{\mathrm{n}}(T)\| = \|x(T)\|$ the deviation in trajectory can be related to the angular deviation by means of the following geometric relationship

$$\|x_{\mathrm{n}}(T) - x(T)\| = 2\|x_{\mathrm{n}}(T)\| \sin(\theta_T/2),$$

which shows the given expression for δ^* and concludes the proof. ■

From Theorem 7.5, optimal attacks are of the form of a feedback controller (that depends on the instantaneous values of u_{n}, x_{n}, and x through $\tilde{w}$), which switches abruptly between two (time-varying) expressions, and where the switching instants are determined by the function γ. Next, we propose an algorithm to determine the optimal switching times of the function γ. To this aim, we choose by convention the vector $\tilde{w}$ that minimizes the counterclockwise angle between ρ and $\tilde{w}$. Our method is illustrated in Algorithm 3 and relies on the following rationale to identify the control input that leads to optimal deviations: if the counterclockwise angle between $\rho(t)$ and $-\rho_{\mathrm{n}}(T)$ is smaller than π, then $\gamma(t) = 1$; if such angle is larger than π, then $\gamma(t) = -1$; if such angle equals to zero, then $\gamma(t) = 0$. Finally, we observe that when the angle between the vectors $\rho(t)$ and $-\rho_{\mathrm{n}}(T)$ equals to π, either choice $\gamma(t) = 1$ or $\gamma(t) = -1$ will result in an optimal solution of (7.8). In

Algorithm 3, we let $\gamma(t) = 1$ in this situation. We formalize the optimality of Algorithm 3 in the following theorem.

Theorem 7.6. ***(Optimality of Algorithm 3)*** *Let w be the output of Algorithm 3. Then, w is a solution to* (7.8).

Proof. Let w be the output of Algorithm 3, let γ denote the corresponding switching function, and let u_{n} be decomposed as in Theorem 7.5. Let

$$\varphi_T := \int_0^T \frac{\|w\| - \|z\|}{\|r\|} dt,$$

denote the angular deviation between nominal and attacked trajectories, obtained by integrating the difference between the tangential velocities, and recall that every optimal attack satisfies $w^* = \gamma\sqrt{u_{\max}^2 - v_{\mathrm{r}}^2\|\rho\|^2}\frac{\tilde{w}}{\|\tilde{w}\|}$, and $\delta^* = 2\|x_{\mathrm{n}}(T)\|\sin(\theta_T/2)$, where θ_T is defined in (7.10). To show that w is a minimizer of (7.8), we equivalently show that $\varphi_T = \theta_T$. We prove this statement by contradiction, and distinguish among two cases.

(Case 1) $|\theta_T| > |\varphi_T|$. By replacing the integral expressions, we obtain

$$\left|\int_0^T \frac{\|w^*\| - \|z\|}{\|r\|} dt\right| > \left|\int_0^T \frac{\|w\| - \|z\|}{\|r\|} dt\right|,$$

which implies that there must exist t such that $\|w^*(t)\| > \|w(t)\|$. Since both w and w^* satisfy (7.9) and $|\gamma| = 1$ at all times, the above relationship results in a contradiction.

(Case 2) $|\theta_T| < |\varphi_T|$. We first observe that the scenario $|\theta_T| < |\varphi_T| < \pi$ immediately results in a contradiction, since w^* is, by assumption, an optimal solution to (7.8) and thus

Algorithm 3: Optimal solutions to (7.8)

Input: $x_{\mathrm{n}}(T)$, $u_{\max}$
Output: w solution to (7.8)

repeat
  Measure instantaneous values of x, x_{n}, u_{n};
  $\phi \leftarrow$ Angle between $x(t)$ and $-x_{\mathrm{n}}(T)$;
  if $\phi = 0$ **then**
    $\gamma \leftarrow 0$;
  else if $0 < \phi \leq \pi$ **then**
    $\gamma \leftarrow 1$;
  else
    $\gamma \leftarrow -1$;
  $v_{\mathrm{r}} \leftarrow u_{\mathrm{n}}^{\mathsf{T}} \rho_{\mathrm{n}} / \|\rho\|^2$;
  $w \leftarrow \gamma \sqrt{u_{\max}^2 - v_{\mathrm{r}}^2 \|\rho\|^2} \frac{\tilde{w}}{\|\tilde{w}\|}$;
until $x_{\mathrm{n}} = x_{\mathrm{n}}(T)$;
return w

a minimizer of $|\theta_T - \pi|$. On the other hand, $|\varphi_T| > \pi$ is also a contradiction since in the algorithm $w(t) = 0$ whenever $\varphi_t = \pi$, which shows the result and concludes the proof. ■

Fig. 7.2 illustrates optimal trajectories resulting from Algorithm 3, and shows a comparison between optimal attack trajectories and suboptimal attacks obtained when $\gamma = 1$ at all times. It is worth noting that the control law described in Algorithm 3 is of feedback type, that is, the instantaneous value of the control inputs v_{r}, w, and u are computed by using the current (measured) values of x, x_{n}, and u_{n}. Thus, differently from [109], optimal undetectable attacks can be cast by using instantaneous measurements of u_{n} and x_{n}, and without the full knowledge of the nominal open loop signals.

In the following remark, we discuss the set of positions that can be reached by a robot under attack.

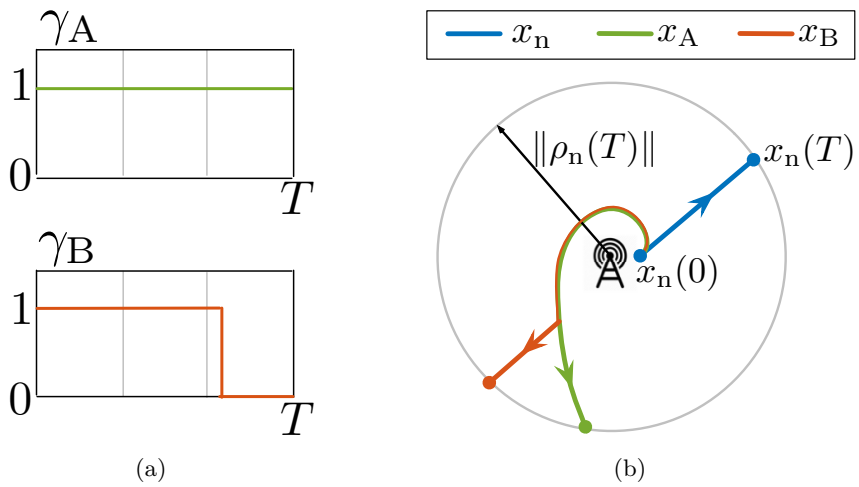

Figure 7.2: (a) Suboptimal and optimal switching functions, and (b) corresponding trajectories. The circle shows that $\|\rho_n(T)\| = \|\rho_A(T)\| = \|\rho_B(T)\|$.

Remark 7.7. ***(Reachable positions under attacks)*** *The set of positions that can be reached by an (undetectable) attacker depend only on the choice of* u_n *performed by the trajectory planner, and can be computed as follows. Let* x_1 *and* x_{-1} *denote the trajectories resulting from* (7.3) *with an undetectable attack input of the form* (7.9) *with* $\gamma = 1$ *and* $\gamma = -1$ *at all times, respectively. Moreover, let* $\text{arc}(x_1(T), x_{-1}(T))$ *be the arc of a circle that is centered at the station position* b *with radius* $\|\rho_n(T)\|$*, and containing* $x_n(T)$ *(see Fig. 7.3 for an illustration). For every* $\bar{x} \in \text{arc}(x_1(T), x_{-1}(T))$*, there exists a control input that steers the robot from* $x(0)$ *to* $x(T) = \bar{x}$*. In fact, it can be shown that the output of Algorithm 3 with* $x_n(T) = -\bar{x}$ *reaches the desired final state* $\bar{x}$ *(see Fig. 7.3).* □

7.3 Secure navigation

This section is devoted to the characterization and design of secure trajectories. We consider scenarios where undetectable attacks can exist (see Theorem 7.3) and focus on

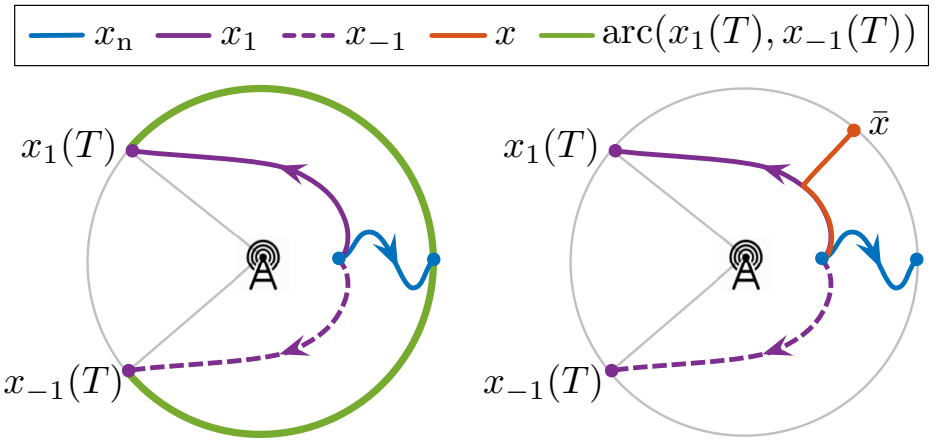

Figure 7.3: Positions reachable by attackers (left) and example of attack trajectory obtained from Algorithm 3 (right).

the problem of designing nominal control inputs that ensure that every attack is detected. We say that a trajectory x_{n} is *secure* if, for all attacks u, one of the following mutually exclusive conditions is satisfied:

(C1) $x = x_{\mathrm{n}}$ at all times; or

(C2) if $x \neq x_{\mathrm{n}}$ at some time, then the attack is detectable.

A control input is *secure* if the resulting trajectory is secure.

Theorem 7.8. ***(Secure control inputs)*** *Let $|\Omega(x_{\mathrm{n}})| = 1$ at all times. The control input u_{n} is secure if and only if the following conditions hold simultaneously:*

(1) there exists a function $\kappa : \mathbb{R}_{\geq 0} \to \{-1, 1\}$ satisfying

$$u_n = \kappa \frac{\rho_n}{\|\rho_n\|} u_{\max}, \tag{7.11}$$

(2) the trajectory ρ_{n} satisfies $\rho_{\mathrm{n}} \neq 0$ at all times.

Proof. (*Only if*) To prove that (C1)-(C2) imply (1)-(2), we equivalently show that if (1)-(2) do not simultaneously hold, then there exists an undetectable attack that violates (C1)-(C2). We distinguish among two cases.

(Case 1) There exists a time instant τ such that (7.11) does not hold, that is, $u_{\mathrm{n}}^{\mathsf{T}}(\tau)\rho_{\mathrm{n}}(\tau) < u_{\max}$. Consider the attack input u satisfying $u^{\mathsf{T}}\rho = u_{\mathrm{n}}^{\mathsf{T}}\rho_{\mathrm{n}}$ at all times, and $\|u(\tau)\| = u_{\max}$. By construction, u is undetectable (see Theorem 7.3) and satisfies $u \neq u_{\mathrm{n}}$, which violates (C1) and (C2).

(Case 2) There exists τ such that $\rho_{\mathrm{n}}(\tau) = 0$. Under this assumption, every u satisfying $u^{\mathsf{T}}\rho = u_{\mathrm{n}}^{\mathsf{T}}\rho_{\mathrm{n}}$ at all times and $u(\tau) \neq u_{\mathrm{n}}(\tau)$ is undetectable. In fact, whenever $\rho_{\mathrm{n}} = 0$ undetectability imposes no constraints on the attack input, and concludes the proof of the implication.

(*If*) Assume the two conditions (1)-(2) hold. If the attack input does not satisfy $u^{\mathsf{T}}\rho = u_{\mathrm{n}}^{\mathsf{T}}\rho_{\mathrm{n}}$, then the attack is detectable and (C2) is verified. On the other hand, assume u is undetectable, that is, $u^{\mathsf{T}}\rho = u_{\mathrm{n}}^{\mathsf{T}}\rho_{\mathrm{n}}$ (and thus $\|\rho\| = \|\rho_{\mathrm{n}}\|$) at all times. Then,

$$u_{\max}\|\rho_{\mathrm{n}}\| = |u_{\mathrm{n}}^{\mathsf{T}}\rho_{\mathrm{n}}| = |u^{\mathsf{T}}\rho| \leq u_{\max}\|\rho\|,$$

where we substituted (7.11) and used the triangle inequality. Since $\|\rho\| = \|\rho_{\mathrm{n}}\|$, exact equality must hold and the vectors u and ρ are linearly dependent with $\|u\| = u_{\max}$ at all times. To conclude, we note that $u = -u_{\mathrm{n}}$ results in a violation of the undetectability assumption $u^{\mathsf{T}}\rho = u_{\mathrm{n}}^{\mathsf{T}}\rho_{\mathrm{n}}$, therefore $u = u_{\mathrm{n}}$ at all times, which shows (C1) and concludes the proof. ■

Theorem 7.8 provides an explicit characterization of secure control inputs: it shows that every secure input has maximum magnitude at all times, and its direction is parallel to vector ρ_{n}. Two significant implications follow from Theorem 7.8. First, the result shows that appropriate control design prevents the existence of undetectable attacks. Second, it shows that whenever the nominal quantities do not satisfy conditions (1)-(2), then undetectable attacks always exist. Further, we note that this result extends the conclusions of Theorem 7.3 by showing that condition (7.5) is also sufficient for the existence of undetectable attacks for general choices of u_{n}.

Remark 7.9. ***(Game-theoretic interpretation of the results)*** *The security problem considered in this work can equivalently be studied in a game-theoretic framework, and, specifically, as a Stackelberg game [112]. In fact, the secure trajectories in Theorem 7.8 can be viewed as the strategies that maximize the payoff of the trajectory planner, which anticipates the fact that the attacker will adopt its best response. This strategy is open-loop and independent of the attacker's action, which takes place subsequently. The undetectable attacks in Theorem 7.5, instead, can be viewed as the best response of the attacker given the strategy of the trajectory planner and the attacker's objectives. The attacker's strategy is of feedback form, because the best response of the attacker depends on the strategy of the trajectory planner to maintain undetectability and maximize the payoff. We remark that alternative formulations of the problem are also possible, where, for instance, the actions of the trajectory planner and the attacker occur concurrently.* □

Next, we focus on characterizing the set of initial and final positions that can be reached via secure trajectories. To this aim, we chose the coordinate system so that $b = 0$ and $x_{\mathrm{n}} = \rho_{\mathrm{n}}$, and let sign() be the sign function, with $\mathrm{sign}(0) = 0$.

Theorem 7.10. ***(Reachable positions via secure control inputs)*** *Let* $|\Omega(x_{\mathrm{n}})| = 1$ *and* u_{n} *be a secure control input. Then, for all* $T \in \mathbb{R}_{\geq 0}$*,*

$$x_{\mathrm{n}}(T) \in \mathcal{S}(x_{\mathrm{n}}(0)),$$

where $\mathcal{S}(x_{\mathrm{n}}(0)) = \{x \,:\, x = \alpha x_{\mathrm{n}}(0), \alpha \in \mathbb{R}_{>0}\}$*. Moreover, for any* $\bar{x}_{\mathrm{n}} \in \mathcal{S}(x_{\mathrm{n}}(0))$ *the secure control input* (7.11) *with*

$$\kappa = \mathrm{sign}(\|\bar{x}_{\mathrm{n}}\| - \|x_{\mathrm{n}}(0)\|), \tag{7.12}$$

steers the robot from $x_{\mathrm{n}}(0)$ *to* $x_{\mathrm{n}}(T) = \bar{x}_{\mathrm{n}}$*, with* $T = \frac{\|\bar{x}_{\mathrm{n}}\|^2}{4u_{\max}}$*.*

Proof. (Reachable set) We first show that for every secure control input the quantity x_1/x_2 is time-invariant, that is, $\frac{d}{dt}\frac{x_1}{x_2} = 0$. By expanding the time derivative we obtain

$$\dot{x}_1 x_2^{-1} - x_1 x_2^{-2} \dot{x}_2 = 0,$$

where we substituted (7.1) and (7.11). Next, we prove that $\alpha > 0$. Assume, by contradiction, that $x(T) = \alpha_T x_{\mathrm{n}}(0)$, and $\alpha_T < 0$. By continuity of x_{n}, there exists $\tau \in [0, T)$ such that $x(\tau) = \alpha_\tau x_{\mathrm{n}}(0)$, with $\alpha_\tau = 0$. But this violates the assumption that u is secure (condition (2) in Theorem 7.8), which contradicts the assumption and proves the claim.

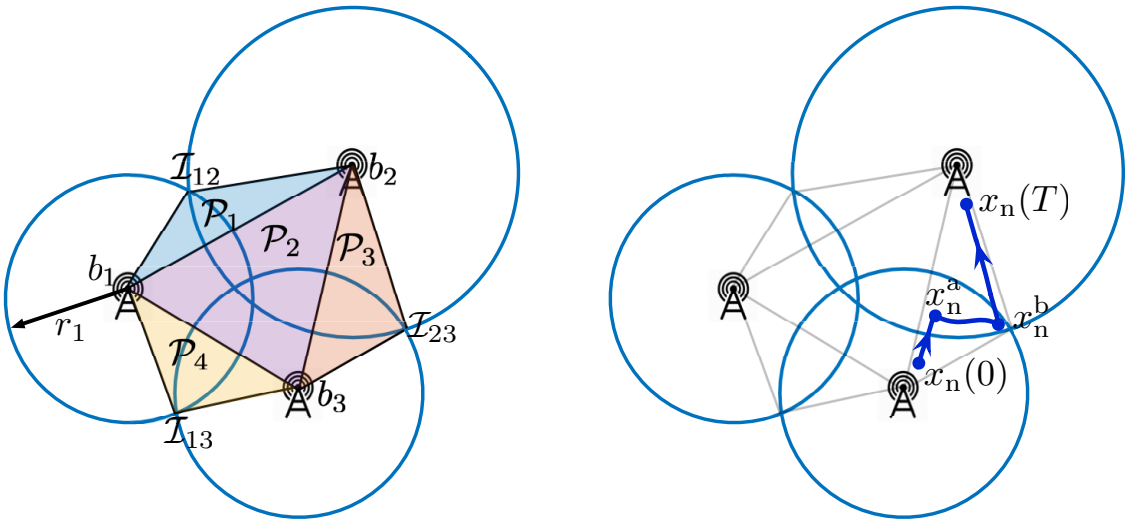

Figure 7.4: (Left) Notation used in Example 7.11. (Right) Intermediate waypoints.

(Expression for secure control input) Let u_{n} be as in (7.11) and let $n := \|x_{\mathrm{n}}\|^2$. Then, by substituting (7.11), we obtain

$$\dot{n} = \frac{d}{dt} x_{\mathrm{n}}^{\mathsf{T}} x_{\mathrm{n}} = 4\dot{x}_{\mathrm{n}} x_{\mathrm{n}} = 4\kappa u_{\max},$$

Moreover,

$$\begin{aligned} n(T) = \|x_{\mathrm{n}}(T)\|^2 &= \int_0^T 4\kappa u_{\max} dt \\ &= \mathrm{sign}(\|\bar{x}_{\mathrm{n}}\| - \|x_{\mathrm{n}}^0\|) u_{\max} T = \|\bar{x}_{\mathrm{n}}\|^2, \end{aligned}$$

where we have substituted the expression for κ and T. To conclude, we note that since $x_{\mathrm{n}}(T) \in \mathcal{S}(x_{\mathrm{n}}(0))$ and $\bar{x}_{\mathrm{n}} \in \mathcal{S}(x_{\mathrm{n}}(0))$, we necessarily have $x_{\mathrm{n}}(T) = \bar{x}_{\mathrm{n}}$, which shows the claimed result and concludes the proof. ■

Theorem 7.10 shows that the set of configurations that are reachable via secure trajectories from x_0 are described by the line passing through the points x_0 and the origin of the reference frame. We conclude this section by illustrating how the above results can be combined when $|\Omega(x_{\rm n})| \geq 2$.

Example 7.11. ***(Secure navigation)*** *Consider the scenario illustrated in Fig. 7.4, consisting of $n_{\rm b} = 3$ radio stations. For all $i, j \in \{1, 2, 3\}$, we let $\mathcal{I}_{ij} = \{x : \|x - b_i\| = r_i$ and $\|x - b_j\| = r_j\}$ denote the intersection points between the circles that identify the communication ranges of the radio stations. Further, let*

$$\mathcal{P}_1 = \{b_1, \mathcal{I}_{12}, b_2\}, \qquad \mathcal{P}_2 = \{b_1, b_2, b_3\},$$

$$\mathcal{P}_3 = \{b_2, \mathcal{I}_{23}, b_3\}, \qquad \mathcal{P}_4 = \{b_1, b_3, \mathcal{I}_{13}\},$$

denote the polygons that originate from the locations of the RSSI stations (i.e., b_i) and the intersection points (i.e., $\mathcal{I}_{ij}$), see Fig. 7.4(a) for an illustration. As an illustrative example, consider any initial position $x_{\rm n}(0) \in \{x \ : \ x \in \mathcal{P}_3$ and $\Omega(x) = \{3\}\}$, that is, any initial position that is located in the polygon $\mathcal{P}_3$ and within the communication range of station 3. Moreover, consider any final position $\bar{x}_{\rm n} \in \{x \ : \ x \in \mathcal{P}_3$ and $\Omega(x) = \{2\}\}$, that is, any final position that is located in the polygon $\mathcal{P}_3$ and within the communication range of station 2 (see Fig. 7.4(b)). Moreover, define the sets

$$\chi_{\rm n}^{\rm A} := \{x : x = \alpha x_{\rm n}(0), \alpha \in \mathbb{R}_{>0}, \text{ and } \Omega(x) = \{2, 3\}\},$$

$$\chi_{\rm n}^{\rm B} := \{x : x = \alpha \bar{x}_{\rm n}, \alpha \in \mathbb{R}_{>0}, \text{ and } \Omega(x) = \{2, 3\}\},$$

which describe the positions that are reachable from $x_{\mathrm{n}}(0)$ *and* $\bar{x}_{\mathrm{n}}$*, respectively, and that belong to the intersection between the communication ranges of stations* 2 *and* 3*. Notice that these sets are nonempty since the intersection between the communication ranges of stations* 2 *and* 3 *is non-empty. Now, let* $x_{\mathrm{n}}^{\mathrm{a}} \in \chi_{\mathrm{n}}^{\mathrm{A}}$ *and* $x_{\mathrm{n}}^{\mathrm{b}} \in \chi_{\mathrm{n}}^{\mathrm{B}}$*. Then, a secure control input from* $x(0)$ *to* $\bar{x}$ *is as follows:*

(i) Apply the secure control input given by (7.11) *with* $\kappa = \mathrm{sign}(\|x_{\mathrm{n}}^{\mathrm{a}}\| - \|x_{\mathrm{n}}(0)\|)$ *until* $x_{\mathrm{n}} = x_{\mathrm{n}}^{\mathrm{a}}$*;*

(ii) Apply any control input u_{n} *that satisfies* $\Omega(x_{\mathrm{n}}) = \{2, 3\}$ *until* $x_{\mathrm{n}} = x_{\mathrm{n}}^{\mathrm{b}}$*;*

(iii) Apply the secure control input given by (7.11) *with* $\kappa = \mathrm{sign}(\|\bar{x}_{\mathrm{n}}\| - \|x_{\mathrm{n}}^{\mathrm{b}}\|)$ *until* $x_{\mathrm{n}} = \bar{x}_{\mathrm{n}}$*;*

We note that the geometry of the problem and Theorem 7.10 guarantee the existence of the secure control input defined in steps (i)-(iii). An illustration of the trajectory resulting from the above algorithm is presented in Fig. 7.4. □

Chapter 8

Conclusions and Future Work

One fundamental challenge for modern network systems is to guarantee their robustness, namely their efficient operation in the face of failures of their components, changes in the behavior of their users, or targeted malicious attacks. This dissertation contains a collection of models and theoretical tools to study the robustness of network systems, with two main application focuses: traffic control and cyber-physical security. With respect to traffic control, we analyzed the impact of app-informed travelers in traffic congestion, and we designed tractable control algorithms to control automated intersections. With respect to security in cyber-physical systems, we studied the sensitivity of robustness with respect to perturbations of the communication edges, and we designed control inputs to prevent the action of malicious attackers against robotic navigation. We conclude this dissertation with some final remarks on each of these topics, together with a discussion of possible extensions.

8.1 Traffic Control in Transportation Systems: Summary and Directions

In Chapter 3, we proposed a dynamical routing model for understanding the impact of app-informed travelers in traffic networks. We studied the stability of such routing model coupled with a dynamical traffic model, and we showed that the general adoption of routing apps: (i) maximizes the throughput of flow across the traffic system, but (ii) can deteriorate the stability of the equilibrium points. To ensure asymptotic stability, we propose a control technique that relies on regulating the rate at which routing apps react to changes in traffic congestion.

In Chapter 4, we developed a simplified traffic model to capture the behavior of urban traffic networks controlled by automated traffic intersections. We casted an optimization problem to minimize the overall congestion in the network, and we showed that this problem is equivalent to the problem of optimizing the degree of controllability of the dynamical system. Our results show that the availability of a global, although approximate, model of the system interconnection can considerably improve the network efficiency, and allows for a more efficient and tractable analysis as compared to traditional techniques.

In Chapter 5, we proposed a real-time optimization framework to design routing suggestions for the drivers with the goal of optimizing the travel time experienced by all users in dynamical traffic networks that operate at non-equilibrium points. Our results reveal a tradeoff between efficiency and resilience in a transportation system, demonstrating that controlling the routing often results in roads that operate close to their capacity, thus deteriorating the resilience of the overall system.

In the following, we discuss some of the aspects that require further investigation.

Presence of Noise. In this dissertation, we have focused on traffic models that are *deterministic*. However, real-world traffic infrastructures are systematically subject to stochastic fluctuations in the user behavior, noise in the sensor measurements, and models are often inaccurate or approximate. We emphasize that the traffic models adopted in this work are *macroscopic*, that is, they capture the *aggregate behavior of the system in the long run*. Deterministic models are adopted in these settings thanks to their tractability, and because they typically offer a baseline for the development of more-accurate stochastic models. The development of stochastic traffic control techniques is an interesting research problem, and preliminary works facing these challenges are [113, 114].

Needs for Communication and Actuation Infrastructure. In Chapters 4 and 5 we discussed the use of vehicles communication to adjust the operation of automated intersections and of app-based routing in traffic networks. Unfortunately, the implementation of these real-time control policies requires the availability of an effective and reliable communication infrastructure that will allow the system operator to communicate with the automated vehicles. Although ongoing research efforts are currently tackling these challenges, the development and implementation of a reliable communication infrastructure is, to date, still an ongoing research effort. To this aim, research is needed to develop effective and reliable communication protocols. Ongoing research in this area is [115] (see also references therein).

Security of Transportation Systems. While the introduction of automation and communication capabilities brings novel opportunities for control and optimization,

these features also open a number of security concerns. In fact, lack of appropriate encryption in the transmitted signals or the opportunity to physically tamper with the road-side units may enable malicious attackers to compromise the effective operation of a transportation infrastructure and of its components. To this aim, research is needed to develop tools that can ensure the robust operation of modern transportation systems despite malicious intrusions. These security concerns have been highlighted in recent works [116, 117].

8.2 Security in Linear Networks and Robotics: Summary and Directions

In Chapter 6, we extended the classical notion of observability radius of dynamical systems to networks, thus providing a measure of the ability to maintain observability of the network modes against structured perturbations of the edge weights. We characterized network perturbations preventing observability, and we described a heuristic algorithm to compute perturbations with smallest Frobenius norm. Additionally, we studied the observability radius of networks with random weights, derived fundamental bounds relating the observability radius to certain connectivity properties, and explicitly characterized the observability radius of line and star networks. Our results show that different network structures exhibit inherently different robustness properties, and thus provide guidelines for the design of robust complex networks.

In Chapter 7, we considered the problem of designing the trajectories of a robot when its localization signals are maliciously compromised by an attacker. We demonstrated the existence of undetectable attacks in relation to the region of the plane where the robot is

located, and we presented an efficient algorithm to design optimal undetectable trajectories. Conversely, we showed how a trajectory planner can leverage the layout of the radio stations to design control inputs that allow the detection of any attack. Our results demonstrate for the first time that appropriate control design can enhance the security of systems operating in adversarial environments.

Nonlinear Dynamics. In our analysis in Chapter 6, we focused on network systems described by linear dynamics. However, common real-world components are characterized by nonlinearities. Although our results still hold locally, i.e., in a neighborhood of the point of operation where the nonlinear system is linearized, it is an exceedingly difficult problem to characterize robustness for systems with nonlinear dynamics. We expect that the theory developed in [118, 119] can be a useful starting point to develop general theories that hold for systems with nonlinear dynamics.

Uncertainty and Noise in Sensory Data. In Chapter 7 we characterized undetectable attacks and secure trajectories for deterministic systems. When the dynamics or the sensors are driven by noise, different and more relaxed notions of attack detectability should be adopted, as done for instance in [120] for the case of linear dynamics. Loosely speaking, undetectable attacks are easier to cast in stochastic systems, because an attacker has the additional possibility of hiding its action within the noise limits. Thus, the conditions derived in this work for deterministic systems serve as fundamental limitations also for stochastic systems.

Bibliography

[1] G. Bianchin and F. Pasqualetti, "Routing apps may deteriorate performance in traffic networks: Oscillating congestions and robust information design," *IEEE Transactions on Automatic Control*, 2020. submitted.

[2] G. Bianchin, Y.-C. Liu, and F. Pasqualetti, "Secure navigation of robots in adversarial environments," *IEEE Control Systems Letters*, vol. 4, no. 1, pp. 1–6, 2020.

[3] Y.-C. Liu, G. Bianchin, and F. Pasqualetti, "Secure trajectory planning against undetectable spoofing attacks," *Automatica*, vol. 112, p. 108655, 2020.

[4] G. Bianchin and F. Pasqualetti, "Gramian-based optimization for the analysis and control of traffic networks," *IEEE Transactions on Intelligent Transportation Systems*, pp. 1–12, 2019.

[5] G. Bianchin, P. Frasca, A. Gasparri, and F. Pasqualetti, "The observability radius of networks," *IEEE Transactions on Automatic Control*, vol. 62, no. 6, pp. 3006–3013, 2017.

[6] G. Bianchin and F. Pasqualetti, "Oscillating congestion in dynamical traffic networks with real-time app routing," *IEEE Conf. on Decision and Control*, 2020. submitted.

[7] G. Bianchin, F. Pasqualetti, and S. Kundu, "Resilience of traffic networks with partially controlled routing," in *American Control Conference*, (Philadelphia, PA, USA), pp. 2670–2675, July 2019.

[8] G. Bianchin and F. Pasqualetti, "A network optimization framework for the analysis and control of traffic dynamics and intersection signaling," in *IEEE Conf. on Decision and Control*, (Miami, FL, USA), pp. 1017–1022, Dec. 2018.

[9] T. Menara, G. Bianchin, M. Innocenti, and F. Pasqualetti, "On the number of strongly structurally controllable networks," in *American Control Conference*, (Seattle, WA, USA), pp. 340–345, May 2017.

[10] G. Bianchin, P. Frasca, A. Gasparri, and F. Pasqualetti, "The observability radius of network systems," in *American Control Conference*, (Boston, MA, USA), pp. 185–190, July 2016.

[11] G. Bianchin, F. Pasqualetti, and S. Zampieri, "The role of diameter in the controllability of complex networks," in *IEEE Conf. on Decision and Control*, (Osaka, Japan), pp. 980–985, Dec. 2015.

[12] G. Bianchin, A. Cenedese, M. Luvisotto, and G. Michieletto, "Distributed fault detection in sensor networks via clustering and consensus," in *IEEE Conf. on Decision and Control*, pp. 3828–3833, 2015.

[13] G. Bianchin and F. Pasqualetti, "Time-delay attacks in network systems," in *Cyber-Physical Systems Security*, pp. 157–174, Springer International Publishing, 2018.

[14] G. Bianchin and F. Pasqualetti, "Gramian-based optimization." `https://github.com/gianlucaBianchin/Gramian-Based-Traffic-Optimization`, 2018. [Online; accessed 20-February-2020].

[15] G. Bianchin, "Coordinated control of mixed robot and sensor networks in distributed area exploration," Master's thesis, University of Padova, 2014.

[16] M. Sprung, M. Chambers, and S. Smith-Pickel, "Transportation statistics annual report 2018," tech. rep., U.S. Department of Transportation, 2018.

[17] D. A. Lazar, S. Coogan, and R. Pedarsani, "The price of anarchy for transportation networks with mixed autonomy," in *American Control Conference*, pp. 6359–6365, June 2018.

[18] V. Bonifaci, T. Harks, and G. Schäfer, "Stackelberg routing in arbitrary networks," *Mathematics of Operations Research*, vol. 35, no. 2, pp. 330–346, 2010.

[19] M. Patriksson, *The traffic assignment problem: models and methods*. Mineola, NY: Dover Publications, 2015.

[20] N. Mehr and R. Horowitz, "How will the presence of autonomous vehicles affect the equilibrium state of traffic networks?," *IEEE Transactions on Control of Network Systems*, pp. 1–10, 2019. in press.

[21] J. G. Wardrop, "Some theoretical aspects of road traffic research," *Proceedings of the institution of civil engineers*, vol. 1, no. 3, pp. 325–362, 1952.

[22] J. Vanbiervliet, B. Vandereycken, W. Michiels, S. Vandewalle, and M. Diehl, "The smoothed spectral abscissa for robust stability optimization," *SIAM Journal on Optimization*, vol. 20, no. 1, pp. 156–171, 2009.

[23] R. E. Kalman, Y. C. Ho, and S. K. Narendra, "Controllability of linear dynamical systems," *Contributions to Differential Equations*, vol. 1, no. 2, pp. 189–213, 1963.

[24] F. Pasqualetti, S. Zampieri, and F. Bullo, "Controllability metrics, limitations and algorithms for complex networks," *IEEE Transactions on Control of Network Systems*, vol. 1, no. 1, pp. 40–52, 2014.

[25] F. L. Cortesi, T. H. Summers, and J. Lygeros, "Submodularity of energy related controllability metrics," in *IEEE Conf. on Decision and Control*, (Los Angeles, CA, USA), pp. 2883–2888, Dec. 2014.

[26] G. Kumar, D. Menolascino, and S. Ching, "Input novelty as a control metric for time varying linear systems," *arXiv preprint arXiv:1411.5892*, 2014.

[27] A. Olshevsky, "Minimal controllability problems," *IEEE Transactions on Control of Network Systems*, vol. 1, no. 3, pp. 249–258, 2014.

[28] N. Monshizadeh, S. Zhang, and M. K. Camlibel, "Zero forcing sets and controllability of dynamical systems defined on graphs," *IEEE Transactions on Automatic Control*, vol. 59, no. 9, pp. 2562–2567, 2014.

[29] M. Fardad, A. Diwadkar, and U. Vaidya, "On optimal link removals for controllability degradation in dynamical networks," in *IEEE Conf. on Decision and Control*, (Los Angeles, CA, USA), pp. 499–504, Dec. 2014.

[30] T. Kailath, *Linear Systems*. Prentice-Hall, 1980.

[31] P. C. Müller and H. I. Weber, "Analysis and optimization of certain qualities of controllability and observability for linear dynamical systems," *Automatica*, vol. 8, no. 3, pp. 237–246, 1972.

[32] A. V. D. Schaft, *L2-gain and passivity techniques in nonlinear control*, vol. 2. Springer, 2000.

[33] R. Sepulchre, M. Jankovic, and P. Kokotovic, *Constructive nonlinear control*. London: Springer-Verlag London, 2012.

[34] C. F. Daganzo, "The cell transmission model part II: network traffic," *Transp. Research Part B: Methodological*, vol. 29, no. 2, pp. 79–93, 1995.

[35] S. Coogan and M. Arcak, "A compartmental model for traffic networks and its dynamical behavior," *IEEE Transactions on Automatic Control*, vol. 60, no. 10, pp. 2698–2703, 2015.

[36] E. Lovisari, G. Como, and K. Savla, "Stability of monotone dynamical flow networks," in *IEEE Conf. on Decision and Control*, pp. 2384–2389, Dec. 2014.

[37] J. W. Weibull, *Evolutionary game theory*. MIT press, 1997.

[38] S. Fischer and B. Vöcking, "On the evolution of selfish routing," in *Algorithms - ESA 2004*, pp. 323–334, Berlin, Heidelberg: Springer, 2004.

[39] W. Krichene, B. Drighès, and A. M. Bayen, "Online learning of nash equilibria in congestion games," *SIAM Journal on Control and Optimization*, vol. 53, no. 2, pp. 1056–1081, 2015.

[40] G. Como, K. Savla, D. Acemoglu, M. A. Dahleh, and E. Frazzoli, "Stability analysis of transportation networks with multiscale driver decisions," *SIAM Journal on Control and Optimization*, vol. 51, no. 1, pp. 230–252, 2013.

[41] G. Como, K. Savla, D. Acemoglu, M. A. Dahleh, and E. Frazzoli, "Robust distributed routing in dynamical networks - part I: Locally responsive policies and weak resilience," *IEEE Transactions on Automatic Control*, vol. 58, no. 2, pp. 317–332, 2013.

[42] H. K. Lo and W. Y. Szeto, "Modeling advanced traveler information services: static versus dynamic paradigms," *Transp. Research Part B: Methodological*, vol. 38, no. 6, pp. 495–515, 2004.

[43] K. H. Schlag, "Why imitate, and if so, how?: A boundedly rational approach to multi-armed bandits," *Journal of Economic Theory*, vol. 78, no. 1, pp. 130 – 156, 1998.

[44] E. Hopkins, "A note on best response dynamics," *Games and Economic Behavior*, vol. 29, no. 1, pp. 138 – 150, 1999.

[45] W. H. Sandholm, "Potential games with continuous player sets," *Journal of Economic Theory*, vol. 97, no. 1, pp. 81 – 108, 2001.

[46] R. K. Ahuja, T. L. Magnanti, and J. B. Orlin, *Network flows*. New Jersey: Prentice Hall, 1988.

[47] G. Como, E. Lovisari, and K. Savla, "Convexity and robustness of dynamic traffic assignment and freeway network control," *Transp. Research Part B: Methodological*, vol. 91, pp. 446–465, 2016.

[48] Q. Ba, K. Savla, and G. Como, "Distributed optimal equilibrium selection for traffic flow over networks," in *IEEE Conf. on Decision and Control*, (Osaka, Japan), pp. 6942–6947, Dec. 2015.

[49] Y. Zhang and P. Ioannou, "Combined variable speed limit and lane change control for highway traffic," *IEEE Transactions on Intelligent Transportation Systems*, vol. 18, no. 7, pp. 1812–1823, 2017.

[50] G. Gomes and R. Horowitz, "Optimal freeway ramp metering using the asymmetric cell transmission model," *Transp. Research Part C: Emerging Technologies*, vol. 14, no. 4, pp. 244–262, 2006.

[51] S. Coogan, E. Kim, G. Gomes, M. Arcak, and P. Varaiya, "Offset optimization in signalized traffic networks via semidefinite relaxation," *Transp. Research Part B: Methodological*, vol. 100, pp. 82–92, 2017.

[52] C. Diakaki, M. Papageorgiou, and K. Aboudolas, "A multivariable regulator approach to traffic-responsive network-wide signal control," *Control Engineering Practice*, vol. 10, no. 2, pp. 183–195, 2002.

[53] P. Hunt, D. Robertson, R. Bretherton, and M. Royle, "The SCOOT on-line traffic signal optimisation technique," *Traffic Engineering & Control*, vol. 23, no. 4, pp. 190–192, 1982.

[54] P. Mirchandani and L. Head, "A real-time traffic signal control system: architecture, algorithms, and analysis," *Transp. Research Part C: Emerging Technologies*, vol. 9, no. 6, pp. 415–432, 2001.

[55] N. Gartner, F. Pooran, and C. Andrews, "Implementation of the opac adaptive control strategy in a traffic signal network," in *IEEE Conf. on Intelligent Transp. Systems*, (Oakland, CA), pp. 195–200, Aug. 2001.

[56] P. Lowrie, "Scats, sydney co-ordinated adaptive traffic system: A traffic responsive method of controlling urban traffic," *Technical report*, 1990.

[57] P. Varaiya, "Max pressure control of a network of signalized intersections," *Transp. Research Part C: Emerging Technologies*, vol. 36, pp. 177–195, 2013.

[58] M. Papageorgiou, C. Diakaki, V. Dinopoulou, A. Kotsialos, and Y. Wang, "Review of road traffic control strategies," *Proceedings of the IEEE*, vol. 91, no. 12, pp. 2043–2067, 2003.

[59] K. Aboudolas, M. Papageorgiou, and E. Kosmatopoulos, "Store-and-forward based methods for the signal control problem in large-scale congested urban road networks," *Transp. Research Part C: Emerging Technologies*, vol. 17, no. 2, pp. 163–174, 2009.

[60] L. B. De Oliveira and E. Camponogara, "Multi-agent model predictive control of signaling split in urban traffic networks," *Transp. Research Part C: Emerging Technologies*, vol. 18, no. 1, pp. 120–139, 2010.

[61] S. Coogan, C. Flores, and P. Varaiya, "Traffic predictive control from low-rank structure," *Transp. Research Part B: Methodological*, vol. 97, no. 2017, pp. 1–22, 2017.

[62] P. Grandinetti, C. C. de Wit, and F. Garin, "Distributed optimal traffic lights design for large-scale urban networks," *IEEE Transactions on Control Systems Technology*, pp. 1–14, 2018.

[63] M. Treiber and A. Kesting, *Traffic flow dynamics*. Springer, 2013.

[64] M. Lighthill and G. Whitham, "On kinematic waves II. A theory of traffic flow on long crowded roads," *Proc. Royal Society*, vol. A, no. 229, pp. 281–345, 1955.

[65] G. Bianchin and F. Pasqualetti, "A network optimization framework for the analysis and control of traffic dynamics and intersection signaling," in *IEEE Conf. on Decision and Control*, (Miami, FL), pp. 1017–1022, Dec. 2018.

[66] C. Canudas-De-Wit, "An average study of the signalized cell transmission model," 2017.

[67] W. Xia and M. Cao, "Analysis and applications of spectral properties of grounded laplacian matrices for directed networks," *Automatica*, vol. 80, pp. 10–16, 2017.

[68] D. Luenberger and Y. Ye, *Linear and nonlinear programming*. Springer, 1984.

[69] R. Bartels and G. Stewart, "Solution of the matrix equation AX+ XB= C," *Communications of the ACM*, vol. 15, no. 9, pp. 820–826, 1972.

[70] F. Pasqualetti, R. Carli, and F. Bullo, "Distributed estimation via iterative projections with application to power network monitoring," *Automatica*, vol. 48, no. 5, pp. 747–758, 2012.

[71] S. Lämmer and D. Helbing, "Self-control of traffic lights and vehicle flows in urban road networks," *Journal of Statistical Mechanics: Theory and Experiment*, vol. 2008, no. 04, pp. 1742–5468, 2008.

[72] M. Behrisch, L. Bieker, J. Erdmann, and D. Krajzewicz, "SUMO - simulation of urban mobility: An overview," in *International Conf. on Advances in System Simulation*, pp. 63–68, 2011.

[73] T. Roughgarden and É. Tardos, "How bad is selfish routing?," *Journal of the Association for Computing Machinery*, vol. 49, no. 2, pp. 236–259, 2002.

[74] J. R. Correa, A. S. Schulz, and N. E. Stier-Moses, "Selfish routing in capacitated networks," *Mathematics of Operations Research*, vol. 29, no. 4, pp. 961–976, 2004.

[75] G. Perakis, "The "price of anarchy" under nonlinear and asymmetric costs," *Mathematics of Operations Research*, vol. 32, no. 3, pp. 614–628, 2007.

[76] D. A. Lazar, S. Coogan, and R. Pedarsani, "Capacity modeling and routing for traffic networks with mixed autonomy," in *IEEE Conf. on Decision and Control*, pp. 5678–5683, Dec. 2017.

[77] A. Hegyi, B. De Schutter, and H. Hellendoorn, "Model predictive control for optimal coordination of ramp metering and variable speed limits," *Transp. Research Part C: Emerging Technologies*, vol. 13, no. 3, pp. 185–209, 2005.

[78] A. Wächter and L. T. Biegler, "On the implementation of an interior-point filter line-search algorithm for large-scale nonlinear programming," *Mathematical programming*, vol. 106, no. 1, pp. 25–57, 2006.

[79] A. V. Fiacco and G. P. McCormick, *Nonlinear programming: sequential unconstrained minimization techniques*, vol. 4. SIAM, 1990.

[80] G. H. Hardy, J. E. Littlewood, and G. Pólya, *Inequalities*. Cambridge University Press, 1988.

[81] W. M. Wonham, *Linear Multivariable Control: A Geometric Approach*. Springer, 3 ed., 1985.

[82] C. Paige, "Properties of numerical algorithms related to computing controllability," *IEEE Transactions on Automatic Control*, vol. 26, no. 1, pp. 130–138, 1981.

[83] R. Eising, "Between controllable and uncontrollable," *Systems & Control Letters*, vol. 4, no. 5, pp. 263–264, 1984.

[84] D. L. Boley and W.-S. Lu, "Measuring how far a controllable system is from an uncontrollable one," *IEEE Transactions on Automatic Control*, vol. 31, no. 3, pp. 249–251, 1986.

[85] G. Hu and E. J. Davison, "Real controllability/stabilizability radius of lti systems," *IEEE Transactions on Automatic Control*, vol. 49, no. 2, pp. 254–257, 2004.

[86] M. Karow and D. Kressner, "On the structured distance to uncontrollability," *Systems & Control Letters*, vol. 58, no. 2, pp. 128–132, 2009.

[87] B. D. Moor, "Total least squares for affinely structured matrices and the noisy realization problem," *IEEE Transactions on Signal Processing*, vol. 42, no. 11, pp. 3104–3113, 1994.

[88] A. Chapman and M. Mesbahi, "On symmetry and controllability of multi-agent systems," in *IEEE Conf. on Decision and Control*, (Los Angeles, CA, USA), pp. 625–630, IEEE, 2014.

[89] F. Pasqualetti and S. Zampieri, "On the controllability of isotropic and anisotropic networks," in *IEEE Conf. on Decision and Control*, (Los Angeles, CA, USA), pp. 607–612, Dec. 2014.

[90] L. N. Trefethen and D. Bau, *Numerical linear algebra*. SIAM, 1997.

[91] G. H. Golub and C. F. V. Loan, *Matrix computations*. JHU Press, 2012.

[92] J. G. Wendel, "Note on the Gamma function," *American Mathematical Monthly*, pp. 563–564, 1948.

[93] H. Mayeda and T. Yamada, "Strong structural controllability," *SIAM Journal on Control and Optimization*, vol. 17, no. 1, pp. 123–138, 1979.

[94] H. A. D. andH. N. Nagaraja, *Order statistics*. John Wiley & Sons, 2003.

[95] E. Scholtz, *Observer-based monitors and distributed wave controllers for electromechanical disturbances in power systems*. PhD thesis, Massachusetts Institute of Technology, 2004.

[96] F. Pasqualetti, A. Bicchi, and F. Bullo, "A graph-theoretical characterization of power network vulnerabilities," in *American Control Conference*, (San Francisco, CA, USA), pp. 3918–3923, June 2011.

[97] L. Dai, *Singular Control Systems*. Springer, 1989.

[98] M. Jun and R. D'Andrea, "Path planning for unmanned aerial vehicles in uncertain and adversarial environments," in *Cooperative control: models, applications and algorithms*, pp. 95–110, USA: Springer, 2003.

[99] D. P. Shepard, T. E. Humphreys, and A. A. Fansler, "Evaluation of the vulnerability of phasor measurement units to GPS spoofing attacks," *International Journal of Critical Infrastructure Protection*, vol. 5, no. 3-4, pp. 146–153, 2012.

[100] A. Broumandan, A. Jafarnia-Jahromi, V. Dehghanian, J. Nielsen, and G. Lachapelle, "GNSS spoofing detection in handheld receivers based on signal spatial correlation," in *ION Position, Location and Navigation Symposium*, pp. 479–487, April 2012.

[101] X. Jiang, J. Zhang, B. J. Harding, J. J. Makela, and A. D. Domínguez-García, "Spoofing GPS receiver clock offset of phasor measurement units," *IEEE Transactions on Power Systems*, vol. 28, no. 3, pp. 3253–3262, 2013.

[102] Y. Z. Lun, A. D'Innocenzo, F. Smarra, I. Malavolta, and M. D. D. Benedetto, "State of the art of cyber-physical systems security: An automatic control perspective," *The Journal of Systems and Software*, vol. 149, no. 2019, pp. 174–216, 2019.

[103] F. Pasqualetti, F. Dörfler, and F. Bullo, "Attack detection and identification in cyber-physical systems," *IEEE Transactions on Automatic Control*, vol. 58, no. 11, pp. 2715–2729, 2013.

[104] Y. Mo and B. Sinopoli, "Secure control against replay attacks," in *Allerton Conf. on Communications, Control and Computing*, (Monticello, IL, USA), pp. 911–918, Sept. 2010.

[105] J. P. Hespanha and S. D. Bopardikar, "Output-feedback linear quadratic robust control under actuation and deception attacks," in *American Control Conference*, (Philadelphia, PA, USA), pp. 489–496, July 2019.

[106] Y. Shoukry, P. Nuzzo, N. Bezzo, A. L. Sangiovanni-Vincentelli, S. A. Seshia, and P. Tabuada, "Secure state reconstruction in differentially flat systems under sensor attacks using satisfiability modulo theory solving," in *IEEE Conf. on Decision and Control*, pp. 3804–3809, Dec 2015.

[107] Q. Hu, D. Fooladivanda, Y. H. Chang, and C. J. Tomlin, "Secure state estimation and control for cyber security of the nonlinear power systems," *IEEE Transactions on Automatic Control*, vol. 5, pp. 1310–1321, Sept. 2018.

[108] J. Kim, C. Lee, H. Shim, Y. Eun, and J. H. Seo, "Detection of sensor attack and resilient state estimation for uniformly observable nonlinear systems having redundant sensors," *IEEE Transactions on Automatic Control*, vol. 64, no. 3, pp. 1162–1169, 2019.

[109] Y.-C. Liu, G. Bianchin, and F. Pasqualetti, "Secure trajectory planning against undetectable spoofing attacks," *arXiv*, p. arXiv:1902.10869, 2019.

[110] I. M. Gelfand and S. V. Fomin, *Calculus of Variations*. New York: Dover Publications, 2000. Reprint of 1963 translation from Russian by R. A. Silverman.

[111] R. F. Hartl, S. P. Sethi, and R. G. Vickson, "A survey of the maximum principles for optimal control problems with state constraints," *SIAM Review*, vol. 37, no. 2, pp. 181–218, 1995.

[112] T. Başar and G. J. Olsder, *Dynamic Noncooperative Game Theory*. SIAM, 2 ed., 1999.

[113] A. Sumalee, R. X. Zhong, T. L. Pan, and W. Y. Szeto, "Stochastic cell transmission model (sctm): A stochastic dynamic traffic model for traffic state surveillance and assignment," *Transp. Research Part B: Methodological*, vol. 45, no. 3, pp. 507–533, 2011.

[114] R. Chen and C. G. Cassandras, "Stochastic flow models with delays and applications to multi-intersection traffic light control," *IFAC-PapersOnLine*, vol. 51, no. 7, pp. 39 – 44, 2018. 14th IFAC Workshop on Discrete Event Systems WODES 2018.

[115] Z. Wang, G. Wu, and M. J. Barth, "Cooperative eco-driving at signalized intersections in a partially connected and automated vehicle environment," *IEEE Transactions on Intelligent Transportation Systems*, pp. 1–10, 2019.

[116] B. Ghena, W. Beyer, A. Hillaker, J. Pevarnek, and J. A. Halderman, "Green lights forever: Analyzing the security of traffic infrastructure," in *Workshop on Offensive Technologies*, 2014.

[117] Y. Feng, S. Huang, Q. A. Chen, H. X. Liu, and Z. M. Mao, "Vulnerability of traffic control system under cyber-attacks using falsified data," in *Transportation Research Board Annual Meeting*, 2018.

[118] A. Isidori, *Nonlinear Control Systems*. Communications and Control Engineering Series, Springer, 3 ed., 1995.

[119] C. D. Persis and A. Isidori, "A geometric approach to nonlinear fault detection and isolation," *IEEE Transactions on Automatic Control*, vol. 46, no. 6, pp. 853–865, 2001.

[120] C.-Z. Bai, F. Pasqualetti, and V. Gupta, "Data-injection attacks in stochastic control systems: Detectability and performance tradeoffs," *Automatica*, vol. 82, pp. 251–260, 2017.